

EPR STUDIES OF TRANSITION METAL IONS IN SOME DIA MAGNETIC SINGLE CRYSTALS

THESIS

**SUBMITTED TO
BUNDELKHAND UNIVERSITY
JHANSI, U.P., INDIA
FOR
THE DEGREE OF
DOCTOR OF PHILOSOPHY
IN
PHYSICS**

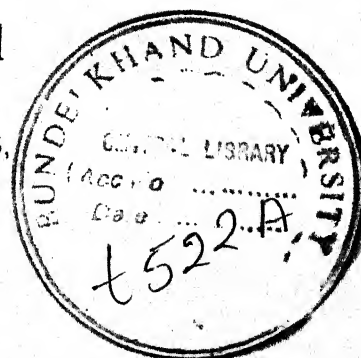
BY

ABHISHEK RICHHARIYA

UNDER THE SUPERVISION OF

Dr. N. L. SHUKLA

**READER AND HEAD,
DEPARTMENT OF PHYSICS,
ATARRA P.G. COLLEGE,
ATARRA (BANDA), U.P.
(SUPERVISOR)**



2002

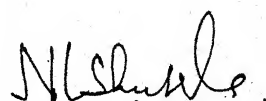
*This work is dedicated to my dearest
Mummy and Papa*

CERTIFICATE

This is to certify that the present thesis entitled “**EPR Studies of Transition Metal Ions in some Diamagnetic Single Crystals**” embodies the unaided research work of Mr. Abhishek Richhariya. This work was carried out under my supervision and has not been submitted elsewhere for a degree.

Mr. Abhishek Richhariya has attended the research center, Post Graduate Department of Physics, Atarra P.G. College, Atarra (Banda), U.P., more than three hundred days.

Dated: 18/12/2002


(Dr. N.L. Shukla)
Reader and Head
Department of Physics
Atarra P.G. College,
Atarra (Banda) U.P.
(Supervisor)

DECLARATION

I hereby declare that the thesis entitled **“EPR Studies of Transition Metal Ions in some Diamagnetic Single Crystals”** being submitted for the degree of Doctor Philosophy in Physics, Bundelkhand University, Jhansi, U.P., is an original piece of research work done by me under the supervision of **Dr. N.L. Shukla**, Reader and Head, Department of Physics, Atarra P.G. College, Atarra (Banda), U.P., and to the best of my knowledge, any part or whole of this thesis has not been submitted for a degree or any other qualification of any university or examining body in India/elsewhere

Dated: 18/12/2002

Abhishek Richhariya
(Abhishek Richhariya)

ACKNOWLEDGEMENTS

Before everyone and everything, I thank and praise the GOD ALMIGHTY for making it possible that this work exists in the present state.

I take this opportunity to express my gratitude to **Dr. N.L. Shukla**, Reader and Head, Department of Physics, Atarra P.G. College, Atarra (Banda) for exposing me to the field of spectroscopy, his kind guidance and his interest without which the present work would have been impossible.

I am thankful to **Professor (Dr.) B. N. Mishra**, Retd. Professor of Physics, Allahabad University, Allahabad, for his keen interest and help at various stages of this work. I am highly thankful to him for his valuable time that he managed to spare for the discussions regarding the work from time to time. I am equally thankful to **Prof. (Dr.) D.N. Pandey**, Ex-Principal, Atarra P.G. College, Atarra (Banda) for his interest and encouragement during the progress of the research work. I have been greatly benefited by the discussions we had during the progress of the work.

I wish to express my deep sense of indebtedness to my respected parents

Mr. Ashok Richhariya and **Mrs. Indu Richhariya** since the work in the present shape is due to their lively interest, constructive suggestions, all round persuasion and encouragement. They are a perennial source of inspiration and blessings to me. I owe a special debt of thanks to my dear sisters **Vijaeta Richhariya** and **Shweta Richhariya** for their

support, care and moral upliftment in the tough moments during the progress of the work.

My thanks are due to all of my friends who have helped me during the course of the work. I also extend my thanks to **Mr. Rajneesh Khare** and **Mr. Bharat Morbhatt** for helping me at various stages of the work

December 18, 2002

Abhishek Richhariya
(**Abhishek Richhariya**)

LIST OF PUBLICATIONS

1. Effect of exposure to lithium and iodine vapours of transition ions doped ceramics. N.L. Shukla and Abhishek Richhariya. Presented at the Fourth Conference of International Academy of Physical Sciences, February 25-27, 2001 at MGCGV, Chitrakoot.
2. Experimental investigations on $(\text{ZrO}_2)_{0.8}(\text{Y}_2\text{O}_3)_{0.2}$ ceramic compound. N.L. Shukla and Abhishek Richhariya. Presented at the Fourth Conference of International Academy of Physical Sciences, February 25-27, 2001 at MGCGV, Chitrakoot.
3. Intensities of various spectra in Mn^{2+} : NaNO_2 , N.L. Shukla, A.P. Srivastava, Rajneesh Khare and Abhishek Richhariya. Presented in the Fifth Conference of International Academy of Physical Sciences, April 07-09, 2002 at Bundelkhand University, Jhansi.

CONTENTS

CHAPTER-1

INTRODUCTION	1-11
--------------	------

CHAPTER-2

THEORETICAL CONSIDERATION OF ELECTRON	12-47
---------------------------------------	-------

PARAMAGNETIC RESONANCE

2.1	Introduction	12
2.2	Crystal Field Effects	13
	(i) Weak Crystal Field	14
	(ii) Intermediate Crystal Field	15
	(iii) Strong Crystal Field	15
2.3	Hyperfine Interaction	16
2.4	The Spin Hamiltonian	16
2.5	Covalency Effects and Super Hyperfine Structure	19
2.6	Kramers' Theorem and the Jahn- Teller [J-T] effect	21
2.7	Spin-Lattice and Spin-Spin Relaxation	22
2.8	EPR of liquids	24
2.9	Powder EPR spectra	28
2.10	The Expected Powder lineshapes	33
	(i) Patterns without hyperfine splitting	33
	(ii) Patterns with hyperfine splitting	35
2.11	(i) Computation of Resonance Fields	35
	(ii) Method for $S = 1/2$ ions	37
	Figures 2.1 – 2.4	39
	References	43

CHAPTER-3

EXPERIMENTAL TECHNIQUES		48-70
3.1	EPR Spectrometer	48
3.2	Crystal Rotator and Determination of Axis	49

3.3	Determination of EPR Parameters	50
	(i) Line Width	50
	(ii) g-value measurement	50
	(iii) Relaxation time (Measurements in r.f. region)	52
	(iv) Line shape determination	55
	(v) Moment determination	59
	(vi) Extreme hyperfine splitting and g-values	61
	(vii) Line width and Separation between the hyperfine lines	61
	Figures 3.1-3.6	63
	References	70

CHAPTER-4

	ELECTRON PARAMAGNETIC RESONANCE OF Cu^{2+} ION IN HEXAIMIDOZOLE CADMIUM NITRATE	71-100
4.1	Introduction	71
4.2	Experimental	71
4.3	(i) Room Temperature Spectrum	72
	(ii) Low Temperature spectrum (77°K)	72
	(iii) Variable Temperature Study	74
4.4	Summary of the Results	75
4.5	Jahn-Teller Effect in Cu^{2+}	76
4.6	Spin-Hamiltonian for Cu^{2+}	81
	(i) Estimation of the spin Hamiltonian parameters	82
	(ii) Calculation of Jahn-Teller energy	82
	(iii) Calculation of activation energy	84
4.7	Discussion	85
	(i) Activation energy	85
	(ii) High Temperature Spectrum	86
	Tables 4.I and 4.II	87
	Figures 4.1 – 4.10	88
	Reference	99

CHAPTER-5

ELECTRON PARAMAGNETIC RESONANCE OF Mn^{2+} IN NICKEL 101-112

ACETATE TETRADYRATE

5.1	Introduction	101
5.2	Crystal Structure	102
5.3	Result and Discussion	103
	(i) Analysis of the spectra	103
	(ii) Effect of Ni^{2+} on the EPR of Mn^{2+}	103
	Table 5.I	108
	Figures 5.1 – 5.2	109
	References	111

CHAPTER-6

ELECTRON PARAMAGNETIC RESONANCE OF Mn^{2+} ION IN 113-125 HEPTAHYDRATED SULFATES OF NICKEL AND MAGNESIUM

6.1	Introduction	113
6.2	Crystal Structure	114
6.3	Results and Discussion	115
	(i) Analysis of the Spectra	115
	(ii) Effect of Ni^{2+} on the EPR of Mn^{2+}	116
	Table 6.I	120
	Figures 6.1 – 6.3	121
	References	124

APPENDIX

GENERAL REFERNCES

CHAPTER – 1

INTRODUCTION

The Electron Paramagnetic Resonance (EPR) has become one of the most powerful tools for studying the wide varieties of physical, chemical and biological effects and also for the study of magnetic behaviour of paramagnetic substances. It was first observed by E.J. Zavoisky [1] in 1945 at USSR. Later on Cumberow and Halliday [2], Bleaney and Penrose [3] obtained well resolved resonance spectra of paramagnetic ions of the first transition series. A. Abragam, B. Bleaney, J.H.E. Griffiths, K.W.H. Stevens and their co-workers did the major developmental work in the techniques of EPR at the Clarendon laboratory, Oxford.

If a static magnetic field is applied to a system of free electrons ($L=0$, $S= \frac{1}{2}$), the electrons align themselves either parallel or antiparallel to the applied magnetic field. On applying electromagnetic field of frequency ν in a direction perpendicular to a DC magnetic field, the transitions of the electrons from lower level to upper level according to the selection rule $\Delta M_s = \pm 1$ take place and sharp absorption of power occurs provided the relation.

$$h\nu = g\beta H \quad (1.1.1)$$

is satisfied. Mostly the population ratio of the two energy states is given by the Maxwell-Boltzmann distribution relation:

$$n_1 / n_2 = e^{-\Delta E / kT}$$

where n_1 and n_2 are the number of free electrons in the upper and lower state respectively and E is the energy separation between the two states. In case of single spin system the population of the ground state is slightly in excess of the population of the upper state. Factually for a temperature of about 300°K and magnetic field 3000 gauss, the excess population in the ground state is only about 0.07 percent; yet the whole phenomenon of EPR depends upon this difference. If this resonance absorption of the radiation is to continue, there must be some other mechanism, apart from the stimulated emission which allows the electrons of the upper state to lose energy and drop to lower state, otherwise after sometime the population of the lower state will be zero and absorption will cease. Spin - lattice interaction, spin-spin interaction and exchange interaction are the important processes by which electrons lose energy and come to ground state and the absorption becomes a steady process [4].

The Hyperfine splitting of an Electron Paramagnetic Resonance line is obtained when the interaction between the unpaired electron and the magnetic nucleus takes place within the molecule. It is of extreme importance in determining the distribution of unpaired electron density and leads us to reach the valuable information regarding the intra and inter molecular

interactions. The total Hamiltonian of the system inclusive of EPR and Hyperfine processes is given by:-

$$\mathcal{H} = g \beta \vec{H} \cdot \vec{S} + A \vec{S} \cdot \vec{I} \quad (1.1.3)$$

assuming the ion to be free. But the unpaired electron is not always free and is bound in the molecule by a number of forces. The above Hamiltonian will be modified for a macroscopic body containing a paramagnetic as well as a large number of diamagnetic components. A brief discussion is given in chapter two of the thesis.

The substances possessing a resultant electronic magnetic moment exhibit the phenomenon of EPR. The materials possessing this property are transition elements, electrons trapped in radiation damages, impurities in semiconductors, free radicals and many other biological materials. The EPR study gives the various significant information about the system which are mentioned below:

The phenomenon of Electron Paramagnetic Resonance under certain conditions is found useful in providing the information about the bulk properties like susceptibility and specific heat of the system.

The resonance spectrum is extremely sensitive to the surrounding of the paramagnetic ion in the system. Thus it also provides information about the symmetry of the surroundings,

the nature and the strength of the bonding between the ion and its immediate diamagnetic neighbour.

The width of the resonance lines in a fully resolved spectrum depends on a number of factors such as (a) spin – lattice interaction (b) spin-spin interaction and (c) exchange interaction etc. The study of the width of the EPR lines provides complete information about the strength and nature of the these magnetic as well as non magnetic interactions present in the system.

Electronic transitions provide resonance spectra which help to obtain reliable interpretation about the nuclear spin of the paramagnetic ion. The values of nuclear dipole and nuclear quadrupole moments may also be found approximately.

From the analysis of the observed hyperfine structure we can draw conclusions concerning the nature of the sample and the character of the delocalization of the molecular orbital of the unpaired electron.

Thus there are various parameters of EPR spectrum e.g. lineshape, line width, g-value, intensity of the signal and hyperfine splitting constant etc., from which a variety of information about the paramagnetic molecule can be obtained. Apart from these points, the information derived from the EPR

spectrum also depends upon the nature and form of the specimen used.

Concentrated specimens used for EPR study usually provide single line spectrum [5-8]. In the case of polycrystalline samples, one gets linewidth and g-value averaged out over all possible orientations of the crystallites present in the samples. The Hyperfine structure [9-15] is studied in the diluted solutions of the complexes. When magnetically diluted single crystals are used for EPR study [16-20] we obtain most significant information. Results of directional anisotropies in line width and g-value which are obtained only from single crystal study, gives information about the configurations of the ions present in the complexes. A. Abragam et al have developed most of the theory on crystal fields and electron paramagnetic resonance [21,22,23]. It is not always possible to grow a magnetically dilute single crystal. However, it has been shown possible to obtain the similar type of information from powder and glass state EPR spectra [8,22].

Among the transition group elements, Copper is of great importance because of the reason that most of the discoveries associated with microwave spectra of solid state have been first observed in Cu^{2+} salts [28-30]. McGarvey [9], Cohn [10], Kozyrev [11], Kivelson and Wilson [15], Chary and Sastry [24],

Misra and Sharma [25-27], have investigated the paramagnetic resonance spectra of the transition metal ions.

The research work contained in this thesis is compiled and presented in six chapters. The first chapter contains a brief explanation of the phenomenon of EPR and the experimental techniques used.

The matter contained in the second chapter gives a detailed explanation of the theory of EPR investigations of the systems for the present work. A brief discussion on the crystal field effects, covering the weak intermediate crystal field and strong crystal field is given. The spin Hamiltonian and various types of interaction have also been discussed. The theory related to the EPR spectra of liquid, powder and their expected line shapes are described. Besides, the above discussion, the method of the computation of resonance field has also been mentioned in short.

The third chapter of the thesis deals with the experimental technique of EPR. A brief description of the experimental setup used in the EPR studies- varian V-4002 x band EPR spectrometer fitted with V-4540 variable temperature accessory, a crystal rotator and a quartz dewar used for studies at liquid nitrogen temperature (77°K), is given

The fourth chapter of the thesis comprises of the EPR studies carried out on $\text{Cu}^{2+}:\text{CdIm}_6(\text{NO}_3)_2$. the spectra of the sample have been recorded at room temperature and liquid nitrogen temperature. Their respective studies have been carried out. The temperature dependence of the spectra has been interpreted in terms of the dynamic-static Jahn-Teller effect of the trigonal Cu-sites in the system. The non-equivalent sites observed at low temperatures are being accounted for and understood in terms of static-Jahn-Teller distortion of Cu^{2+} sites. The spin Hamiltonian parameters are discussed and the Jahn-Teller energy has been calculated.

The fifth chapter of the thesis contains the detail of the EPR study carried out on nickel acetate tetrahydrate doped with Mn^{2+} . The study was focused at the spectra obtained at room temperature. The Mn^{2+} ion was found to substitute for Ni^{2+} in the bimolecular unit cell of $\text{Ni}(\text{CH}_3\text{COO})_2 \cdot 4\text{H}_2\text{O}$ and exhibit the characteristic magnetic inequivalency. Besides, the Mn^{2+} resonance lines exhibited a direct dependency of the line width on the Zeeman field intensity, and a shift in the g_z value towards the negative site, from the corresponding value for Mn^{2+} iso structural magnesium acetate tetrahydrate $[\text{Mg}(\text{CH}_3\text{COO})_2 \cdot 4\text{H}_2\text{O}]$. These features have been explained in terms of the interaction of Mn^{2+} ion with the Ni^{2+} host ions.

In chapter six, the EPR study of Mn^{2+} has been studied in the iso structural single crystals of nickel sulfate hepta hydrate ($\text{NiSO}_4 \cdot 7\text{H}_2\text{O}$) and magnesium sulfate heptahydrate ($\text{MgSO}_4 \cdot 7\text{H}_2\text{O}$) at room temperature. The Mn^{2+} ion was found to substitute for the divalent cations in the tetra molecular unit cells of $\text{NiSO}_4 \cdot 7\text{H}_2\text{O}$ and $\text{MgSO}_4 \cdot 7\text{H}_2\text{O}$, and exhibit the characteristic magnetic inequivalency. Besides, the Mn^{2+} resonance lines in $\text{NiSO}_4 \cdot 7\text{H}_2\text{O}$ exhibit a direct dependence of line width on the Zeeman-field intensity and a shift in the g_z value towards the negative side, from the corresponding value for Mn^{2+} in $\text{MgSO}_4 \cdot 7\text{H}_2\text{O}$. These features have been explained in terms of the interaction of Mn^{2+} ion with the Ni^{2+} host ions.

REFERENCES

1. E.J. Zavoisky, J. Phys. (USSR) **9**(1945) 211; *ibid* **10**(1946) 197.
2. R.L. Cumberow and D. Halliday, Phys. Rev. **70** (1946), 433.
3. B. Bleaney and R.P. Penrose, Nature 157, (1946) 339.
4. G.E. Pake, Paramagnetic Resonance, W.A. Benjamin Inc., New York (1962).
5. H. Kumagai, K. Ono, I. Hayashi, H. Abe, I. Shimada, H. Shono, H. Ibamoto and S. Tachimori, J. Phys. Soc. Japan, **9** 369 (1954).
6. C. Maclean and G.J.W. Kor; Appl. Sci. Res., **48**, 425 (1955).
7. B.N. Misra and S.K. Gupta, J. Mag. Resonance, **12** 126 (1973).
8. F.K. Neubuhl, J. Chem. Phys., **33** 1074(1960).
9. B.R. McGarvey, J. Chem. Phys., **60**, 71 (1956).
10. M. Cohn and J. Townsend, Nature, **173**, 1090 (1954).
11. B.M. Kozyrev, Disc. Faraday Soc; **19**, 135 (1955).
12. B. B. Garrett and L.O. Morgan, J. Chem. Phys., **44**, 890 (1966).

13. B.N. Misra, S.D. Sharma and S.K. Gupta, *IL. Nuovo Cimento* **19**, 129 (1974).
14. M.P. Eastman, G.R. Kooser, M.R. Das and J.H. Freed, *J. Chem. Phys.*, **51**, 2690 (1969).
15. D. Kivelson and R. Wilson, *J. Chem. Phys.*, **44**, 154, 4440, 4445 (1966).
16. B. Bleaney and D.J.E. Ingram, *Proc. Roy. Soc.*, **A205**, 336 (1951).
17. M. Weger and W. Low; *Phys Rev.*, **111**, 1526 (1958).
18. H.C. Box and H.G. Freund, *J. Chem. Phys.*, **40**, 817 (1968).
19. B. Bleaney, K.D. Bowers and D.J.E. Ingram, *Proc. Roy. Soc.*, **A228**, 147 (1955).
20. R. Janakiraman and G.C. Upreti, *J. Chem. Phys.*, **54**, 2336 (1971).
21. A. Abragam and B. Bleaney, *Electron Paramagnetic Resonance of Transition Ions*, Clarendon Press, Oxford (1970).
22. D. Kivelson and R. Neiman, *J. Chem. Phys.*, **35**, 156 (1961).
23. K.D. Bowers and J. Owen, *Reports on Progress in Physics*, **18**, 304 (1955).

24. M.N. Chary and B.A. Sastry, Indian J. Pure and Appl. Phys., **15**, 172 (1977).
25. B.N. Misra and S.D. Sharma, J. Chem. Phys., **63**, 5322 (1975).
26. B.N. Misra and S.D. Sharma, J. Mag. Reso., **24**, 1 (1976).
27. B.N. Misra and S.D. Sharma, Indian J. Pure and Appl. Phys., **15**, 719 (1977).
28. D.J.E. Ingram, Proc. Phys. Soc., **A62**, 664 (1949).
29. B. Bleaney and D.J.E. Ingram, Proc. Roy. Soc., **A63**, 408. (1950).
30. B. Bleaney, K.D. Bowers and D.J.E. Ingram, Proc. Phys. Soc., **A 64**, 758 (1951).

CHAPTER – 2

THEORETICAL CONSIDERATION OF ELECTRON PARAMAGNETIC RESONANCE

2.1 INTRODUCTION

When a free ion with a resultant angular momentum \bar{J} is subjected to a static magnetic field \bar{B} then it has $2J + 1$ energy levels and the energies of the various states are given as:

$$E_{M_J} = g\beta BM_J \quad (2.1.1)$$

where $M_J = J - 1, \dots, -J + 1, J$, B is the static magnetic field. g is the spectroscopic splitting factor and β is the Bohr magneton. The electrons in the unfilled 3d, 4d, 4f, 5d and (5f, 6d) shells are responsible for paramagnetism in iron, palladium, rare earth, platinum and actinide group complexes. A resonance absorption line corresponding to the energy difference. E between the E_{M_J} levels differing in M_J value by ± 1 should be observed. Therefore, the resonance condition becomes:

$$\Delta E = h\nu = g\beta B \quad (2.1.2)$$

The resonance condition for free electron is shown in Fig. 2.1. The intensities of these transitions are given by the square of the matrix element connecting M_J^{th} and $(M_J + 1)^{\text{th}}$ levels. The intensities are governed by the following relation.

$$[\text{Intensity}]_{M_J \leftrightarrow M_J \pm 1} \propto [J(J + 1) - M_J(M_J \pm 1)] \quad (2.1.3)$$

Thus transitions with different $M_J \leftrightarrow M_J \pm 1$ values will have different intensities. For the case of $J = 5/2$ the five transitions

corresponding to $\Delta M_J = \pm 1$ would have intensities in 5:8:9:8:5 ratio.

2.2 CRYSTAL FIELD EFFECTS

The energy levels of ions in a crystalline environment differ from the free ion energy levels. When a metal ion is placed in a crystalline field, the degeneracy of the d-orbitals will be removed by the electrostatic interactions. The spin degeneracy will remain until a magnetic field is applied. When the species contains more than one unpaired electron, the spin degeneracy can also be resolved by crystal field. Thus the spin levels may be split even in the absence of a magnetic field; this phenomenon is called zero field splitting. The theoretical explanation of zero field splitting in S-state ions was given by van Vleck and Penny [1], Sharma et. al. [2], Narayana [3], Chatterjee et al.[4] and Watanabe [5].

The EPR splitting of energy levels occurs under the effect of two types of fields; crystal field around the ion and the applied magnetic field. The crystal field is also called the internal splitting field and the energy splitting caused by this field are called 'Crystal field splitting' or 'Internal field splitting' or 'Zero field splitting' (ZFS) since it happens in the

absence of external magnetic field. For the paramagnetic ion in a crystal, there are two types of interactions; interactions between the paramagnetic ions (dipolar) and interactions between the paramagnetic ion and the nearest neighbours (ligand field). Former interaction is large in concentrated paramagnetic complexes but can be reduced effectively to a negligibly small value by dilution i.e. by doping small amounts of paramagnetic complex in an isomorphous diamagnetic host. Thus each ion may be considered isolated from other paramagnetic ions and to be independent. The latter interactions of paramagnetic ion with diamagnetic ligands modify the magnetic properties of the paramagnetic ions. The crystal field (CF) theory assumes that the ligands influence the magnetic ion through the electric field which they produce at its site and their orbital motions get modified. The crystal field interaction is affected by the electrostatic screening by the outer electronic shells. Depending upon its magnitude relative to other interactions, the crystalline field interaction is generally classified into three categories.

2.2 (i) Weak Crystal Field

When the crystal field interaction is weaker than the spin-orbit coupling (this is the case with the rare-earth and certain actinide compounds). It is due to the fact that the unfilled

shell, 4f or 5f lies fairly deep within the ion and is shielded by the closed 5s and 5p or 6s and 6p shells respectively.

2.2 (ii) Intermediate Crystal Field

When the crystal field interaction is greater than spin-orbit coupling but is less than the Coulombic interaction between electrons. The best example of these are hydrated salts of the iron group. This situation is described by regarding the orbital motion as clamped due to crystal field and making it unable to respond to an applied magnetic field. This is known as "quenching of orbital angular momentum" and the magnetic properties are all due to spin which is affected only weakly by crystal field through spin-orbit coupling.

2.2 (iii) Strong Crystal Field

The crystal field is said to be strong when the crystal field interaction is of the order of Coulombic interaction between electrons. For the 4d and 5d transition group ions there is a tendency of covalent bonding due to which the orbitals of the metal ion and neighbouring ligands overlap appreciably. In this case due to strong covalent bonding the crystal field assumption remains no longer valid.

2.3 HYPERFINE INTERACTION

Hyperfine interaction are mainly magnetic dipole interactions between the electronic magnetic moment and the nuclear magnetic moment of the paramagnetic ion. The origin of this can be understood simply by assuming that the nuclear moment produces a magnetic field B_N at the magnetic electrons and the modified resonance condition is:

$$\Delta E = h\nu = g\beta|B+B_N| \quad (2.3.1)$$

The hyperfine interaction is highly characteristic one. Identification of paramagnetic and its isotopics in characteristic by the hyperfine structure (HFS) in the EPR spectra is the simplest method. The interaction of the magnetic electron with nuclei of the ligands gives rise to super hyperfine structure (SHFS) on the HFS in the EPR spectra.

2.4 THE SPIN HAMILTONIAN

The EPR, the unpaired electron is not isolated or free, but frequently interacts with a variety of nuclei and electrons. Therefore the right handside in eqn. (2.1.2) becomes the sum of various terms. The state of affairs may be expressed from the quantum mechanical view point in terms of a Hamiltonian.

The electronic interactions which contribute to the total energy of the ion may be described by the following Hamilton [6-10].

$$\mathcal{H} = \mathcal{H}_0 + \mathcal{H}_{cr} + \mathcal{H}_{s-o} + \mathcal{H}_{s-s} + \mathcal{H}_z + \mathcal{H}_{hf} + \mathcal{H}_q + \mathcal{H}_n + \mathcal{H}_e \quad (2.4.1)$$

Where

\mathcal{H}_0 = Free ion energy [$\sim 10^5 \text{ cm}^{-1}$]

\mathcal{H}_{cr} = Electrostatic energy [$\sim 10^4 \text{ cm}^{-1}$]

\mathcal{H}_{s-o} = Spin orbit interaction energy
[$\sim 10^2 - 10^3 \text{ cm}^{-1}$]

\mathcal{H}_{s-s} = Spin-spin interaction energy [$\sim 1 \text{ cm}^{-1}$]

\mathcal{H}_z = Interaction of electron with the external field or Zeeman energy = $\beta B(L+2S)$ [$\sim 1 \text{ cm}^{-1}$]

\mathcal{H}_{hf} = Dipole-dipole interaction between the electron and nuclear-magnetic moments
[$\sim 10^{-1} \text{ cm}^{-1} - 10^{-3} \text{ cm}^{-1}$]

\mathcal{H}_q = Quadrupole interaction between electron and nucleus [$\sim 10^3 \text{ cm}^{-1}$]

$$\mathcal{H}_n = \text{Nuclear Zeeman energy} = g_N \beta_N B \cdot I$$

$$[\sim 10^4 \text{cm}^{-1}]$$

$$\mathcal{H}_e = \text{Energy of exchange effects between electrons.}$$

Practical EPR spectroscopy concerns itself mainly with the \mathcal{H}_{S-S} , \mathcal{H}_Z and \mathcal{H}_{h-f} i.e. the fine structure, Zeeman splitting and hyperfine interactions as the nuclear Zeeman and quadrupole interactions are usually small. The best way to consider all the energy contributions is to express them in the following form including the nuclear Zeeman and quadrupole terms [10].

$$\mathcal{H} = \beta \vec{B} \cdot \vec{g} \cdot \vec{S} + \vec{S} \cdot \vec{D} \cdot \vec{S} + \vec{S} \cdot \vec{A} \cdot \vec{I} - \beta_N \vec{B} \cdot \vec{g}_N \vec{I} + \vec{I} \cdot \vec{Q} \cdot \vec{I}.$$

(2.4.2)

where \vec{S} and \vec{I} are the electronic spin and nuclear spin operators respectively and are equivalent to \vec{J} operators from mathematical point of view and \vec{g} , \vec{D} , \vec{A} , \vec{Q} and \vec{g}_N are all second rank tensor quantities. The first term represents Zeeman interaction with the applied field B , the presence of orbital momentum is taken into account by allowing the splitting factor \vec{g} to differ from the spin-only value (2.0023). \vec{D} in the second term represents the crystal field splitting. The third term expresses the hyperfine interaction between \vec{S} and \vec{I} . The fourth term expresses the nuclear Zeeman interaction and the last

term expresses the quadrupole coupling between nuclear spin I and the electric field gradient. In principal axes system (Tensors in diagonalised eqn. Form) eqn. (2.4.2) can be written as (neglecting the nuclear Zeeman interaction).

$$\mathcal{H} = \beta (g_x B_x S_x + g_y B_y S_y + g_z B_z S_z) + D [S_z^2 - 1/3 S(S+1)] + E (S_x^2 - S_y^2) + A_x S_x I_x + A_y S_y I_y + A_z S_z I_z + Q' [I_z^2 - 1/3 I(I+1)] + Q'' (I_x^2 - I_y^2) \quad (2.4.3)$$

where $D = D_z - 1/2 [D_x + D_y]$, $E = 1/2 [D_x - D_y]$

$$Q' = Q_z - 1/2 [Q_x + Q_y], \quad Q'' = 1/2 [Q_x - Q_y]$$

and g_x, g_y, g_z and A_x, A_y, A_z are the components of g and A tensors respectively along principal axes. In Eqn. (2.4.3) the Parameters "D" and "E" are generally known as fine structure parameters and are the measure of the ZFS of energy states described by the spin-Hamiltonian. "D" and "E" represent the axial and rhombic parts of the crystal field splitting respectively. For the so called axial symmetry $E = Q_{||} = 0$ and $g_z = g_{||}$; $g_x = g_y = g_{\perp}$, $A_z = A_{||}$ and $A_x = A_y = A_{\perp}$.

2.5 COVALENCY EFFECTS AND SUPER-HYPERFINE STRUCTURE

A detailed examination reveals that the approximation of ligand ion in CF theory is not strictly valid, and the overlap of

the wave functions of the ligand ions with that of the metal ion must be taken into account. Stevens[11] considered this problem for the first time for the complexes of the ions from 4d and 5d groups which are bonded in a strongly covalent manner. Owen [12,13] studied the same for some ions from 3d group. The main effects of the covalency on EPR can be listed as follows:

- (i). The covalent bond reduces the orbital contributions to the g-factor. The evidence for reduction of the orbital contribution has been obtained from the spectra Ti^{3+} in alum [14], Fe^{2+} in MgO [15, 16] and ZnF_2 [17] and Co^{2+} in MgO [18, 19] and ZnF_2 [17].
- (ii). The hyperfine interaction parameter 'A' is reduced. The experimental evidence comes from the work of Title [20] who studied the paramagnetic resonance of Mn^{2+} in a variety of host lattices and proved that the hyperfine constant. "A", decrease linearly with the increase of covalency.
- (iii). There may be an additional SHFS structure on the HF lines due to the interaction between the magnetic electrons and the surrounding nuclei. The effect was first found by Owen and Stevens in ammonium chlororidate [21], and subsequently for a number of

transition metal ions in ZnF_2 by Tinkham [17] and by several other workers [22-25] in various host lattices.

2.6 KRAMERS' THEOREM AND THE JAHN-TELLER [J-T] EFFECT

The Kramer's theorem [26] states that in a crystalline field of any symmetry, a system having an odd number of electrons will always possess at least a two-fold spin degeneracy which can be lifted by the application of a magnetic field. These states were referred to as Kramer's doublet and assures the observation of EPR in the so called Kramer's (odd number of electrons).

According to J-T effect [27-28], a symmetrical non-linear molecule having a degenerate electronic energy level can not have stable configuration and will therefore distort to a configuration of lower symmetry and thus the degeneracy of the electronic state is lifted, or in other words the disposition of the nuclei adjusts in such a way that the symmetry of a complex gets lowered.

Van Vleck [29] estimated that for iron group, a splitting of few hundred cm^{-1} and for rare earth group about 10^{-2} cm^{-1} may be caused by J-T effect. In the case of paramagnetic ions

embedded in diamagnetic hosts, the symmetry of the ligand field is also reduced due to Jahn-Teller effect. This effect is prominently noticeable in the case of Cu^{2+} in trigonal field [30-32] and Fe^{2+} in octahedral field [15-16].

2.7 SPIN LATTICE AND SPIN-SPIN RELAXATIONS

In EPR three processes are commonly described for transferring energy from the excited spin system to the lattice [spin lattice relaxation (SLR)] direct, Raman and Orbach process. In the direct process for the two-level system, relaxation occurs through transfer of energy from a single spin to a single vibrational mode of the crystalline lattice which has essentially the same frequency [33]. When relaxation is by the direct process, $T_1 \propto 1/B^2T$ [34] (where T_1 is the SLR time) and is independent of the spin concentration. Therefore, the temperature and magnetic field can serve as variables either for the study or for the control of T_1 . Actually, the "direct" process is important only at low temperatures.

At high temperatures, the indirect or Raman process predominates. Here a phonon is inelastically scattered in the process of flipping a spin. Energy is conserved and this process was strongly temperature dependent with $T_1 \propto 1/T^7$ for $T < \theta_D$,

$T_1 \propto 1/T^2$ for $T > \theta_D$ where θ_D is the Debye temperature [35]. Experimental results are in fair agreement with theory at high temperature but not at low temperature where the direct process is important.

In the orbach process, there are two transitions one after the other which occur via an intermediate state. When electron is transferred from a level m to level n in the ground manifold of states by absorbing energy equal to $h\nu$, then by stimulated transition, it goes to a level q which is higher in energy than n by an amount Δ . Spontaneous transition then takes place from level p to m which release a phonon of energy equal to $(h\nu + \Delta)$. The relaxation rate is given by

$$\frac{1}{T_1} \propto e^{-\Delta/kT} \quad (2.7.1)$$

where k is the Boltzmann factor. This relaxation process is active in the case of rare-earth ions.

The theory of spin-spin relaxation (S-SR) has been developed by Van Vleck [36], Pryce and Stevens [37] where two main types of interactions between the ions have been recognized; the dipole-dipole and the exchange interaction. The dipoles are close enough so that they experience various local fields resulting from the dipolar fields of their neighbours. In the case of exchange interaction, the energy transfer takes place by means of mutual spin flips between neighbouring

spins. As the spins are in thermal equilibrium among themselves and if the equilibrium is disturbed, it is re-established exponentially with a time constant T_2 called the SSR time. The resonance line width is proportional to $1/T_2$.

2.8 EPR OF LIQUIDS

The paramagnetic complexes in liquid solutions can be considered as micro-crystals tumbling in a random way as they jostled by the molecular motions of the solvent [38]. Considering the effect of only motional modulation of anisotropic g and A tensors on the line-width Kivelson [39] developed the theory of ESR line width in dilute solutions. Because of the tumbling motion, the orientation of micro-crystals varies with respect to the external magnetic field. The spin Hamiltonian under this condition can be written as:

$$\mathcal{H}_{\text{spin}} = \mathcal{H}^{(0)} + \mathcal{H}^{(1)} + F(t) \quad (2.8.1)$$

where

$$\mathcal{H}^{(0)} = g_0 \beta_0 S_z H_z$$

$$\mathcal{H}^{(1)} = h A_0 S_z + \frac{1}{2} A_0 [I^+ S^- + I^- S^+],$$

$$g_0 = 1/3 (g_x + g_y + g_z)$$

$$A_0 = 1/3 (A_x + A_y + A_z)$$

$F(t)$ is the time dependent part of the Hamilton and depends upon the anisotropy of g and A . Assuming that the spectral lines are well resolved, that the Zeeman term is the largest term in energy and the lines-shapes are Lorentzian, Wilson and Kivelson [40] gave the expression of line-width ΔH as

$$\Delta H = a_1 + a' + a_2 + a_3 + a_4 \quad (2.8.2)$$

$$a_1 = a_0 + a = \frac{1}{43} [(\Delta\gamma H_0)^2] (4 + 3u) + \frac{1}{40} b^2 [I + 1]$$

$$= (3 + 7u) \frac{1}{8} b^2 (I + 1) (A_0 / \omega_0) uf - \frac{1}{30}$$

$$= \Delta\gamma H_0 b_1 (I + 1) (A_0 / \omega_0) (1 + u),$$

$$a_2 = \frac{1}{13} (b\Delta\gamma H_0) (4 + 3u) - \frac{2}{43} (\Delta\gamma H_0)^2 (4 + 3u + 3uf) (A_0 / \omega_0)$$

$$= \frac{1}{20} b^2 I (I + 1) (A_0 / \omega_0) (4 + 3u + 7uf) + \frac{1}{40} b^2 (A_0 / \omega_0) \times (3 + 2\gamma) \quad [21]$$

$$(I+1)-1]$$

$$a_3 = A_0 = \frac{b^2}{40} (5 - u) + \frac{1}{8} b^2 (A_0 / \omega_0) uf = \frac{1}{30} (\Delta\gamma / H_0 b)$$

$$= (A_0 / \omega_0) (7 + 5u + 12uf)$$

$$a_4 = \frac{1}{10} b^2 (A_0 / \omega_0) (1 + u + uf)$$

in these expressions

$$u = (1 + \omega_0^2 \tau_c^2)^{-1/2}, f = \omega_0^2 \tau_c^2 u,$$

$$b = \frac{2}{3} (A_{||} - A_{\perp}) \text{ rad / sec}, \Delta\gamma = \beta_0 \Delta g / h, \Delta g = g_{||} - g_{\perp}$$

Where ω_0 is the microwave frequency in rad/sec and τ_c is the orientational correlation time expressed as:

$$\tau_c = \frac{4}{3} \frac{\pi r^3 \eta}{kT} \quad (2.8.3)$$

and η is the viscosity of the solution. a_0 is called the residual line-width due to some unspecified mechanisms. The most important of these mechanisms is the spin rotational relaxation mechanism, a relaxation mechanism because of the interaction of the rotational magnetic moment of paramagnetic molecule with its spin or nuclear magnetic moment. Atkins and Kivelson [41], following Hubbard theory [42], gave the following expression for the line-width due to this mechanism:

$$a_0 \sim \alpha_{RS} = \frac{2}{\sqrt{3}} \frac{h}{\beta_0 g} \frac{1}{12\pi r^3} [\Delta g^2 + 2\Delta g_{\perp}^2] \frac{kT}{\eta}, \quad (2.8.4)$$

Where $\Delta g_{||} = g_{||} - 2.0023$, $\Delta g_{\perp} = g_{\perp} - 2.0023$, r the molecular radius of the equivalent rotating sphere in the solution and the remaining symbols have their usual meaning.

Among many suggestions to explain the observed line-width an idea analogous to electric field fluctuation mechanism in solids [43, 44] was applied in the case of liquids. In this process the electric fields constituting the crystal or molecular

binding fields are modulated by the molecular vibrations and by collisions with surrounding diamagnetic molecules, and these fluctuations of electric field affect the spin by means of spin-orbit interactions. The lattice vibrations in crystals replace the Brownian motion in solutions as the source of modulation. Kivelson developed [43] the contributions of three most significant electric field fluctuation mechanisms in solutions as:

$$W(1) = 64 (\lambda / \Delta)^2 = \left(\frac{\phi' q_0}{\Delta r_0} \right)^2 \frac{(\omega_0 \tau_c)^2 \tau_c^{-1}}{1 + \omega_0^2 \tau_c^2} \quad (\text{Van Vleck direct})$$

(2.8.5)

$$W(2) = 32 (\lambda / \Delta)^2 = \left(\frac{\phi' q_0}{\Delta r_0} \right)^2 \tau_0^{-1} (\text{Van Vleck Raman}), \omega_0^2 \tau_c^2 \leq 1,$$

(2.8.6)

$$W(3) = 16 (\lambda / \Delta)^2 = \left(\frac{(\phi' q_0)^2}{\Delta r_0} \right)^2 \left(\frac{\Delta}{\delta} \right)^2 \frac{\tau_0^{-1}}{[\exp(h\delta / kT) - 1]}$$

(Orbach),

$$\delta^2 \tau_c^2 \geq 1, \quad (2.8.7)$$

Where λ = spin orbit coupling constant for a given ion, Δ = crystal field splitting parameter, r_0 = characteristic intermolecular distance, τ_c = mean correlation time for intermolecular fluctuations, q_0 = typical root-mean-square

value of q_i ; q_i 's are the amplitudes of intermolecular oscillations, $h\delta$ =exciting energy of the first excited state.

$$\phi' = \sum | (hV_{CF} / \delta q_i) r_0 |$$

is a potential indicating the approximate magnitude of the crystal or molecular binding field. However, out of these three electric field fluctuation mechanisms only Orbach process was found to be useful.

2.9 POWDER EPR SPECTRA

In the polycrystalline samples the polycrystals (crystallites) randomly oriented with respect to the static magnetic field (46-48). Consequently, EPR corresponding to all possible orientations of these small crystallites is obtained. The individual EPR signals usually overlap because of finite individual line widths to form what we normally call a "powder EPR pattern". For discussing the powder line-shapes, we consider a spherical coordinate system shown in Fig. 2.1 in which the orientation of the paramagnetic species defined by the orthogonal axes, x , y and z ; θ and ϕ are the angles specifying the orientation of B in this coordinate system. Now, the number of crystallites with a magnetic field orientation

between θ and $\theta + d\theta$ and between ϕ and $\phi + d\phi$ proportional to the solid angle $d\Omega$ [49] where

$$d\Omega \propto \sin \theta \, d\theta \, d\phi = d \cos \theta \, d\phi \quad (2.9.1)$$

The powder EPR pattern then the ensemble average of the resonance condition over all equally probable elements of solid angle ($d\Omega$) summed over all allowed transitions. The EPR absorption at field H in the magnetic field interval dH may be expressed in terms of a normalized "shape function" [50] $S(H)$ given by

$$S(H) \, dH \propto (4\pi)^{-1} \sum_r \int_H^{H+dH} P_r(\Omega) \, d\Omega(H_r) \quad (2.9.2)$$

Eqn. (2.9.2) integrated over those elements of solid angle $d\Omega(H_r)$ such that $H < H_r < H + dH$, where H_r is the appropriate resonance condition corresponding to r th transition. In general, $d\Omega$ is a multi-valued function of H_r , there being more than one value of $\cos \theta$ and ϕ for some resonance fields H_r . $P_r(\Omega)$ is the transition probability for the r th component and is normally independent of Ω except in the case where we have strong g -anisotropy (51-54). Thus, $P_r(\Omega)$ may be taken outside the integral sign of Eqn. (2.9.2) in most situations, and the EPR powder patterns for each resonance transition to be multiplied by one of these factors before adding all pattern together to get the total absorption line-shapes.

However, in situations where all elements of solid angle not equally probable, [55], an additional factor such as $p(\Omega)$ must be included in Eqn. (2.9.2), where $P(\Omega) d\Omega$ gives the probability of a site being oriented in an element of solid angle $d\Omega$ at Ω .

The resonance conditions described above represented idealized δ -function line-shapes, which are seldom observed in the actual spectra. Several line broadening mechanisms operative in actual situations Line-broadening from dipole-dipole interactions can be expressed empirically by a normalized "Gaussian Function" of the following form [56].

$$Y_G(H - H_r) = \left(\frac{\ln 2}{\pi} \right)^{1/2} \frac{y_0}{\Delta H} \exp. \left[\frac{(-\ln 2)(H - H_r)^2}{\Delta H^2} \right] \quad (2.9.3)$$

Where $Y_G = \left(\frac{\ln 2}{\pi} \right)^{1/2} \frac{1}{\Delta H}$ and H_r represents the resonant field corresponding to an appropriate resonance condition. The quantity ΔH referred to as the half-width at half-maximum (HWHM) of a pure absorption line in the absence of microwave power saturation. The equation for the corresponding first derivative of the Gaussian Function is:

$$Y'_G(H - H_r) = -\frac{2}{\pi} \frac{(\ln 2)^{3/2}}{\Delta H^3} \cdot (H - H_r) \cdot \exp. \left[-\frac{\ln 2}{\Delta H^2} \cdot (H - H_r)^2 \right] \quad (2.9.4)$$

The peak-to-peak width of the derivate line-shape (ΔH_{pp}) is related to ΔH by the following relation

$$\Delta H = (\ln 2 / 2)^{1/2} \Delta H_{pp} \quad (2.9.5)$$

Line broadening from "Exchange Interaction" can often be approximated theoretically by a normalized Lorentzian function, characterized by the following expression [57]:

$$Y_L(H - H_r) = 1 / \pi \cdot \frac{\Delta H}{\Delta H^2 + (H - H_r)^2} \quad (2.9.6)$$

The corresponding first derivative line-shape is:

$$Y_L'(H - H_r) = -\left(\frac{2}{\pi}\right) \frac{\Delta H (H - H_r)}{[\Delta H^2 + (H - H_r)^2]^2} \quad (2.9.7)$$

For Lorentzian line ΔH and (ΔH_{pp}) are related by the following relation:

$$\Delta H = \frac{(\sqrt{3} \Delta H_{pp})}{2} \quad (2.9.8)$$

Dilute paramagnetic systems (such as radical species diluted in a liquid) often exhibit spectral line-shapes which can normally be approximated by a Lorentzian function. Moreover, in some systems, the presence of more than one independent line-broadening mechanism complicates the spectral shape, and then each component line-width should be given by Eqns. (2.9.3-2.9.5) and (2.9.6.-2.9.8), respectively. Although not common, a combination of Lorentzian and Gaussian lines was

some times observed due to the presence of several types of interaction in the spin system. Such combinations are often represented by a "Voigt" shape function [57].

To account for the above broadening mechanism, an additional term representing the appropriate line line-shape, e.g. Eqn. (2.9.2-2.9.4) and (2.9.5-2.9.7), should be added to in Eqn. (2.9.2), which then involves a double integral. If we neglect the dependence of the lines-shapes functions on orientations [58], which normally is unimportant in the powder lines-shape calculations [59], we can take the line-broadening terms outside of the integral sign in Eqn. (2.9.2), thus giving a convolution of the ideal delta function line-shape.

Since analytical solutions to most powder EPR pattern problems generally impossible to carry out in practice , Eqn. (2.9.2) quite often solved numerically by using a computer. It might be said that without high-speed digital computers that are available these days, this task would be nearly impossible. As a consequence powder EPR spectrometry would have been more limited in its applications than it is today. The normal procedure for obtaining solutions to Eqn. (2.9.2) comprises summation of all contributions to the shape function, $S(H)$, over a grid in $(\cos \theta, \phi)$ space by various numerical integration algorithm [60].

The next section illustrates the powder patterns expected for several systems under different symmetry conditions.

2.10 THE EXPECTED POWDER LINE-SHAPES

2.10.1 Pattern without Hyperfine Splitting:

For paramagnetic systems with axial symmetry, we find from Eqn. (2.18) that the shape function $S(H)$ can be expressed as:

$$S(H) dH \propto \sin\theta d\theta \quad (2.10.1)$$

Or

$$S(H) \propto \sin\theta / (dH/d\theta) \quad (2.10.2)$$

Eqns. (2.10.1) and (2.10.2) reflect the fact that very large number of radicals with axes nearly perpendicular to the field direction will be present in the system and only a few radicals will have their axis aligned close to the field direction. This means that we expect to see two "extrema" in the powder spectra.

The resonance field (H_r) is given by:

$$H_r = \frac{h\nu}{\beta} \frac{1}{(g_{\parallel} \cos^2 \theta + g_{\perp} \sin^2 \theta)} \quad (2.10.3)$$

Eqn. (2.10.3) shows the expected angular variation of H_r (Fig. 2.2). Differentiating Eqn. (2.10.3), in order to evaluate $dH/d\theta$, we write Eqn. (2.10.2) into the form

$$S(H) \propto \left(\frac{h\nu}{\beta}\right)^2 \frac{1}{H_r^3 (g_{\parallel}^2 - g_{\perp}^2) \cos \theta} \quad (2.10.4)$$

We see, therefore, that due to the presence of "cos θ " term in the denominator of Eqn. (2.10.4), $S(H)$ rises monotonically from a finite value determined by g_{\parallel} to infinity, i.e., at a field determined by g_{\parallel} , as $\theta \rightarrow 90^\circ$. This behaviour is shown by the s-function line-shape in Fig. 2.2(a) where the powder patterns obtained for various amounts of line-broadening are also depicted. The two extrema, therefore, correspond to g_{\parallel} and g_{\perp} , respectively, so that the resonance field lies between $h\nu/g_{\parallel}\beta$ and $h\nu/g_{\perp}\beta$. The corresponding first derivative spectra would be of the type shown in Fig. 2.2. (c). Levedev [61] gives a more complete description of such theoretical line-shapes for systems with axial symmetry.

For powder specimens with an orthorhombic g-tensor, there are three turning points in the EPR spectrum corresponding to the three principal g-tensor components, g_{xx} , g_{yy} and g_{zz} ; g_{yy} being the intermediate in the spectrum [49]. The diagnostic features of the absorption line-shapes and its first-derivative for such a situation are shown in Fig. 2.3.

2.10.(ii) Patterns with Hyperfine Splitting:

The simple line-shapes patterns in Figs. 2.2 and Fig. 2.3 are modified in the presence of electron-nuclear hyperfine interaction. Assuming the unpaired electron to be interacting with a set of magnetically equivalent $I = 2$ nuclei, the line-shape pattern of Fig. 2.2(c) becomes modified to that shown in Fig. 2.4.(a). The powder pattern becomes more complicated when interacting magnetic nuclei have spin $I > 1/2$, for example, for $I = 3/2$, and an isotropic hyperfine interaction, the pattern would be according to Fig. 2.4.(c).

In several simple situations it may be possible to determine some or all of the components of g and A simply from the experimentally observed spectra. Otherwise, the extraction of rather precise Hamiltonian parameters usually rests on the "Computer Simulation" until the best fit is achieved between experimental and calculated line-shapes.

2.11.(i) COMPUTATION OF RESONANCE FIELDS

The EPR transitions result from a matching of energy levels of a spin in a magnetic field by the microwave quantum used. Thus the validity of the phenomenological SH used may be testified by comparing the observed and computed values of

resonance fields with the help of solution of SH matrix (with the known values of parameters) as and subsequently matching the possible energy level differences to the microwave quantum. The SH matrix can be solved either by perturbation method or by exact numerical diagonalization on digital computers. The perturbation methods are applicable to the cases where the Zeeman term is dominant and are thus of limited applicability only to cases with small ZFS and small hyperfine interaction. The energy levels given in the fine structure in the EPR are labeled by quantum numbers M_s and those giving the hyperfine structure by m_I . Though the labelling is done as if these are pure quantum numbers, they have no other meaning except their use for labelling. In the perturbation expressions which involve these numbers and treat them as pure quantum numbers an error is introduced due to their real value being defined for $\Delta M_s = \pm 1$ and $\Delta m_I = 0$. The transitions possible in violation of the above rules are termed as forbidden transitions and may involve $\Delta M_s = \pm 2, \pm 3$ etc. and $m_I = \pm 1, \pm 2$ etc.

The resonance fields are calculated from the exact solution of SH matrix and by finding an interval $(H, H + \delta H)$ by interactive procedure such that for a value H_j of the magnetic field $F_j \left(= |E_{jj} - E_{j+\Delta M}| - \frac{h\nu}{\beta} \right) \leq 0$ and for $(H_j - \delta H)$, $F_j \geq 0$ where E_j

are the levels involved in the transition, ΔM is a positive or negative integer including zero depending on the transition under consideration being "allowed" or "forbidden", $h\nu$ is the microwave quantum and δH is a small number pre-selected based on the experimental accuracy of the resonance fields ($\delta H \sim 10^{-1} - 10^{-3}$ Gauss). The value H_j thus computed corresponds to the resonance field position for the transition under consideration. The process is repeated until the total number of observed transitions have been considered and their position computed (in Gauss).

2.11.(ii) Method For $S = \frac{1}{2}$ Ions

For $S = \frac{1}{2}$ and $I = 3/2$ or $7/2$ for example Cu^{2+} , Co^{2+} and VO^{2+} the fine structure terms are dropped from the SH and it assumes the simpler form:

$$\mathcal{H} = \beta \bar{S} \cdot \bar{g} \cdot \bar{H} + \bar{I} \cdot \bar{A} \cdot \bar{S} + \bar{I} \cdot \bar{P} \cdot \bar{I} - \beta_N \bar{H} \cdot \bar{g}_N \cdot \bar{I} \quad . \quad [2.11.(ii).1]$$

In most of the cases the last two terms are found to be very small and may generally be dropped from the spin Hamiltonian. For axial symmetry the SH (II-2.7) is sometimes written in terms of more customary symbols in the following form [49):

$$\mathcal{H} = g \beta S_z H_z + \beta g_{\perp} (S_x H_x + S_y H_y) + A S_z I_z + B (S_x I_x + S_y I_y) +$$

$$+ O \left[3I_z^2 - I(I+1) \right] + \gamma \beta_N \vec{H} \cdot \vec{I} - R I_z H_z - R_{\perp} (H_x I_x + H_y I_y) \quad [2.11.(ii).2]$$

Bleaney [50] in his classic paper has obtained the expressions for the resonance fields applying perturbation method and Low [9] has given the expressions for resonance fields for both the allowed and the forbidden transitions. Extensive discussion of the perturbation method and the above SH may be found in literature [12,48]. For the analysis of Cu^{2+} ($S=1/2$, $I=3/2$) and VO^{2+} ($S=1/2$, $I=7/2$) EPR spectra spin Hamiltonian paramagnetics are obtained. The parameters thus obtained were next refined by obtaining minimizing F . Here $F = \sum_i (H'_0 - H_T^i)^2$, where H'_0 and H_T^i are the experimentally observed and calculated resonance field values respectively and H_T^i are computed by the method described earlier through the exact numerical diagonalization of a SH matrix (8×8 for Cu^{2+}) and 16×16 for VO^{2+} .

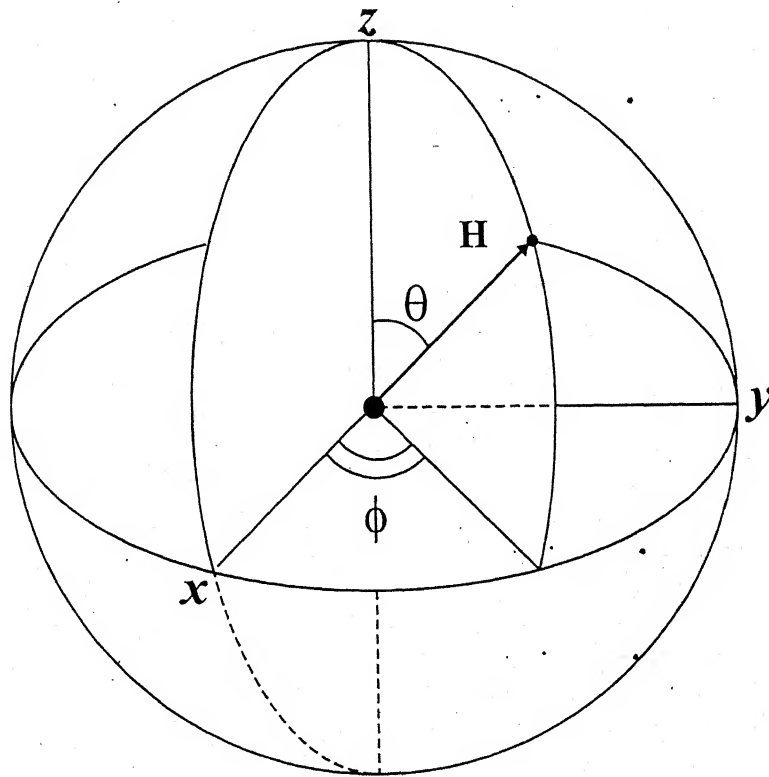


Fig2.1.

Axis system and polar coordinates showing the orientation of H

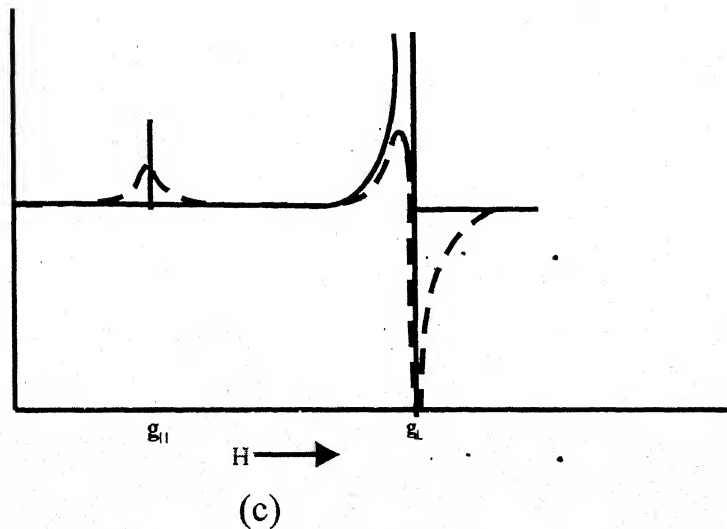
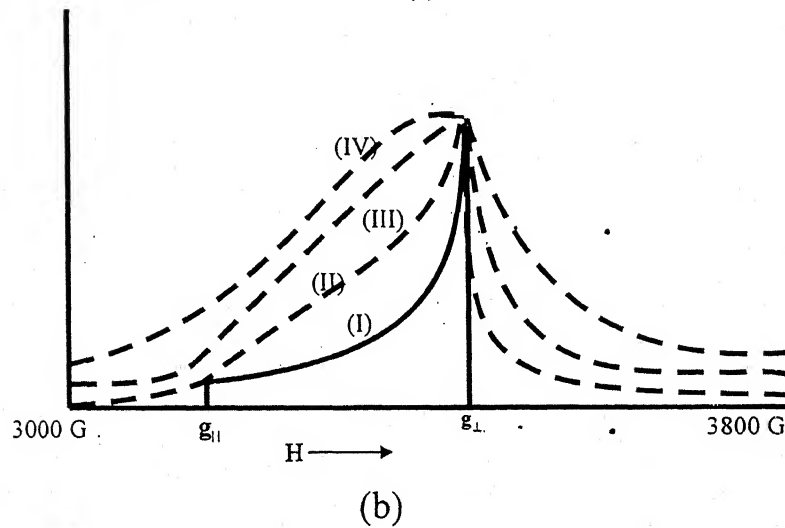
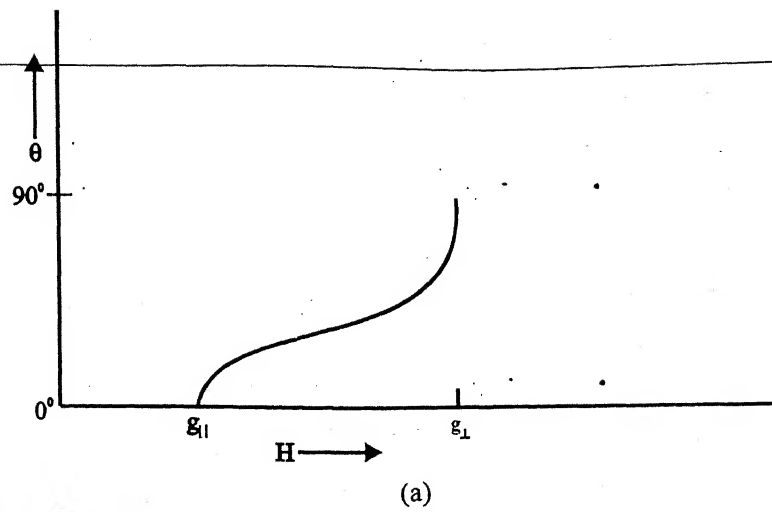
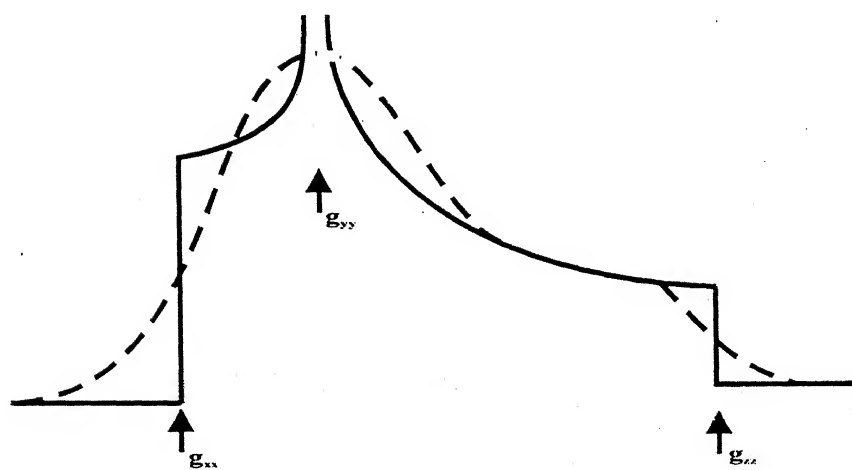


Fig. 2.2: Powder EPR Pattern for a system ($S = 1/2$, $I = 0$) with axial symmetry ($g_{\parallel} > g_{\perp}$)

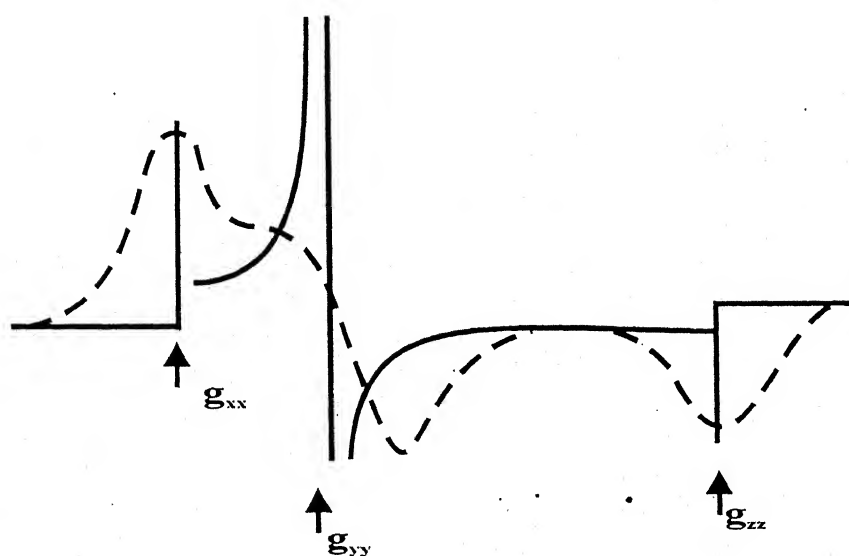
(a) Angular dependence of the resonance field position.

(b) Absorption line shapes: The δ -function line shape (I) is broadened by Lorentzian shape functions of width 10 G (II), 50 G (III) and 100 G (IV) respectively.

(c) Derivative line shape: Solid is the δ -function line shape.



(a)



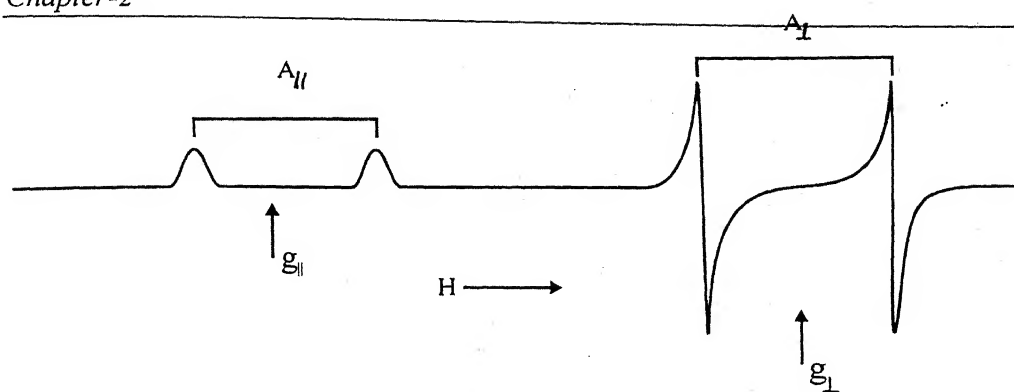
(b)

Fig. 2.3: Powder EPR Pattern for an orthorhombic g-tensor with $I=0$

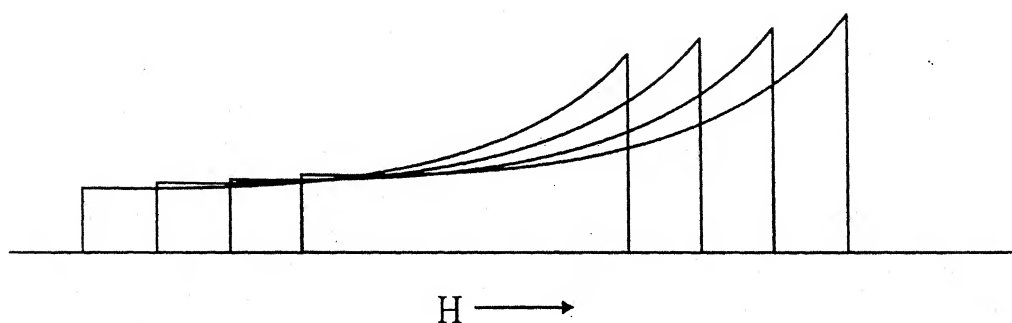
(a) Absorption Curves

(b) Derivative Curves

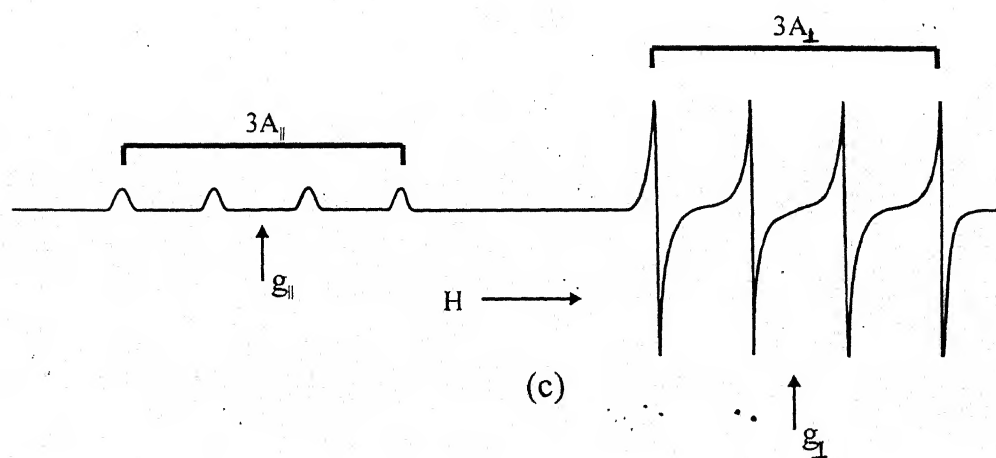
The solid and broken lines are respectively δ -function line and broadened line.



(a)



(b)



(c)

Fig. 2.4: Powder patterns for an $S = 1/2$ axial symmetry system ($g_{\parallel} > g_{\perp}$) with isotropic A- tensor:
 (a) Derivative line showing hyperfine interaction with $I = 1/2$.
 (b) Idealised absorption positions for hyperfine interaction with $I = 3/2$
 (c) Derivative line corresponding to (b) including some line broadening.

REFERENCES

1. J.H. Van Vlack and W.Q. Penny, Phil. Mag., **17**, 961 (1934).
2. R.R. Sharma, T.P. Das and R. Orbach, Phys. Rev., **149**, 257 (1966); 388 (1967) and **171**, 378 (1968).
3. P.A. Narayana, Phys. Rev. Lett., **B10**, 2676 (1974).
4. R. Chatterjee, M.R. Smith and H.A. Buckmaster, Canad. J. Phys., **54**, 1224 (1976).
5. H. Watanabe, Progr. Theor. Phys., **18**, 405 (1957).
6. A Abragam and M.H.L. Pryce, Proc. Roy. Soc., **A205**, 135 (1951).
7. S.A. Al'tshuler, B.M. Kozyrev. "Electron Paramagnetic Resonance", Academic Press, New York (1964).
8. R.S. Anderson, "Electron Spin Resonance", Methods of Experimental Physics, **3**, 441 (1962).
9. R.S. Alger, Electron Paramagnetic Resonance, Techniques and Applications, Inter-science Publications, John Wiley and Sons, New York, London, Sydney (1968).
10. A. Abragam and B. Bleaney, "Electron paramagnetic Resonance of Transition Ions", Oxford University Press (Clarendon), Oxford (1970).

11. K.W.H. Stevens, Proc. Roy. Soc, **A219**, 542 (1953).
12. J. Owen., Discus. Faraday. Soc., **19.**, 127 (1955).
13. J. Owen, Proc. Roy. Soc., **A227**, 183 (1955).
14. B. Bleaney, G.S. Bogle., A.H. Cooke, H.J. Duffus, M.C.M. O'Brien and K.W.H. Stevens, Proc., **A 68**, 57 (1955).
15. W. Low, Ann. New York Acad. Sci., **72**, 69 (1958).
16. W. Low, Phys. Rev., **101**, 1827 (1956).
17. M. Tinkham, Proc. Roy. Soc., **A 236**, 535 and 549 (1956).
18. W. Low, Phys. Rev. **109**, 865 (1958).
19. W. Low and D. Shaltiel, J. Phys. Chem. Solids, **6**, 315 (1958).
20. R.S. Title, Phys. Rev., **131**, 623 (1963).
21. J. Owen and K.W.H. Stevens, Nature, **171**, 836 (1953).
22. S. Ogawa, J. Phys. Soc. Japan, **15**, 1475 (1960).
23. J.E. Drumheller, J. Chem. Phys., **38**, 970 (1963).
24. W.J., Weighle and W.H. Tantttila, J. Chem. Phys., **41**, 274 (1964).
25. T.L. Estle and W.C. Holton, Phys. Rev., **150**, 159 (1968).

26. H.A. Kramers, Proc. Amsterdam Acad. Sci., **33**, 959 (1930).
27. H.A. Jahn and E. Teller, Proc. Roy. Soc., **A161**, 220 (1937).
28. H.A. Jahn, Proc. Roy. Soc., **A 164**, 117 (1938).
29. J.H. Van Vleck, J. Chem. Phys., **7**, 72 (1939).
30. B. Bleaney and K.D. Bowers, Proc. Phys. Soc., **A65**, 667 (1952).
31. D. Biji and A.C. Ross-Innes, Proc. Phys. Soc., **A66**, 954 (1953).
32. B. Bleaney, K.D. Bowers, and R.S. Trenam, Proc. Roy. Soc., **A 228**, 157 (1955).
33. J.A. Giordmaine, L.E. Alsop, F.R. Nash and C.H. Townes, Phys. Rev., **109**, 302 (1958).
34. G.E. Pake, "Paramagnetic Resonance", Benjamin, New York (1962).
35. W. Low, "Paramagnetic Resonance in Solids", Solid State Physics Suppl., **2**, 150 (1960).
36. J.H. Van Vlack, Phys. Rev., **74**, 1168 (1948).
37. M.H.L. Pryce and K.W.H. Stevens, Proc. Phys. Soc., **A63**, 36 (1950).
38. H.M. McConnell, J. Chem. Phys., **25**, 709 (1956).

39. D. Kivelson, J. Chem. Phys., **27**, 1087 (1957): **33**, 1094 (1960).
40. R. Wilson, D. Kivelson, J. Chem. Phys., **44**, **154**, **4440**, **4445** (1966).
41. P.S. Hubbard, Phys. Rev., **131**, 1155 (1962).
42. J.H. Van Vleck, Phys. Rev., **57**, 426 (1940).
43. R.Orbach, Proc. Phys. Soc., **A77**, 821 (1961).
44. D. Kivelson, J. Chem. Phys., **45**, 1324 (1966).
45. F.J. Adrian, J. Colloid Interface Sci., **26**, 317 (1968).
46. P.H. Kasai and R.J. Bishop, Jr. in Zeolite Chemistry and Washington, E.C.(1976), p. 350.
47. W.N. Delgass, G.L. Haller, R. Kellerman and J.H. Lunsford, "Spectroscopy in Heterogeneous Catalysis", Academic Press, New York (1979), p. 183.
48. F.K. Kneubuhl, J. Chem. Phys., **33**, 1074 (1960).
49. C.P. Slichter, "Principles of Magnetic Resonance" (second revised and expanded edition), Springer-Verlag, Berlin (1980), p. 259.
50. C.A. McDowell, P. Raghunathan and J.C. Tait, J. Chem. Phys., **59**, 5858 (1973).
51. B. Blaney, Proc. Phys. Soc., London **75**, 621 (1960).

52. T. Vangard and R. Assa, "Paramagnetic Resonance", Vol., 2, Ed. W. Low, Academic Press, New York (1963), p. 509.
53. A. Isomoto, H. Watari and M. Kotani, J. Phys. Soc. Japan, **29**, 1571 (1970).
54. H.M. McConnell and B.G. McFarland, Quart. Rev. Biophys., **3**, 91 (1970).
55. C.P. Poole, Jr., "Electron Spin Resonance", Interscience, New York (1967), p. 778.
56. Reference 21, p. 783.
57. J. Maruani, Chem. Phys. Lett., PS7PS, 29 (1970).
58. A. Abragam, "The Principles of Nuclear Magnetism", Clarendon Press, Oxford (1961), p. 220.
59. See, for example, (a) R. Lefebvre and J. Maruani, J. Chem. Phys., **42**, 1480 and 1496; (b) R. Breslow and F.J. Owens, Chem. Phys. Lett., **16**, 20 (1972) and references therein (c).

CHAPTER – 3

EXPERIMENTAL TECHNIQUES

3.1 EPR SPECTROMETER

The experimental EPR studies were carried out on a Varian V-4502 EPR spectrometer¹ operating at X-band micro-wave frequency (~ 9.5 GHz) and provided with a 100 kHz field modulation. Fig. 3-1 shows the simplified block diagram of the spectrometer. The Varian V-4540 variable temperature accessory (range 77 K to 570 K) was used with the spectrometer to carry out the temperature variation studies. An all quartz dewar, suitable for use with liquid nitrogen, was used for studies at 77 K. A 9 inch Varian electromagnet, rotatable about the vertical axis and equipped with 'Fieldial' magnetic field regulator, was used. It provides a very homogeneous magnetic field in the air gap (2.625 inches) and the field can be varied from near zero to about 10 KG. DPPH, with $g = 2.0036$, was used as the standard field marker by fixing a small speck of DPPH on the sample. The magnetic field at DPPH resonance was measured by proton resonance using a Varian F-8A flux meter and a Systronics Counter timer Type 701 (Sr. No. 016). The EPR spectra were recorded using a Varian G-14 strip chart recorder. A Varian V-4531 multipurpose rectangular cavity operating in the TE_{102} mode was used.

¹ 'V-4502 EPR spectrometer system manual' Varian Associates, California

3.2 CRYSTAL ROTATOR AND DETERMINATION OF AXIS

Angular variation EPR studies of the doped crystals were carried out using a Varian E-229 goniometer sample rotater, which rotates the crystal in increments of 0.5° by means of a gear drive about a vertical axis. This goniometer is physically attached to the multipurpose cavity. In addition, for spatial orientations a crystal holder, shown in Fig. (3-2) was employed. This provides the rotation of the crystal within the cavity about a horizontal and a vertical axis without removing it from the cavity. This facilitates the alignment of any desired axis of the crystal along the Zeeman field direction. Here the rotation of the crystal about a horizontal axis was achieved by means of a thread and shaft arrangement (also called string drive method).

The directions of the crystal field axes (X, Y, Z) were determined from the angular variation of the EPR spectra employing the following method: the crystal was rotated independently about a horizontal and a vertical axis and the direction of maximum spread of the fine structure of Mn^{2+} EPR spectra was obtained. This direction is termed as the Z-axis. Then the crystal was rotated in a plane perpendicular to the Z-axis and the directions of maximum

and minimum spreads of the spectra in this plane were determined, which are called the X- and the Y-axis, respectively.

3.3 DETERMINATION OF E.P.R. PARAMETERS

(i). Line Width:

In X-band region, the peak to peak line width of the first derivative record was measured very accurately and with the help of calibration of the chart it was converted in magnetic field units. For accurate measurement of the magnetic field the spectra were calibrated at large number of points with the help of a proton probe used along with the frequency counter. In R.F. region, the photographs of EPR absorption lines were enlarged. The line width between the half power points was determined and was converted in oersteds by multiplying it with the value of the field per unit division obtained above. The method used for the determination of line-widths is given in Fig. 3.3.

(ii). g-value measurement:

The spectroscopic splitting factor or 'g-value' is a measure of the contribution of the spin and orbital motion of the electron to its

total angular momentum, and for an electron completely free from orbital effect, its value is 2.0023. The g-value of DPPH (1,2) has been found equal to 2.0036 ± 0.0003 , that is, the accuracy in the fourth decimal place is needed. The g-value of DPPH can be calculated from the experimental record in the following manner:

The value of magnetic field H from proton resonance is given by

$$h \gamma_p = g_p \beta_p H \quad (3.3.1)$$

$$\text{i.e.} \quad H = [h / g_p \beta_p] \gamma_p$$

Similarly for Electron Paramagnetic Resonance

$$h \gamma_e = g_e \beta_e H \quad (3.3.2)$$

$$\text{i.e.} \quad g_e = [h \gamma_e / \beta_e] \cdot 1/H$$

Since H is known and therefore g_e can be calculated. γ_p and γ_e are in mc and H is in oersteds. The gyromagnetic ratio of proton in water(3) i.e. $\gamma = 2.67513 \pm 0.00002 \times 10^4 \text{ gauss}^{-1} \text{ sec}^{-1}$ was used. The accuracy in g-value is achieved by attaining the maximum possible accuracy in the ratio of the Electron Paramagnetic Resonance frequency γ_e and the proton resonance frequency γ_p at the given field. So at least five to six proton frequency marks should be applied on the chart while the field is scanned to get the resonance spectrum. The frequency at the center of the EPR

spectrum was measured with respect to all the marks and the value of H corresponding to mean frequency was calculated. The frequency of the Klystron was separately measured and substituting these two values, the value of g was calculated.

The g -value of the sample other than DPPH was measured by comparison (4) using pure DPPH as a standard. Since the frequency of resonance is kept constant, so equation of resonance for pure DPPH and sample using eq. (3.3.2) are given by :

$$h\gamma_e = g_{\text{DPPH}} \beta_e H_1 \quad (3.3.3)$$

and
$$h\gamma_e = g_{\text{sample}} \beta_e H_2 \quad (3.3.4)$$

using these two expressions we can write

$$g_{\text{sample}} = g_{\text{DPPH}} \cdot H_1/H_2 \quad (3.3.5)$$

where H_1 is the field at resonance for DPPH and H_2 is the field at resonance of the sample. Thus g value of the sample under study can be measured by utilizing equation (3.3.5)

(iii) Relaxation time (Measurements in r.f. region)

Block (5) proposed a set of equations to describe to the behaviour of magnetic properties of an assembly of nuclei placed in an external magnetic field. He obtained the expressions for absorption as well as dispersion as a function of frequency of the electromagnetic field H_0 applied along the z -axis and an r.f. field H_1

perpendicular to z-axis. Bloch's expression for the magnetic susceptibility and absorption are given below:

$$u = \chi'(\omega).H_1 = M_0 \frac{|\gamma|H_1T_2^2(\omega_0 - \omega)}{1 + T_2^2(\omega_0 - \omega)^2 + (\gamma H_1)^2T_1T_2} \quad (3.3.6)$$

$$v = \chi''(\omega).H_2 = M_0 \frac{|\gamma|H_1T_2}{1 + T_2^2(\omega_0 - \omega)^2 + (\gamma H_1)^2T_1T_2} \quad (3.3.7)$$

where $M_0 = \chi_0.H_0$; $|\gamma| = \omega_0 / H_0$ gyromagnetic ratio

and T_1, T_2 are the spinlattice and spin—spin relaxation time respectively. These equations have been used in the case of electron spin resonance to determine the relaxation time.

The important methods for the determination of relaxation time in radio frequency region are following:

1. Bridge method (6)
2. Induction method (6)
3. Oscillator detector method (9)

In case when pure absorption lines are studied, the oscillator detector method has been found as the most convenient and sufficiently sensitive. To determine spin lattice relaxation time which is not possible with this in usual manner, a new technique has been developed by Wolf (9). Here it is possible to vary H_1 and to measure it. The expression for half line width δ_1 and δ_2 at half power points for two values of r.f. field H_1 and H_2 respectively,

based on the Lorentzian form of the absorption line and on the Bloch equations, can be written as:

$$\delta_1 = \sqrt{[1 + \gamma(H_1)^2 T_1 T_2] / \gamma T_2} \quad (3.3.8)$$

$$\delta_2 = \sqrt{[1 + \gamma(H_2)^2 T_1 T_2] / \gamma T_2} \quad (3.3.9)$$

The nature of variation of δ with H_1 is shown in Fig. 3.4. If $H_1 < H_2$, then $\delta_1 < \delta_2$. The expression for T_1 and T_2 can be written by squaring and rearranging the equations (3.3.8) and (3.3.9)

$$T_1 = \Delta D^2 / \gamma \sqrt{[\Delta H^2 \Delta p^2]} \quad (3.3.10)$$

$$T_2 = \Delta H^2 / \gamma \sqrt{[\Delta H^2 \Delta p^2]} \quad (3.3.11)$$

$$\text{Where } \Delta D^2 = \delta_2^2 - \delta_1^2; \Delta H^2 = H_2^2 - H_1^2 \text{ and } \Delta p^2 = \delta_1^2 H_2^2 - \delta_2^2 H_1^2 \quad (3.3.12)$$

The value of the r.f. magnetic field in the sample coil is given by

$$H_1 = 2\pi N K \sqrt{2} / 10 I \cdot I_L \quad (3.3.13)$$

Where N = Number of turns in the sample coil = 10

l = length of the coil. = 1.2 cm

K = nogoka factor for short solenoid, which in this case is 0.68. and

$$I_L = \text{r.f. current in the tank coil} = E/Z_t$$

where E is the r.f. voltage across the tank coil line and Z_t is its impedance. The value of Z_t has been calculated by the standard formula and E has been measured by a V.T.V.M. The sample is placed in this coil and it acts as the transmitting and receiving coil.

The values of T_1 and T_2 have been calculated by using the formulae (3.3.10) and (3.3.11) by substituting the measured values of δ_1 and δ_2 and the values of the r.f. field H_1 and H_2 respectively.

The relaxation times were also measured at different temperature by taking the EPR spectra for two values of r.f. magnetic field H_1 and H_2 at different temperatures. For temperature variation silvered double walled thermos flask was used which could maintain a constant temperature for a sufficient long time. The samples were kept in it for a long time in order to attain the temperature of the bath. Freezing mixture, dry ice and liquid oxygen was used for low temperature work. The temperature was measured at regular intervals, with the help of properly calibrated copper constantan thermocouples. The EPR spectra of the samples were photographed from an oscilloscope display when the fluctuation in the thermocouple was minimum.

(iv). Line shape determination:

A great deal of information can be obtained from the careful analysis of the shape of a resonance absorption line. Two types of line shapes have been proposed, the Lorentzian and the Gaussian.

If the amplitude of high frequency field is small i.e. sufficiently below than that required for saturation, the imaginary part of the Susceptibility $\chi''(\omega)$ can be written as:

For Lorentzian shape:

$$\chi''(\omega) = [(\chi_0 \omega_0 T_2) / 1 + T_2^2 (\omega_0 - \omega)^2] \quad (3.3.14)$$

$$= \pi \chi_0 \omega_0 G_L(\omega_0 - \omega) \quad (3.3.15)$$

Where $G_L(\omega_0 - \omega)$ is the Lorentian shape factor and is given by

$$G_L(\omega_0 - \omega) = [T_2 / 1 + T_2^2 (\omega_0 - \omega)^2] \quad (3.3.16)$$

For Gaussian shape:

$$\chi''(\omega) = [(\chi_0 \omega_0 T_2) \exp. \{-T_2^2 (\omega_0 - \omega)^2 / \pi\}] \quad (3.3.17)$$

$$= \pi \chi_0 \omega_0 G_G(\omega_0 - \omega) \quad (3.3.18)$$

Where G_G is the Gaussian shape factor and is given by

$$G_G(\omega_0 - \omega) = 1/\pi [T_2 \exp. \{-T_2^2 (\omega_0 - \omega)^2 / \pi\}] \quad (3.3.19)$$

Since the measurements of the line widths in our experiment have been done in terms of magnetic field and keeping the frequency constant, so it is more convenient to convert the expressions (3.3.14) and (3.3.17) as given below:

$$\text{Lorentzian shape } \chi''(H) = \frac{2\chi_0 H_0}{\Delta H_{1/2}} \left[\frac{1}{1 + 4 \left\{ \frac{H_0 - H}{\Delta H_{1/2}} \right\}^2} \right] \quad (3.3.20)$$

$$\text{Gaussian Shape } \chi''(H) = (4\pi \ln 2)^{1/2} \frac{\chi_0 H_0}{\Delta H_{1/2}} \left[\exp \left\{ -4 \ln 2 \cdot \frac{(H_0 - H)^2}{\Delta H_{1/2}} \right\} \right] \quad (3.3.21)$$

Where $\Delta H_{1/2}$ is the full width between half power points in oersteds. Since the intensity of absorption is directly proportional to the $\chi''(H)$ and intensity is measured by the amplitude of the absorption line, therefore $\chi''(H)$ can be replaced by a constant times Y_{\max} , the maximum amplitude of the absorption line. Thus the line shape can be normalized in terms of maximum amplitude and one can write:

$$\text{For Lorentzian Shape } \frac{Y(H)}{Y_{\max}} = \left[\frac{1}{1 + 4 \frac{(H_0 - H)^2}{\Delta H_{1/2}}} \right] \quad (3.3.22)$$

$$\text{For Gaussain Shape } \frac{Y(H)}{Y_{\max}} = \exp \left\{ -4 \ln 2 \cdot \frac{(H_0 - H)^2}{\Delta H_{1/2}} \right\} \quad (3.3.23)$$

In a similar manner, the expressions for first derivative of $\chi''(H)$ can be written and normalized. The expression for normalized derivative curves are:

Lorentzian Shape:

$$\frac{Y'(H)}{Y'_{\max}} = \left[\frac{d\chi''(H)}{dH} \right] / \left[\frac{d\chi''(H)}{dH} \right]_{\max} = \frac{32}{9} \left[\frac{H_0 - H}{\Delta H_{pp}} \right] \left[1 + \frac{4}{3} \left(\frac{H_0 - H}{\Delta H_{pp}} \right)^2 \right]^{-2} \quad (3.3.24)$$

Guassian Shape

$$\frac{Y'(H)}{Y'_{\max}} = \left[\frac{d\chi(H)}{dH} \right] / \left[\frac{d\chi(H)}{dH} \right]_{\max} = 2e^{1/2} \left[\frac{H_0 - H}{\Delta H_{pp}} \right] \exp. \left\{ -2 \left(\frac{H_0 - H}{\Delta H_{pp}} \right)^2 \right\}$$

(3.3.25)

where ΔH_{pp} is the full width between maximum slope points of first derivative record.

The normlized theoretical Lorentzian and Guassian line shape graphs of pure absorption as well as first derivative curves have been drawn with the help of the equations (3.3.22-3.3.25) by taking the calculated values of $Y(H)/Y_{\max}$ and $Y'(H)/Y'_{\max}$ For arbitrary values of $(H_0-H)/\Delta H_{1/2}$ and $(H_0-H)/\Delta H_{pp}$ respectively. These theoretical line shape graphs are given in Fig. 3.5. The Lorentzian shape is slightly sharper in the center and decrease much more slowly in the wing beyond the half amplitude or first derivative points. The line shapes of pure EPR absorption curves and of their first derivatives have been tested by platting the points corresponding to the different values of $Y(H)/Y_{\max}$ and $Y'(H)/Y'_{\max}$ for each values of $(H_0-H)/\Delta H_{1/2}$ and $(H_0-H)/\Delta H_{pp}$ from different experimental records respectively, on the respective theoretical Lorentzian and Gaussian line shape graphs.

(v) Moment determination :

The expression for the n th moment $\langle H^n \rangle$ of a resonance absorption as defined by Van Vleck (7) can be written as

$$\langle H^n \rangle = \frac{H_j - H_{j-1}}{A} \sum_{j=1}^m (H_j - H_0)^n Y_j \quad (3.3.26)$$

where Y_j is the amplitude of the resonance absorption line at the magnetic field H_j and there are m intervals in all and A is the area under resonance absorption curve. It is convenient to take equal intervals $(H_j - H_{j-1})$ along the field direction so that

$$A = (H_j - H_{j-1}) \sum_{j=1}^m Y_j \quad (3.3.27)$$

we can determine H_0 of a symmetrical line by computing the first moment.

$$\langle H^1 \rangle = \frac{H_j - H_{j-1}}{A} \sum_{j=1}^m (H_j - H_0) Y_j \quad (3.3.28)$$

which will vanish for the proper choice of H_0 . If the expression of $\langle H^1 \rangle$ is not zero, then let

$$\langle H^1 \rangle = B = \frac{\sum_{j=1}^m (H_j - H_0) Y_j}{\sum_{j=1}^m Y_j} \quad (3.3.29)$$

The correction factor B is the displacement as shown in Fig. 3.6 (a).

In the light of this correction factor the expression for the n th moment can be written as

$$\langle H^n \rangle_{\text{corr}} = \frac{H_j - H_{j-1}}{A} \sum_{j=1}^m (H_j - H_0 - B)^n Y_j \quad (3.3.30)$$

Thus the expressions for second and fourth moment can be written as:

$$\langle H^2 \rangle = \frac{H_j - H_{j-1}}{A} \left(\frac{1}{2} \Delta H_{1/2} \right)^2 \sum_{j=1}^m \left(\frac{H_j - H_0 - B}{\frac{1}{2} \Delta H_{1/2}} \right)^2 Y_j \quad (3.3.31)$$

and the fourth moment

$$\langle H^4 \rangle = \frac{H_j - H_{j-1}}{A} \left(\frac{1}{2} \Delta H_{1/2} \right)^4 \sum_{j=1}^m \left(\frac{H_j - H_0 - B}{\frac{1}{2} \Delta H_{1/2}} \right)^4 Y_j \quad (3.3.32)$$

It has been shown that for a purely Gaussian line shape

$$\frac{\langle \langle H^4 \rangle_{\text{AV}} \rangle^{1/4}}{\langle \langle H^2 \rangle_{\text{AV}} \rangle^{1/2}} = 1.32 \quad (3.3.33)$$

If the value of this ratio is greater than 1.32 the line will have Lorentzian shape.

The expressions for the area and the moment of a first derivative absorption curve can be written as:

$$A = (H_j - H_{j-1})^2 \sum_{j=1}^m j (Y'_j - B_1) \quad (3.3.34)$$

$$\langle H^2 \rangle = \frac{(H_j - H_{j-1})^2}{A} \sum_{j=1}^m \sum_{i=j}^m (H_j - H_0 - B_2)^2 (Y'_j - B_1) \quad (3.3.35)$$

$$\langle H^4 \rangle = \frac{(H_j - H_{j-1})^2}{A} \sum_{j=1}^m \sum_{i=j}^m (H_j - H_0 - B_2)^4 (Y'_j - B_1) \quad (3.3.36)$$

$$\text{where } B_1 = \frac{1}{m} \sum_{j=1}^m Y'_j \quad (3.3.37)$$

$$B_2 = \frac{1}{2} \frac{\sum_{j=1}^m (H_j - H_0)^2 (Y'_j - B_1)}{\sum_{j=1}^m (H_j - H_0)^2} \quad (3.3.38)$$

B_1 and B_2 are the correction factors due to the improper choice of base line and vertical axis as shown in Fig. 3.6 (b). If the base line is not properly chosen i.e. $B_1 \neq 0$, then the area of the line will be effected and an improper choice of H_0 (i.e. $B_2 \neq 0$) will not effect the integrated area but will produce error in the value of the moments.

(vi). Extreme Hyperfine Splitting and g-values :

The determination of g-value is made as described earlier using expression (3.3.5). The extreme hyperfine splitting i.e. the separation between the outermost peaks have been measured in magnetic field units.

(vii). Line width and Separation between the hyperfine Lines:

Horizontal axis of the derivative record is converted in terms of static magnetic field and taking the center of the spectrum as origin, the value of $(H-H_0)$ is determined on either side of the first derivative EPR line. The derivative curve is then integrated about different points along the axis and the integrated area versus magnetic field is plotted. The number of the lines and their relative

intensities are thus speculated by visual observations. The Lorentzian and Gaussian line shape expressions denoted by equations (3.3.20) and (3.3.21) can be written as given below.

For Lorentzian Shape:

$$Y_L = \sum \frac{A}{1 + (\alpha - \varepsilon)^2} \quad (3.3.39)$$

For Gaussian Shape

$$Y_G = A \sum e^{-(\alpha - \varepsilon)^2} \quad (3.3.40)$$

Where

$$\alpha = \frac{H}{1/2 \Delta H_{1/2}} \text{ and } \varepsilon = \frac{H_0}{1/2 \Delta H_{1/2}} \quad (3.3.41)$$

A is the maximum intensity of the EPR line. Further assuming that each individual line has definite shape and all the lines are of same width and have equal separation, the value of Y_L and Y_G are obtained for a particular value of ε and different values of α with the help of above expressions (3.3.39) and (3.3.40). Such curves are drawn for different values of ε . These theoretically computed resonance absorption curves are fitted on the experimental integrated observed spectrum and best fit is used to evaluate the line width and separation between the lines. Values of electron nuclear coupling constants can be obtained with the help of the known values of separation ΔH between hyperfine components after applying suitable overlapping corrections (8).

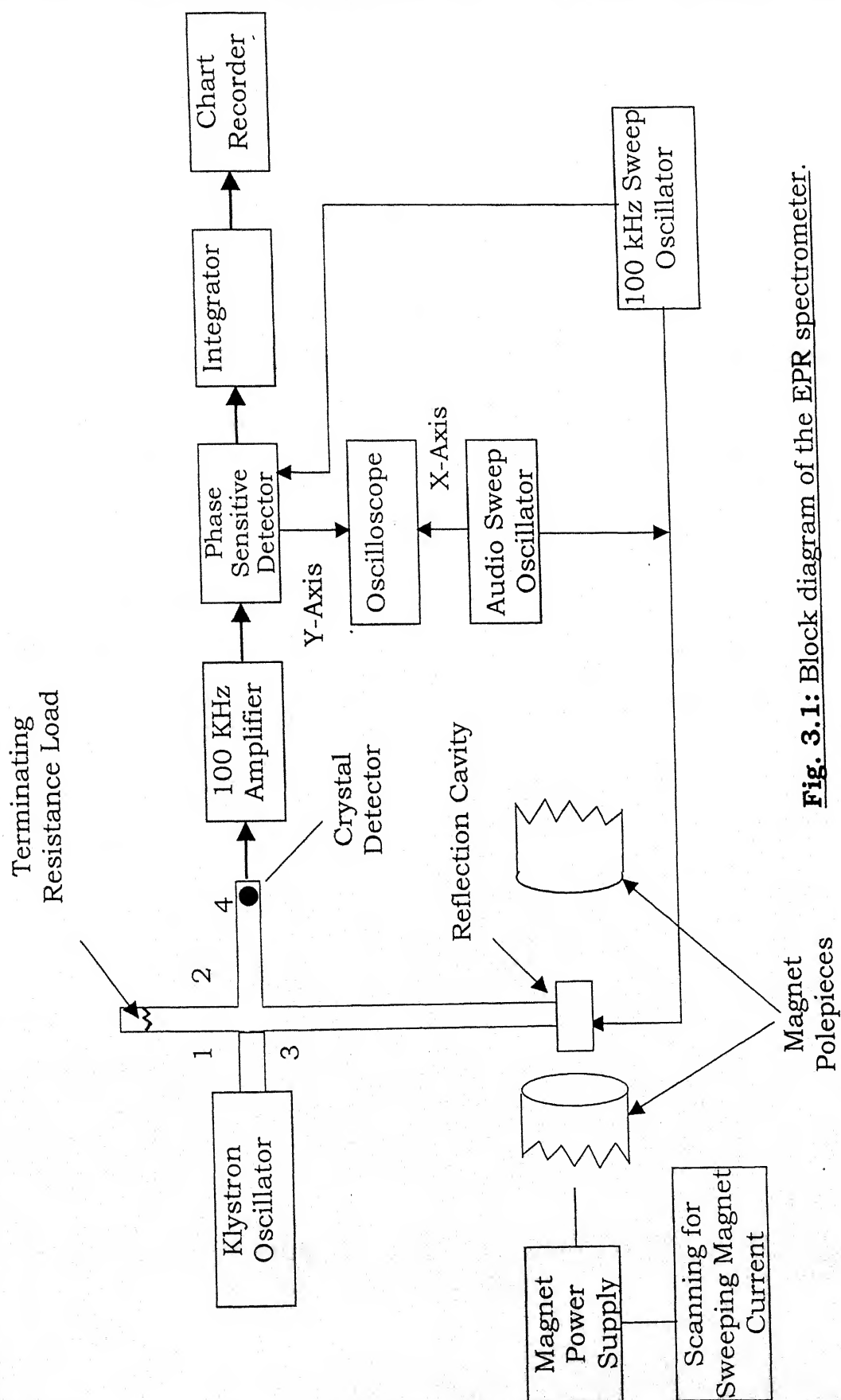


Fig. 3.1: Block diagram of the EPR spectrometer.

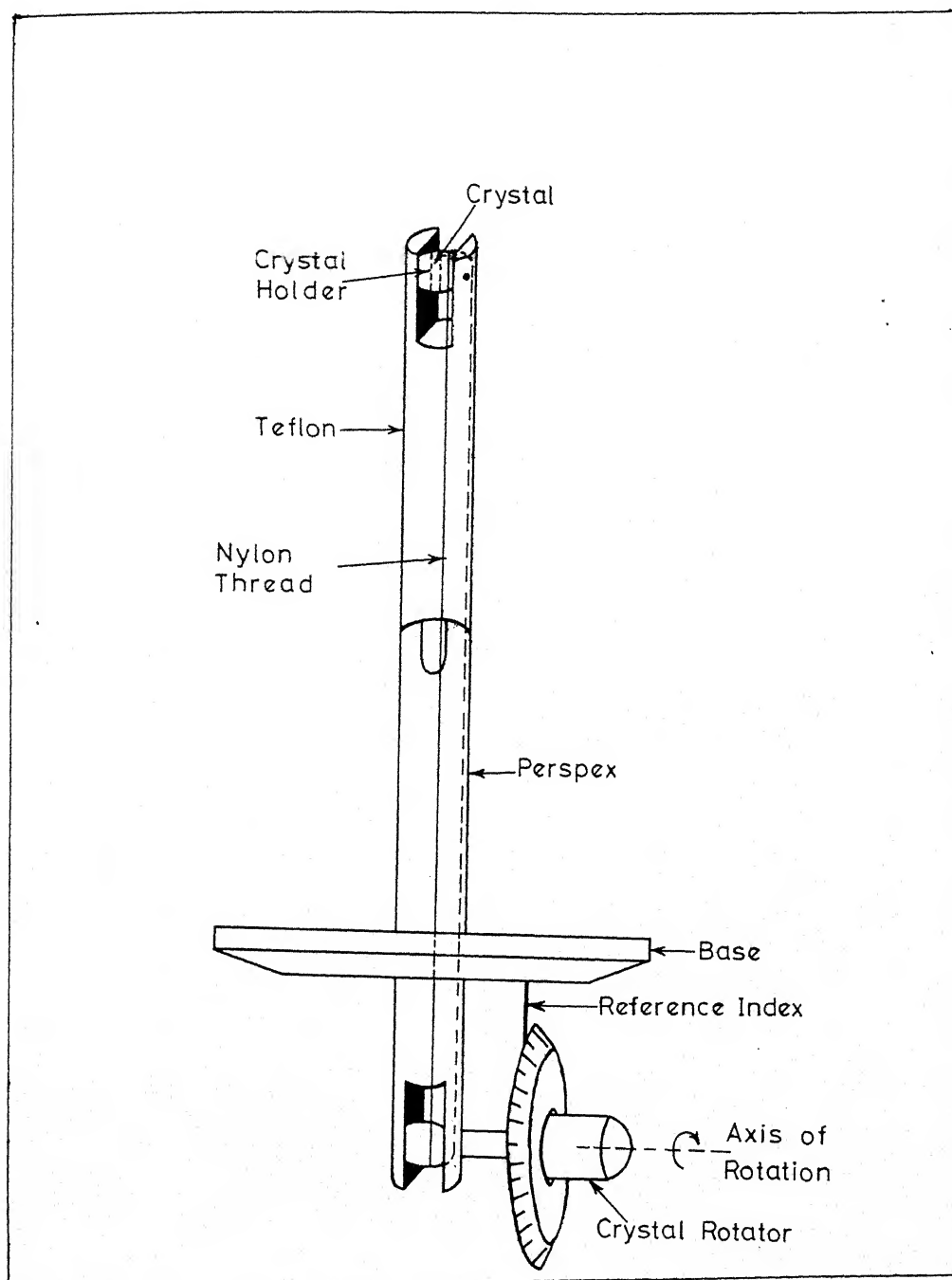
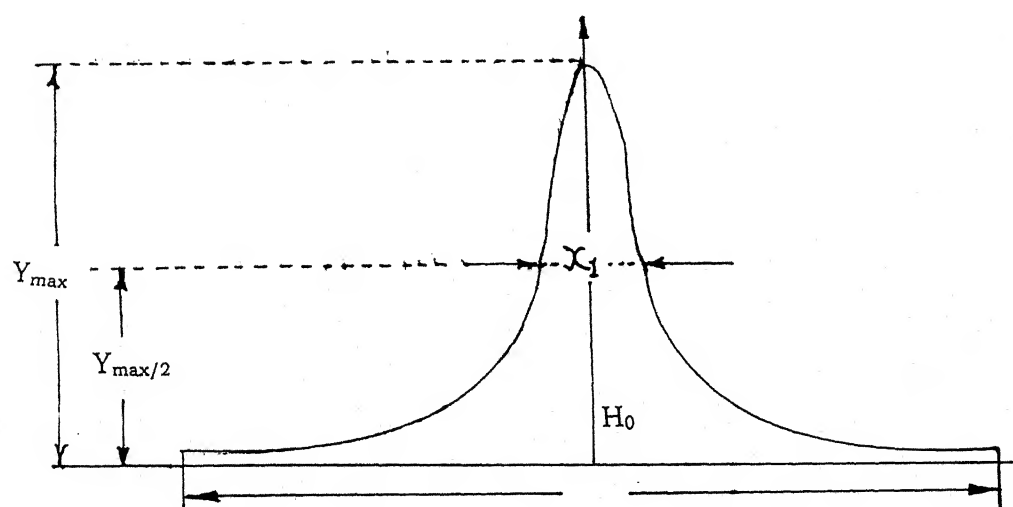
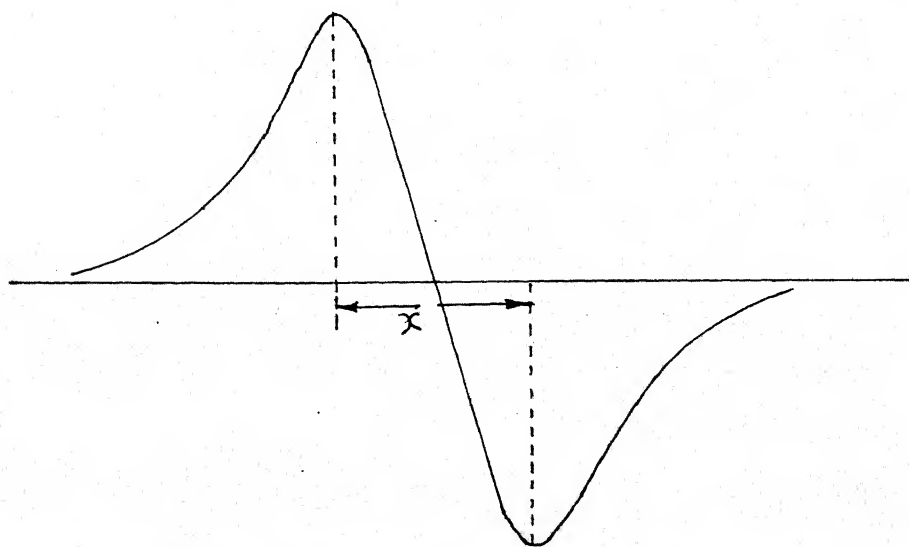


Fig. 3.2: Device to rotate the single crystal inside the cavity about a horizontal axis.



(a) Full width at half power points $\Delta H_{1/2} = 2H_0 X_1/N_2$



(b) Full width at Maximum slope points $\Delta H_{pp} = X$ in oersteds

Fig. 3.3 Method of line width evaluation.

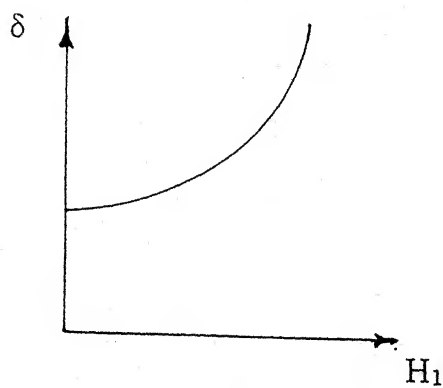


Fig. 3.4 Variation of δ with R.F. Magnetic Field H_1 .

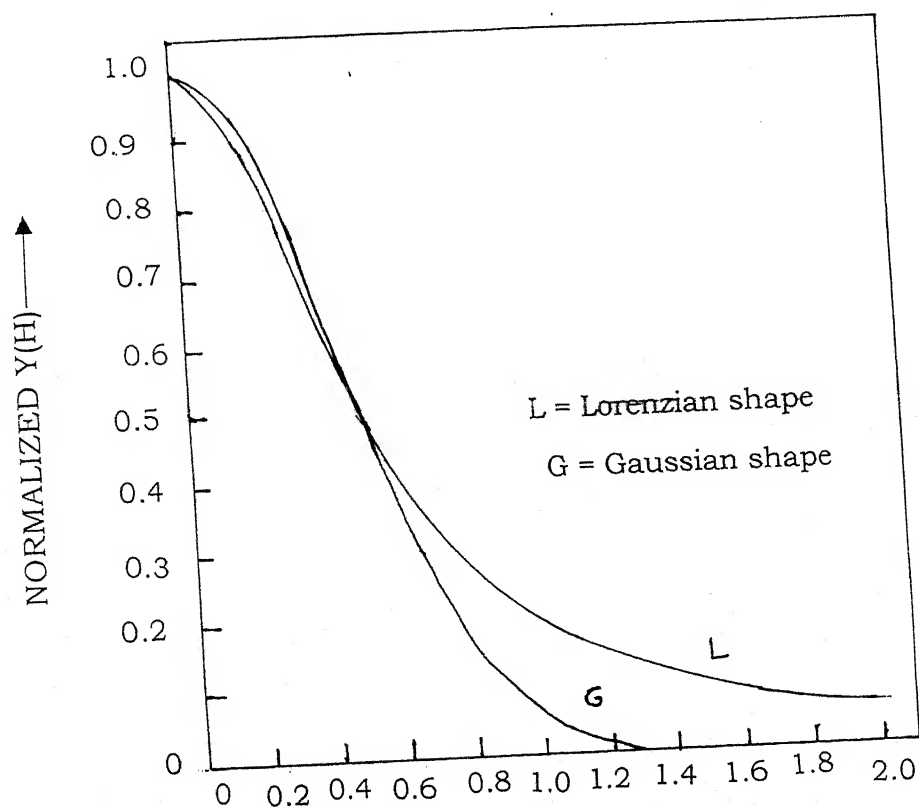


Fig. 3.5 (a) Lorentzian and Gaussian absorption curves with the same linewidth at half power points.

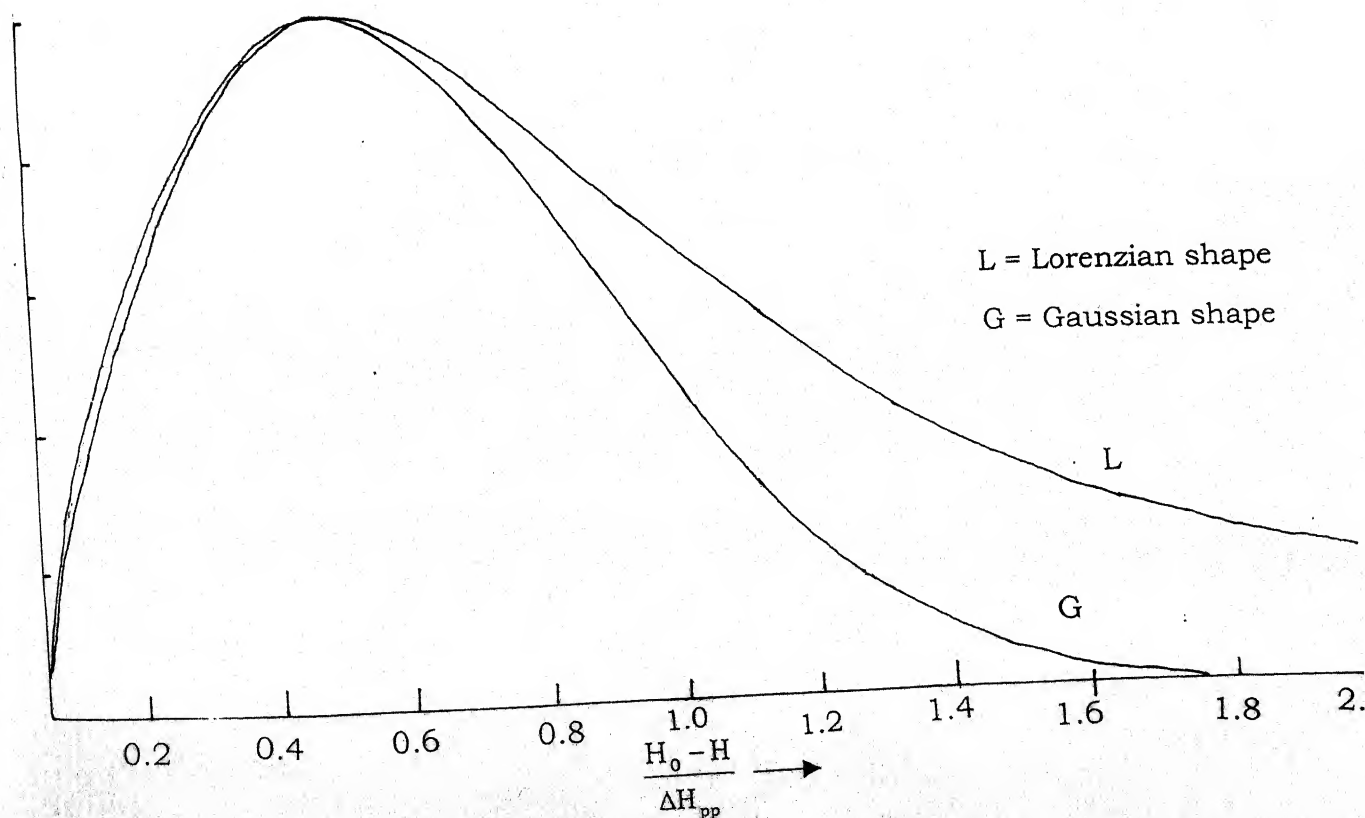


Fig. 3.5 (b) Lorentzian and Gaussian absorption first derivative curves with the same peak to peak line width.

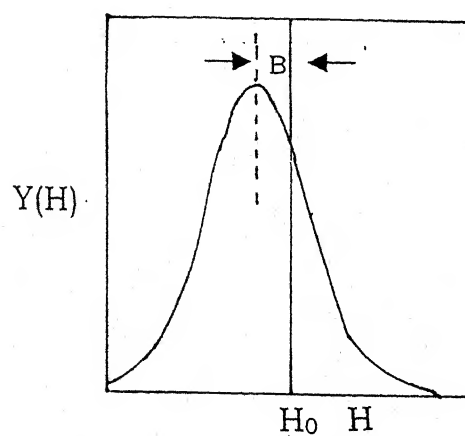


Fig. 3.6(a) Correction factor B that results from an improper choice of the resonant field H_0 .

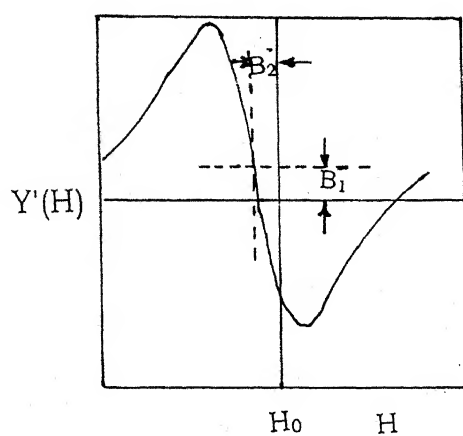


Fig. 3.6 (b) The derivative line for an improper choice of base line and resonant field H_0 .

REFERENCES

1. C.H. Townes and J. Turkevich, Phys. Rev. **77**, 148 (1950).
2. C. Kikuchi and V.W. Cohen, Phys. Rev., **93**, 394, (1954).
3. R.L. Driscoll and P.L. Bender, Phys. Rev. Letters, **1**, 413 (1958).
4. B. Venktaraman, B.G. Segal and G.K. Frenkel, J. Chem. Phys. **30**, 1006 (1959).
5. F. Bloch, Phys. Rev., **70**, 460 (1946).
6. E.R. Andrew, "**Nuclear Magnetic Resonance**", Chapter III, Cambridge University Press, 1955.
7. J.H. Van Vleck, Phys. Rev. **74**, 1168 (1948).
8. B. Venkataraman, Ph.D. Thesis, Faculty of Pure Science, Columbia University, U.S.A., (1995).
9. E. De. Wolf, K. Verhandi, Ulaamse, Acad. Wetensch, **55**, 1-96 (1957).

CHAPTER – 4

ELECTRON PARAMAGNETIC RESONANCE OF Cu^{2+} ION IN HEXAIMIDOZOLE CADMIUM NITRATE

4.1 INTRODUCTION

The doubly degenerate ground state 2e_g of $\text{Cu}^{2+}(3d^9)$ is usually apt to couple with the lattice vibrations of appropriate symmetry, which results in the splitting of the ground state. Experimentally the EPR spectrum is found to be extremely temperature dependent in such systems. At high temperatures the spectrum is almost isotropic, showing small variations in the g and A values. On lowering the temperature the spectrum becomes anisotropic after a certain temperature often referred to as the transition temperature and marked variation in g and A values is observed. This phenomenon has been explained on the basis of Jahn-Teller effect. The high temperature spectrum corresponds to the thermally averaged low temperature spectrum, whereas the anisotropic spectrum of low temperature corresponds to the three equally probable configurations caused by tetragonal distortions.

4.2 EXPERIMENTAL

Single crystals of Cu^{2+} doped $\text{Cd}(\text{Im})_6(\text{NO}_3)_2$ were prepared (1). To get the appropriate concentration the crystals were grown a number of times with different concentration of the copper salts. Crystals have slight greenish tinge. Density

measurements were used to ascertain the complex. Electronic spectrum of the single crystal was also recorded.

4.3.(i) Room Temperature Spectrum

At 300 °K a single site Cu^{2+} spectrum with resolved hyperfine structure, displaying little anisotropy is observed. The spectrum has a maximum spread along C-axis. All four Cu^{2+} hyperfine lines along this direction have almost same linewidth. In a plane perpendicular to C-axis, the spectrum does not exhibit any anisotropy. Minimum values of g and A are observed perpendicular to C-axis. A marked linewidth dependence on m_I could be observed along this direction. Spectra are presented in Fig. 4.1. g and A values along and perpendicular to the C-axes are given in Table 4.I.

4.3.(ii) Low Temperature spectrum (77°K)

At this temperature, the spectrum has an entirely different character, displaying observable anisotropy. Preliminary studies indicate the presence of non-equivalent sites of Cu^{2+} with resolved hyperfine and ligand hyperfine structures. The powder spectrum was recorded to estimate the

approximate principal g and A values. This spectrum, shown in Fig. 4.2 is characteristic of Cu^{2+} ion in an elongated octahedron environment with axially symmetric g and A tensors. The anisotropic behaviour was first examined in a plane perpendicular to the three-fold axis i.e. C -axis. The presence of non-equivalent sites and resolved superhyperfine structure were the important features. The spectra were found to display a 60° periodicity. Next the anisotropic behaviour was examined in $(11\bar{2}0)$ plane. The spectrum along C -axis is shown in Fig 4.3. Along this direction all sites are equivalent. As the magnetic field is rotated away from C -axis, one of the sites starts separating towards low field, showing a turning point at about $50^\circ \pm 2^\circ$ from C -axis. This spectrum is also presented in Fig. 4.3. This is assigned as the principal direction labeled as Z -axis. The g and A values are directly calculated from this direction which are consistent with the g and A values measured from the powder spectrum. The superhyperfine lines are not very intense. Only 6 components on $m_I = 3/2$ and 5 components on $m_I = -1/2$ could be identified. The behaviour of the spectra was not found to be symmetrical about C -axis. Along intermediate directions, the spectra are quite complex, however, three distinct non-equivalent sites could be observed along 80° (Ref. Fig. 4.4). g_\perp and A_\perp values were calculated from the 90° to z -axis spectrum.

4.3.(iii) Variable temperature study:

To estimate the transition temperature and the nature of relaxation process, variable temperature experiments were performed along C-axis and on powder sample. The latter did not give much information. The spectra were recorded in the temperature range 275 $^{\circ}\text{K}$ TO 85 $^{\circ}\text{K}$ along C-axis. These are presented in Fig. 4.5 and 4.6. As the temperature is increased from 85 $^{\circ}\text{K}$, the intensity of the hyperfine lines reduces sharply and at about 110 $^{\circ}\text{K}$ the intensity of the low temperature spectrum becomes vanishingly small. However, the superhyperfine lines become more pronounced and can be seen on the diminishing hyperfine lines even upto 200 $^{\circ}\text{K}$. From 120 $^{\circ}\text{K}$ and above, a new spectrum seems to emerge, which becomes very clear about 133 $^{\circ}\text{K}$. The central part of the spectrum, corresponding to the hyperfine lines $m = \pm 1/2$ is weaker than the outlying hyperfine components corresponding to $m=3/2$. This is the spectrum which persists upto room temperature, but all the lines except the highest field line has the same intensity. The g value is found to be higher and A value smaller than the low temperature spectrum. The superhyperfine lines are clearly observed in the temperature range 145 $^{\circ}\text{K}$ to 515 $^{\circ}\text{K}$ and then slowly disappears. A careful examination shows that there is a variation in the magnitude of ligand hyperfine constant with temperature. However, a

detailed variable temperature experiment needs to be performed to ascertain this because the change in magnitude is small and this variation may have very interesting repercussions.

4.4 Summary of the Results

The observed behaviour of the EPR spectra of $\text{Cu}^{2+}:\text{CdIm}_6(\text{NO}_3)_2$ are summarized below:-

1. The high temperature spectrum corresponds to a single site of Cu^{2+} . It shows a small but observable anisotropy with a maximum g value C-axis and minimum along a direction perpendicular to C-axis.
2. The low temperature spectrum corresponds to three non-equivalent tetragonally elongated Cu^{2+} sites. The angle between Z-axis and C-axis is 50° .
3. The transition from high temperature to low temperature spectrum takes place around 115°K .

The temperature dependence of the spectra is attributed to the dynamic-static Jahn-Teller effect of the trigonal Cu site(2). The theory of the Jahn-Teller effect which supports the above behaviour is described in the following section.

4.5 JAHN-TELLER EFFECT IN Cu^{2+}

The electronic configuration of Cu^{2+} is $(1s^2 2s^2 2p^6 3s^2 3p^6) 3d^9$ and the ground state is a doublet D, which has 5-fold orbital degeneracy. In octahedral ligand field, the 2D splits into orbital doublet e_g and a triplet t_{2g} separated by a cubic field of $10D_q(3)$. The e_g doublet is not split by a trigonal field. t_{2g} splits into a singlet $|0\rangle$ and a doublet $|\pm 1\rangle$. For Cu^{2+} in octahedral symmetry e_g lies below t_{2g} . According to Jahn-Teller theorem (4), if a system has an orbital electronic degeneracy, where the nuclei are in symmetric configuration, there exists at least one asymmetric displacement of the nuclei which removes this degeneracy in the ground state. In the case of e_g ground state for the octahedral complex, Van Vleck(5) argued that such a Jahn-Teller distortion occurs via the linear coupling of the e_g^{vib} modes of vibrations of the octahedron to the electronic ground state. These two modes are denoted as Q_θ and Q_ϵ and can be expressed in terms of the displacements of the ligands as shown in Fig. 4.7 (6). Thus

$$\begin{aligned} Q_\theta &= \frac{1}{12} [2(Z_3 - Z_6) - (x_1 - x_4) - (y_2 - y_5)] \\ Q_\epsilon &= [(x_1 - x_4) - (y_2 - y_5)] \end{aligned} \quad (4.5.1)$$

The Q_θ coordinate represents tetragonal distortion of the octahedron lowering the symmetry from O_h to D_{4h} . The $H_{J,T}$ for

linear coupling can be written in the sub surface spanned by $|\theta\rangle$ and $|\epsilon\rangle$ (7) as

$$H_{J.T.} = \frac{1}{2\mu} (P_\theta^2 + P_\epsilon^2) U + \frac{1}{2} \mu \omega^2 (Q_\theta^2 + Q_\epsilon^2) U_1 + V(Q_\theta U_\theta + Q_\epsilon U_\epsilon) \quad (4.5.2)$$

Where U_i are the 2×2 matrices

$$U_1 = \begin{bmatrix} 1 & 0 \\ 0 & 1 \end{bmatrix}; U_\theta = \begin{bmatrix} -1 & 0 \\ 0 & 1 \end{bmatrix}; U_\epsilon = \begin{bmatrix} 0 & 1 \\ 1 & 0 \end{bmatrix}$$

such that

$$\langle \theta | -U_\theta | \theta \rangle = \langle \epsilon | U_\epsilon | \epsilon \rangle = 1$$

and

(4.5.3)

$$\langle \theta | U_\theta | \theta \rangle = -1 \text{ etc.}$$

where μ is the mass of the ligands and ω the frequency of the e_g vibrations. Above equation represents effective Hamiltonian for the static Jahn-Teller effect with the static linear Jahn-Teller couplings. V is the Jahn Teller coupling constant. If the kinetic energy is small compared to the potential energy term, one can diagonalise the Hamiltonian using products of eigen functions of nuclear vibrations and linear combination of the electronic states (Born-Oppenheimer approximations). The associated energy eigen values as function of Q 's then provide energy surfaces on which one can

find absolute minima corresponding to the stable configurations. Using the substitutions.

$$\left. \begin{aligned} Q_\theta &= \rho \cos \theta \\ Q_\epsilon &= \rho \sin \theta \end{aligned} \right\} \quad (4.5.4)$$

We find eigen states of $H_{J.T.}$ as

$$\left. \begin{aligned} \psi_- &= \cos(\phi/2) |\theta\rangle - \sin(\phi/2) |\epsilon\rangle \\ \psi_+ &= \cos(\phi/2) |\epsilon\rangle + \sin(\phi/2) |\theta\rangle \end{aligned} \right\} \quad (4.5.5)$$

The energies corresponding to these states are

$$E_\pm = E_0 + V_p + \frac{1}{2} \mu \omega^2 \rho^2 \quad (4.5.6)$$

The energy surfaces are plotted in Fig. 4.7, where the configuration of minimum energy on the lower surface is all the points on the circle with the radius

$$\rho = |v| / \mu \omega^2 \quad (4.5.7)$$

And the corresponding energy of stabilization is

$$W_{J.T.} = E_0 - E_- = \frac{1}{2} \mu \omega^2 \rho_0^2 = \frac{V^2}{2\mu \omega^2} \quad (4.5.8)$$

It can be seen that this energy is independent of θ so that the energy surfaces have rotational symmetry about the origin. This would mean that there are infinite number of equivalent configuration of minimum energy.

Higher order warping terms in the distortions considered by Opick and Pryce (8) and Liehr et al (9) remove the rotational symmetry in the following manner.

$$H_{warp} = V_3 \rho^3 \cos(3\phi) U_1 + V_2 + \rho^2 (-U_0 \cos^2 \phi + U_e \sin 2\phi) \quad (4.5.9)$$

The energy eigen values of the total Hamiltonian are

$$E_{\pm} = E_0 + \frac{1}{2} \mu \omega^2 \rho^2 + V_3 \rho^2 \cos \phi \pm [V^2 \rho^2 + V_2^2 \rho^4 - 2VV_2 \rho^3 \cos 3\phi]^{\frac{1}{2}} \quad (4.5.10)$$

The bottom of the trough in the lower energy surface is warped with a period of $2\pi/3$ in θ . Hence there are three configurations of stable equilibrium corresponding to $\phi = 0, 2\pi/3, 4\pi/3$ etc. with energies

$$E_{\pm} = E_0 + \frac{1}{2} \mu \omega^2 \rho^2 \pm V_0 \mp V_2 \rho^2 + V_3 \rho^3 \quad (4.5.11)$$

If $\phi = \pi/3, 3\pi/3, 5\pi/3$ correspond to the energy

$$E_{\pm} = E_0 + \frac{1}{2} \mu \omega^2 \rho_0^2 + V_0 \pm V_2 \rho^2 - V_3 \rho^3 \quad (4.5.12)$$

The energies corresponding to Eq. (4.5.9) will be absolute minima i.e. $V_2 \ll V_3$ and $V_3 < 0$. The height of the barrier will be $\langle 2V_3 \rho^3 \rangle|_{\rho=\rho_0}$ the ground state of these minima will be

$$\Psi_+ |_{\theta=0} = | \varepsilon \rangle \text{ if } V < 0 \text{ and } \Psi_- |_{\phi=0} = | \theta \rangle$$

If $V > 0$, characterizing the elongation or contraction of the octahedron.

The three energy minima will have identical energies. The angular cross section of the potential energy surface is shown in Fig. 4.7.

The distortions corresponding to these minima can be obtained by expressing normal coordinates Q_e and Q_θ in terms of the axial distortions of the octahedral complex (XY_6)

$$X = X_1 - X_4, Y = Y_2 - Y_5, Z = Z_3 - Z_6$$

With the condition $X + Y + Z = 0$, then

$$\left. \begin{aligned} X &= (Q_e) - Q_\theta / \sqrt{3} \\ Y &= -Q_e + Q_\theta / \sqrt{3} \\ Z &= 2Q_\theta / \sqrt{3} \end{aligned} \right\} \quad (4.5.13)$$

If we choose $Q_e = \rho \sin \phi$, $Q_\theta = \rho \cos \phi$ then above equation can be written as

$$\begin{aligned} Z &= \frac{2\rho}{\sqrt{3}} \cos \phi; \\ X &= (2\rho / \sqrt{3}) \cos (\phi - 2\pi / 3); Y = (2\rho / \sqrt{3}) \cos (\phi + 2\pi / 3) \end{aligned} \quad (4.5.14)$$

We can note that the cyclic permutations $X \rightarrow Y \rightarrow Z \rightarrow X$ can be described by successive changes of $2\pi/3$ in angle ϕ . That gives the geometrical interpretation of a rotation through $2\pi/3$ around the three-fold axis $[111]$, for a given value of ρ , $\phi = 0$ corresponds to an elongation according to Eq. (4.5.14) along Z-axis, $\phi = 2\pi/3$ along X-axis and $\phi = -2\pi/3$ along Y - axis whereas values of $\phi = \pi$, $2\pi/3 + \pi$ and $\pi - 2\pi/3$ will correspond

to the compressions of the octahedron along the same axes. V_3 is generally found to be negative for Cu^{2+} so that stable configurations are tetragonal elongations and the ground state is $|\varepsilon\rangle = \sqrt{3}(x^2 - y^2)$.

4.6 Spin – Hamiltonian for Cu^{2+}

The total spin-Hamiltonian for the axially symmetric g and A tensors is (actual expressions for g and A in the present case are available in Ref. (10):

$$H_{av} = g H_z S_z + g_{\perp} (S_x I_x + S_y I_y) + A S_z I_z + A_{\perp} (S_x I_x + S_y I_y) \quad (4.6.1)$$

The eigen values of this can be obtained by the standard perturbation methods using $|M, m\rangle$ as basis states where $M = \pm 1/2$, $m = \pm 1/2, \pm 3/2$. The field positions for the allowed transitions corresponding to $\Delta M = \pm 1$, $\Delta m = 0$, when the magnetic field makes an angle θ with the Z -axis are given by

$$H_m = H_0 - A m - \frac{A_{\perp}^2 (A^2 + A_{\perp}^2)}{4g^2 \beta^2 A^2 H_0} [I(I+1) - m^2] - \frac{A^2 - A_{\perp}^2}{8A^2 g^2 \beta^2 H_0} \frac{g g_{\perp}}{g^2} m^2 \sin^2 \theta \quad (4.6.2)$$

where

$$\left. \begin{aligned} g &= \sqrt{g^2 \cos^2 \theta + g_{\perp}^2 \sin^2 \theta} \\ A &= \frac{I}{g_{\beta}} \sqrt{(g^2 A^2 \cos^2 \theta + g_{\perp}^2 A_{\perp}^2 \sin^2 \theta)} \\ H_0 &= \frac{h}{g\beta} \end{aligned} \right\} \dots (4.6.3)$$

(i) Estimation of the spin Hamiltonian parameters:

$g_{||}$, g_{\perp} and $A_{||}$ were calculated directly from the EPR spectra. A_{\perp} was estimated from the perpendicular spectrum and treating this as a parameter. g and A anisotropy curves presented in Fig. 4.8 were plotted using equation (4.5.1). On this curve, g and A values calculated from the intermediate direction spectra in $(11\bar{2}0)$ plane were matched. (The second order correction was applied to g and A values using eqn. (4.6.2). A_{\perp} was slightly adjusted till the curve matched with the experimental values. A_{\perp}^N was calculated directly from Z-axis spectrum. The magnitude is about 10 to 11 Gauss. The spin-Hamiltonian parameters are presented in Table 4.II.

(ii). Calculation of Jahn-Teller energy:

An attempt has been made to estimate the Jahn-Teller energy. The approach adopted here gives an approximately value of the Jahn-Teller energy.

The following expressions are used (11)

$$\Delta g = -2\lambda \left[\frac{\cos^2 \alpha (3 \cos^2 \alpha - 1)}{\Delta_0} + \frac{3 \sin^2 \alpha}{\Delta_0} + \frac{\sin^2 \alpha (3 \cos^2 \alpha + 1)^2}{\Delta_1} \right] \quad (4.6.4a)$$

and

$$\Delta g_{\perp} = -\lambda \left[\frac{\sin^2 \alpha (3 \cos^2 \alpha - 1)^2}{\Delta_0} + \frac{3 \sin^2 \alpha \cos^2 \alpha}{\Delta_0} + \frac{\cos^2 \alpha (3 \sin^2 \alpha - 1)^2 + 1}{\Delta_1} \right] \quad (4.6.4b)$$

The appearance of Δ_0 is to be noted with interest.

The equation will reduce to $\Delta g_z = -\frac{2\lambda}{\Delta}$ and $\Delta g_{\perp} = -\frac{2\lambda}{\Delta}$ if $\alpha = 54.3^\circ$.

Table-4.(ii)

Parameters of $\text{Cu}^{2+} : \text{CdIm}_6 (\text{NO}_3)_2$ at 77°K

S.N	System	$g_{ }$	$A_{ }$ cm^{-1}	g_{\perp}	A_{\perp} cm^{-1}	A_{\perp}^N cm^{-1}	A^N cm^{-1}
1.	$\text{Cu}^{2+} : \text{Cd Im}_6 (\text{NO}_3)_2$	2.307	150	2.067	25	11	14

Δ_0 represents Jahn-Teller energy. The splitting is shown in Fig. 4.9.

If λ , Δ_0 , Δ_1 , g and A values are known, Δ_0 can be calculated.

In the present case, the values of Δ_0 and Δ_1 are found to be 1.45 eV and 1.52 eV (from optical spectrum). The λ term if used has to be weighted properly by the covalency reduction factor. Hence to eliminate this, Δ_0 is calculated from

$\frac{\Delta g}{2 \Delta g_{\perp}}$. Using the experimental values of $g_{\parallel} = 2.307$, $g_{\perp} = 2.067$, $\alpha = 50^{\circ}$, $\Delta_0 = 4800 \text{ cm}^{-1}$ so that $E_{J.T.}(12) = \frac{\Delta_0}{4} = 1200 \text{ cm}^{-1}$.

(iii) Calculation of the activation energy:

If a system undergoes a Jahn-Teller distortion at low temperature, there is always a possibility of a thermally activated orientation from one distorted configuration to the another. This is possible when the system absorbs one or more phonons and makes a real transition to one of the excited states and then decay back to the ground state in one of the any three distorted configurations.

The relaxation time can be expressed through Arrhenius equation (13).

$$\tau = \tau_0 \exp(V_0 / kT) \quad (4.6.5)$$

Where τ is the relaxation time, V_0 is the height of the potential barrier separating different directions of the distortions.

To calculate this parameter, a graph was plotted between line intensity I_p vs. T^{-1} (in $^{\circ}\text{K}$).

The plots are presented in Fig. 4.10.

I_p and T^{-1} were calculated from the spectra obtained at various temperatures. Thus the growth curve of the high

temperature gives the activation energy of 790 cm^{-1} whereas the decay curve plotted from the low temperature spectra gives an activation energy of 700 cm^{-1} (14).

4.7 DISCUSSION

The temperature dependence of the spectra has been interpreted in terms of the dynamic – static Jahn-Teller effect of the trigonal Cu-sites in this system. The three non-equivalent sites observed at low temperature can be understood in terms of the static Jahn-Teller distortions of the Cu^{2+} site. The spin-Hamiltonian parameters are typical for copper in tetragonally elongated geometry. The Jahn-Teller energy has been calculated to be 1200 cm^{-1} , which is a reasonable order of magnitude⁽⁷⁵⁾.

(i). Activation energy:

The effect of thermal activation over the warping barrier resulting in a transition from the static to dynamic Jahn-Teller effect is an important feature and is the most convincing evidence for the occurrence of the Jahn-Teller effect. The activation energy has been calculated to be $700 \pm 50\text{ cm}^{-1}$, which is quite close to the expected value (8).

The activation energy can have the following intuitive interpretation. The dependence of the electronic potential on nuclear coordinates (ρ , θ) can be described in Q_θ and Q_ϵ space by 'Mexican hat'. In addition to this, electronic energy is dependent on θ through so-called warping term $V_3 \rho^3 \cos \phi$. The height of barrier is given by $\langle 2V_3 \rho^3 \rangle \big|_{\rho=\rho_0}$ which will be a measure of activation energy.

Following additional observation may be noted:

1. The high temperature spectrum reaches a peak intensity at about 170°K. Subsequently it decreases with increasing temperature. This may be because of the decrease in spin lattice relaxation time which would tend to broaden the lines.
2. The line-width within the spectra will have dependence on principal quantum number m_l

$$\frac{I}{T_2} \propto \tau_c (\Delta g \beta' H + K m_l)^2 / h^2$$

For the magnetic field parallel to C the term in H is zero. Hence all the lines will have same width.

(ii). High temperature spectrum:

As discussed above the high temperature spectrum can arise because of thermal averaging of the three tetragonal

distortions or population of excited vibronic levels. In cubic field case, both predict the same g value. However in the trigonal field case the motional averaging results in an axial anisotropy of the high temperature spectrum. This can be expressed as (14).

$$\text{Along C-axis, } g' = g \cos^2 \alpha + g_{\perp} \sin^2 \alpha$$

$$\text{Perpendicular to C-axis } g'_{\perp} = \frac{1}{2} (g^2 \sin^2 \alpha + g_{\perp}^2 \cos^2 \alpha + g_{\perp})$$

Where unprimed parameters refer to low temperature values. In our case $\alpha = 500$. The room temperature values compare well with the values calculated from the above formula. Hence the room temperature spectrum arises from the motional averaging of the low temperature spectrum(16-21).

Table 4.I: Room Temperature values

Axis	G	A	Electronic spectrum
C	2.170	59 G	$\Delta E_{xy} = 1.45 \text{ eV}$
$\perp_r \text{ C}$	2.143	50 G	$\Delta E_{xyz} = 1.52 \text{ eV}$

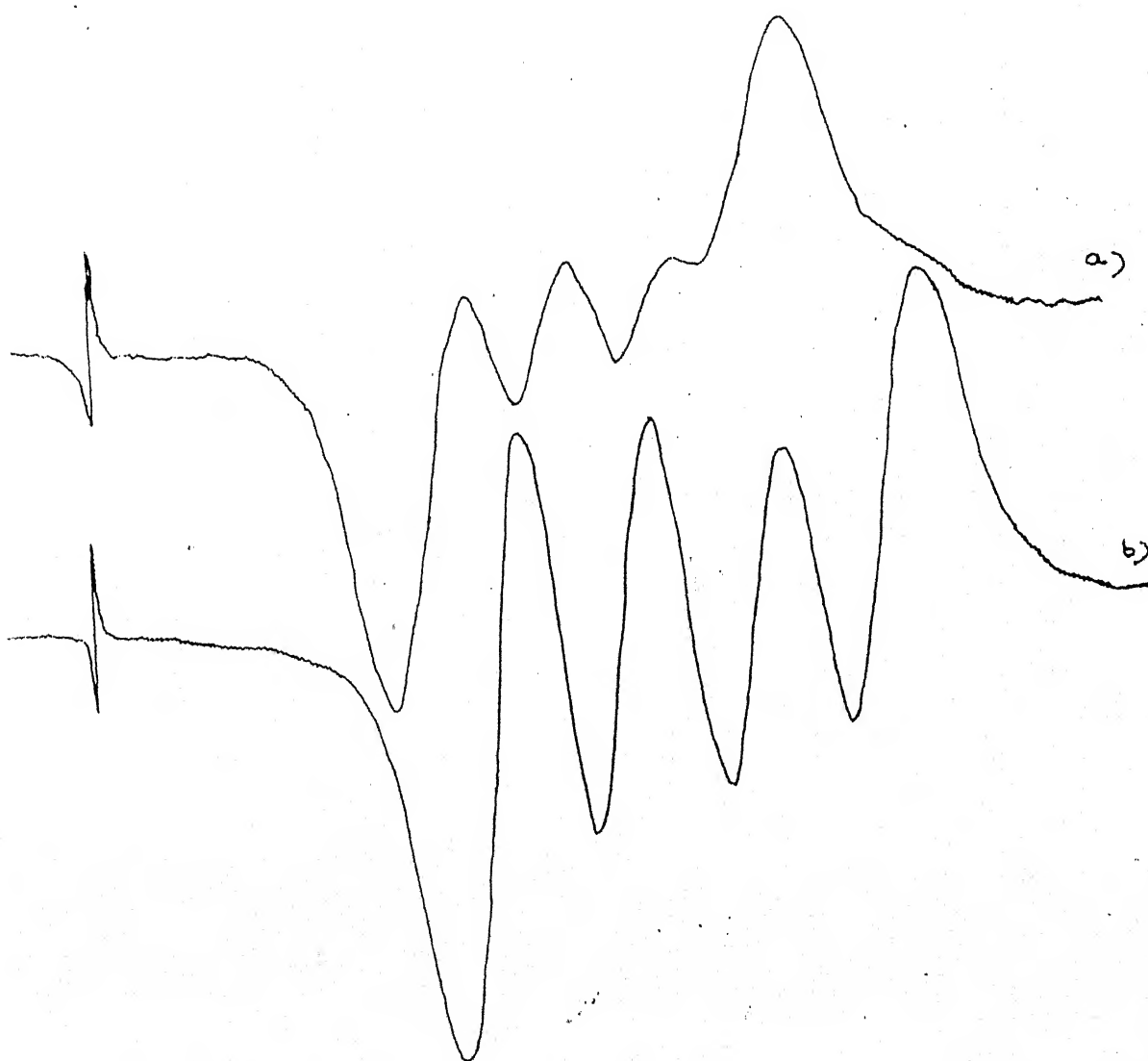


Fig. 4.1: Single crystal EPR spectra of Cu^{2+} : $\text{CdIm}_6(\text{NO}_3)_2$ at 300 °K
(a) $\text{H} \perp \text{c}$ axis.
(b) $\text{H} \parallel \text{c}$ axis.

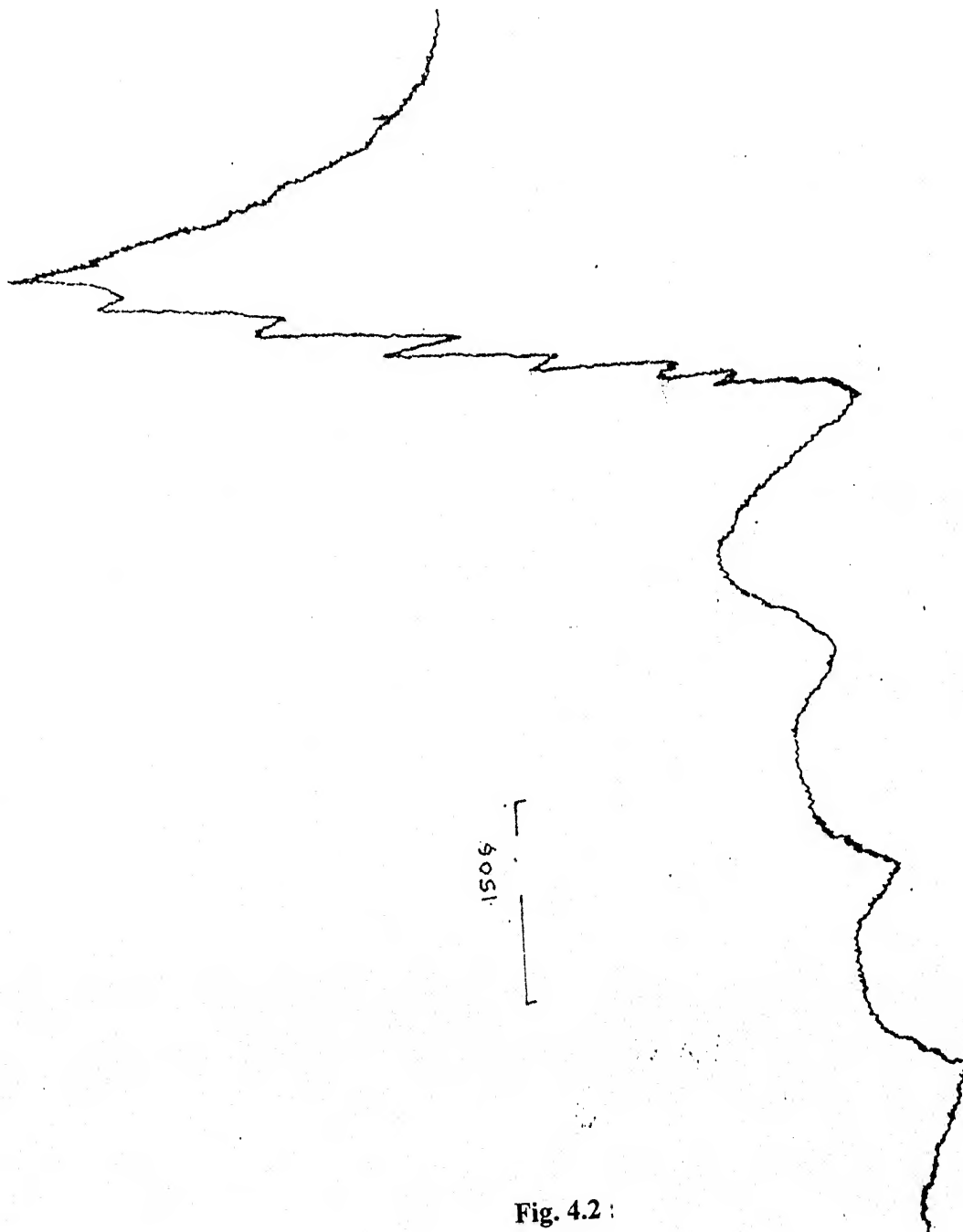


Fig. 4.2 :

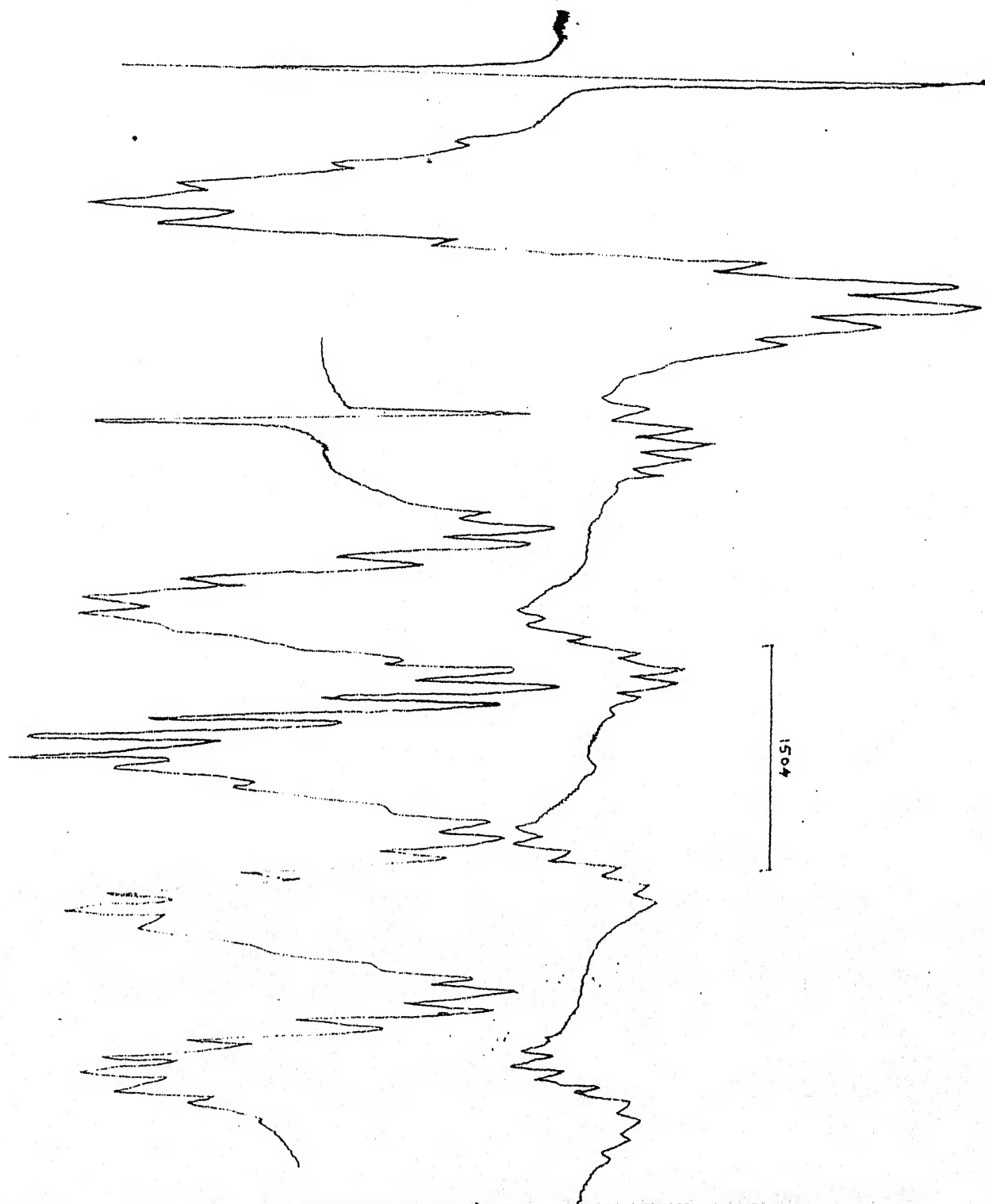


Fig. 4.3: Cu^{2+} : $\text{Cd Im}_6(\text{NO}_3)_2$ EPR spectra at 77°K

(a) $H \parallel c$ axis.

(b) $H \perp c$ axis.

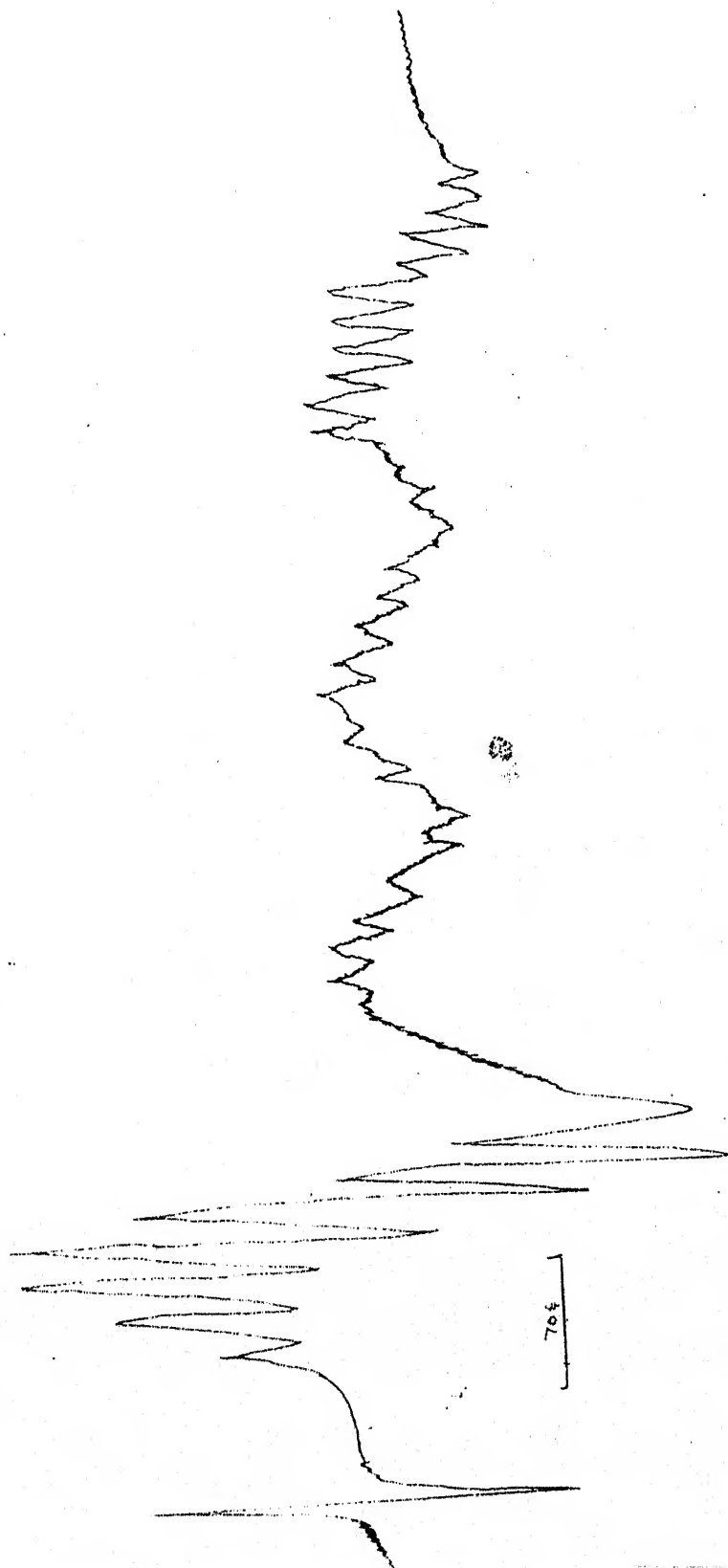
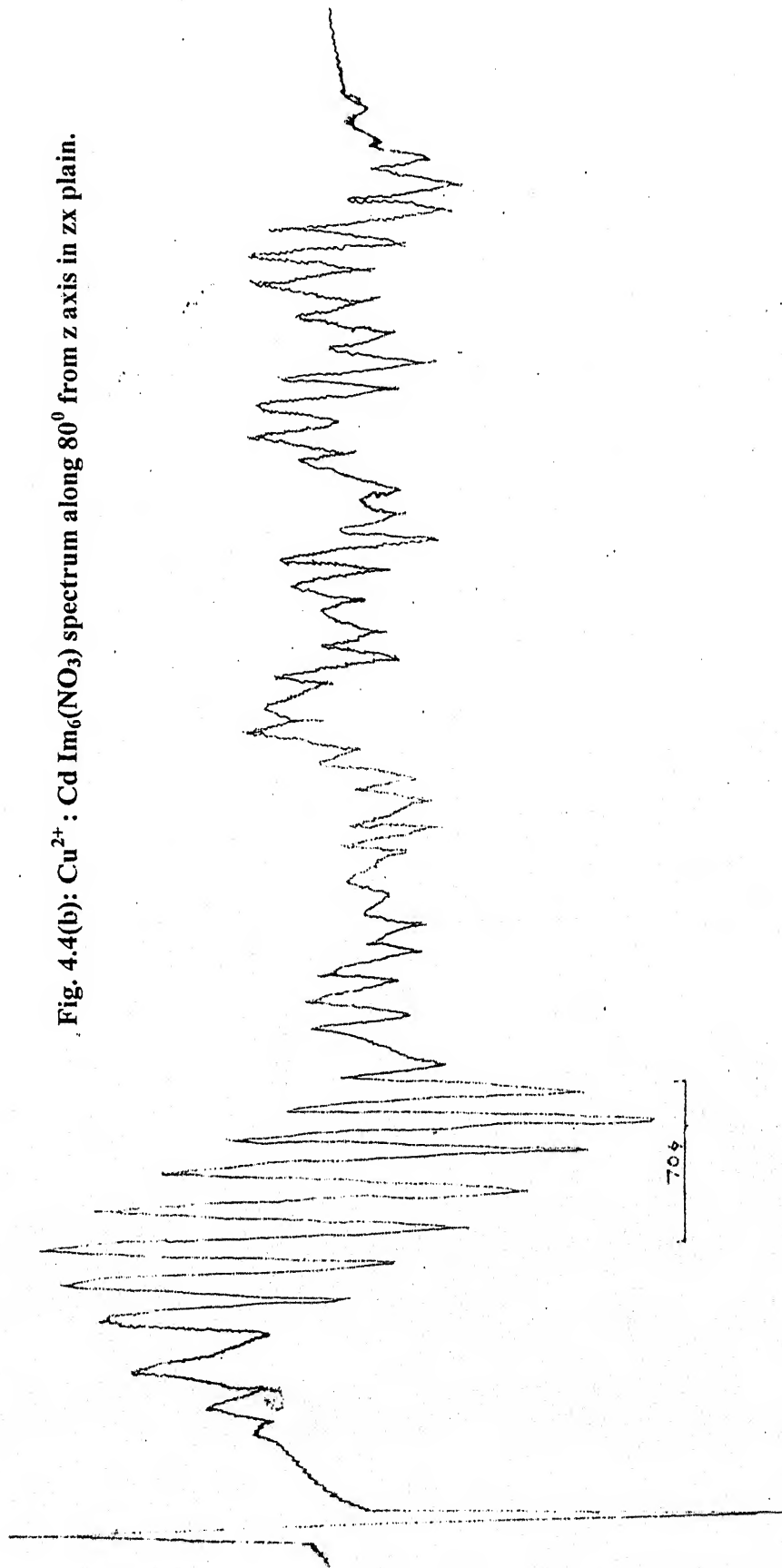


Fig. 4.4(a) : Cu^{2+} : $\text{Cd Im}_6(\text{NO}_3)$ spectra along perpendicular direction to z axis in zx plain.

Fig. 4.4(b): Cu^{2+} : $\text{Cd Im}_6(\text{NO}_3)$ spectrum along z axis in zx plain.



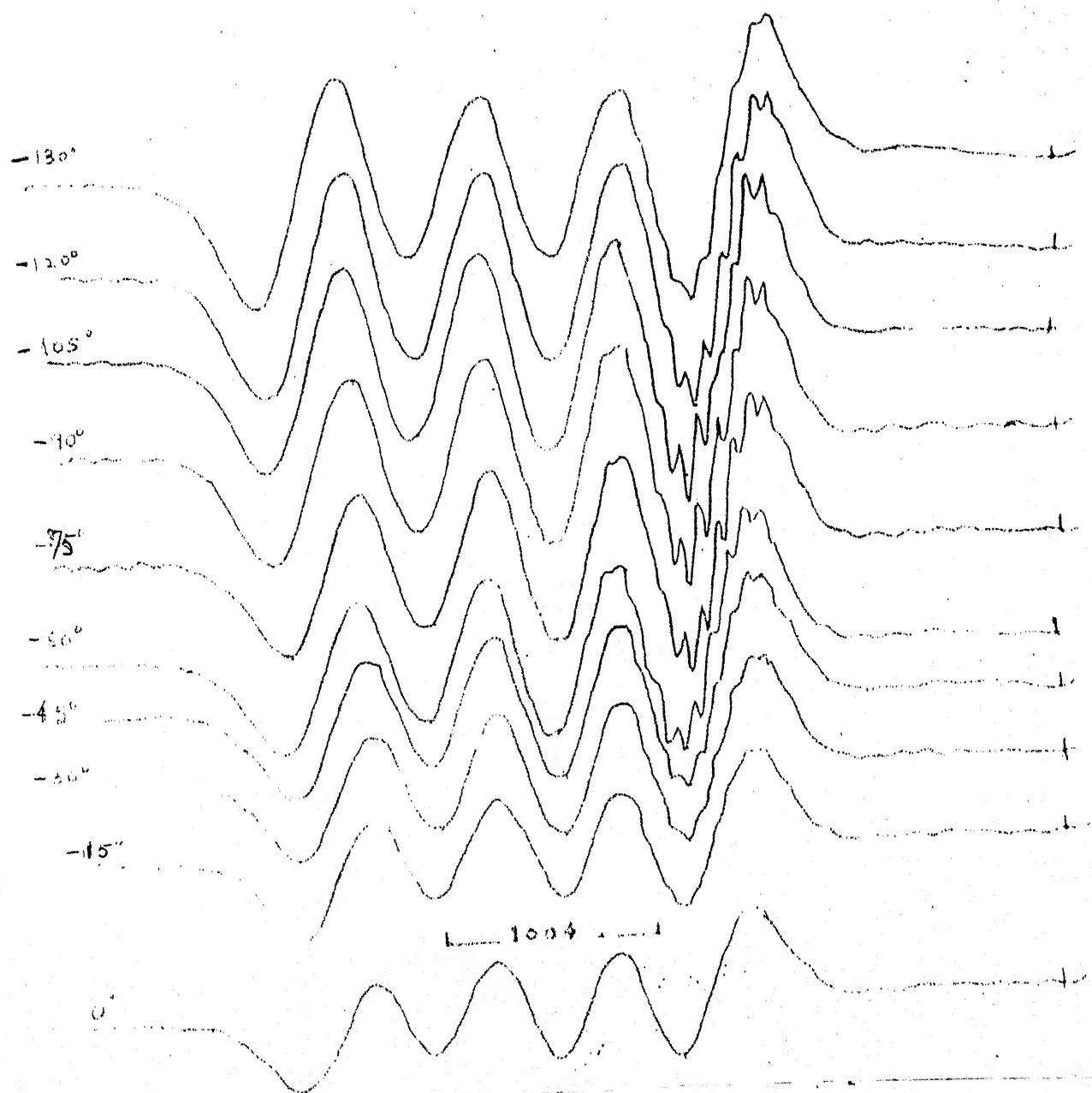
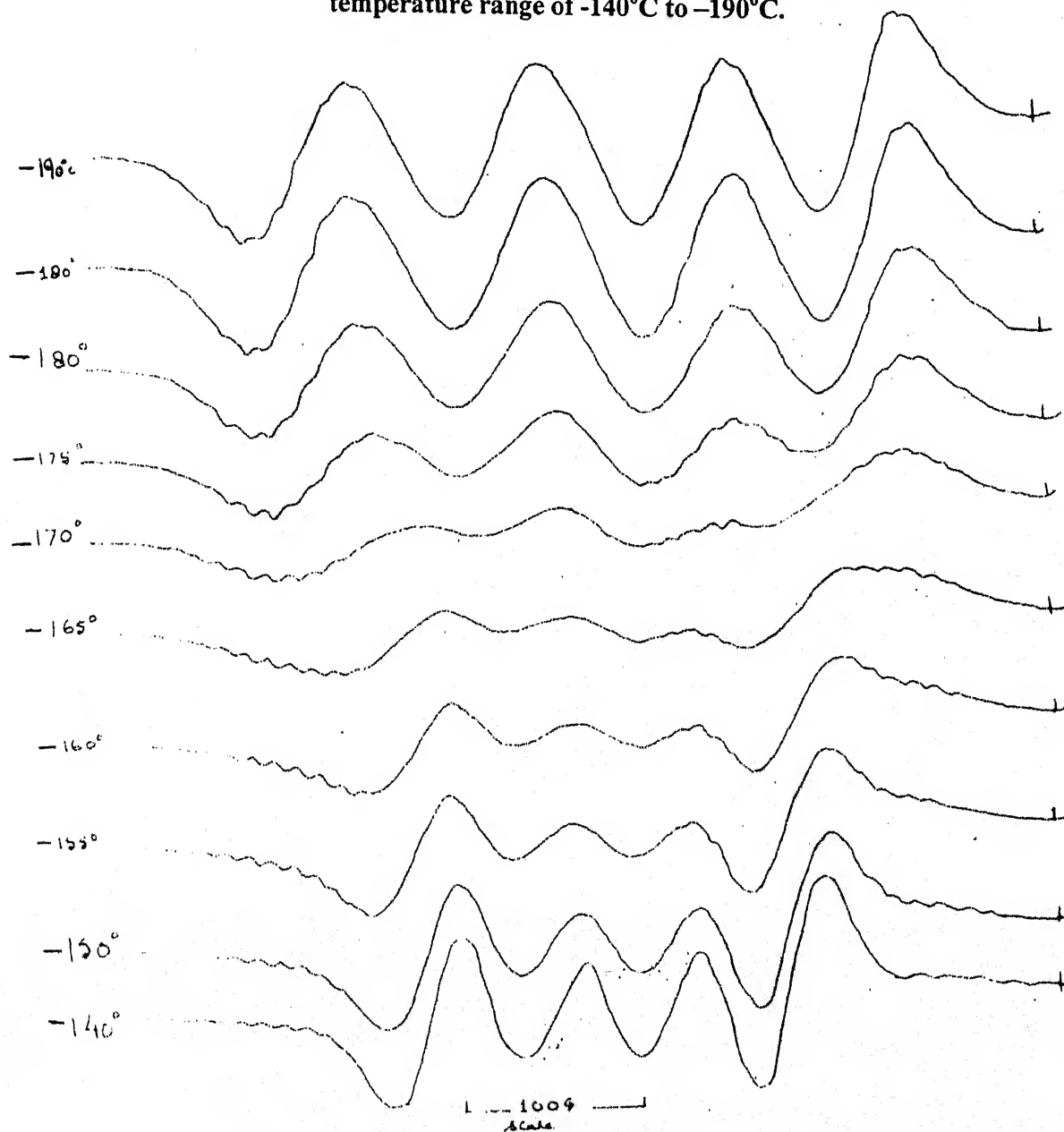


Fig. 4.5: $\text{Cu}^{2+}:\text{CdIm}_6(\text{NO}_3)$ variable temperature experiment along C axis in the temperature range of 0°C to -130°C .

Fig. 4.6: $\text{Cu}^{2+} : \text{Cd Im}_6(\text{NO}_3)$ variable temperature experiment along C axis in the temperature range of -140°C to -190°C .



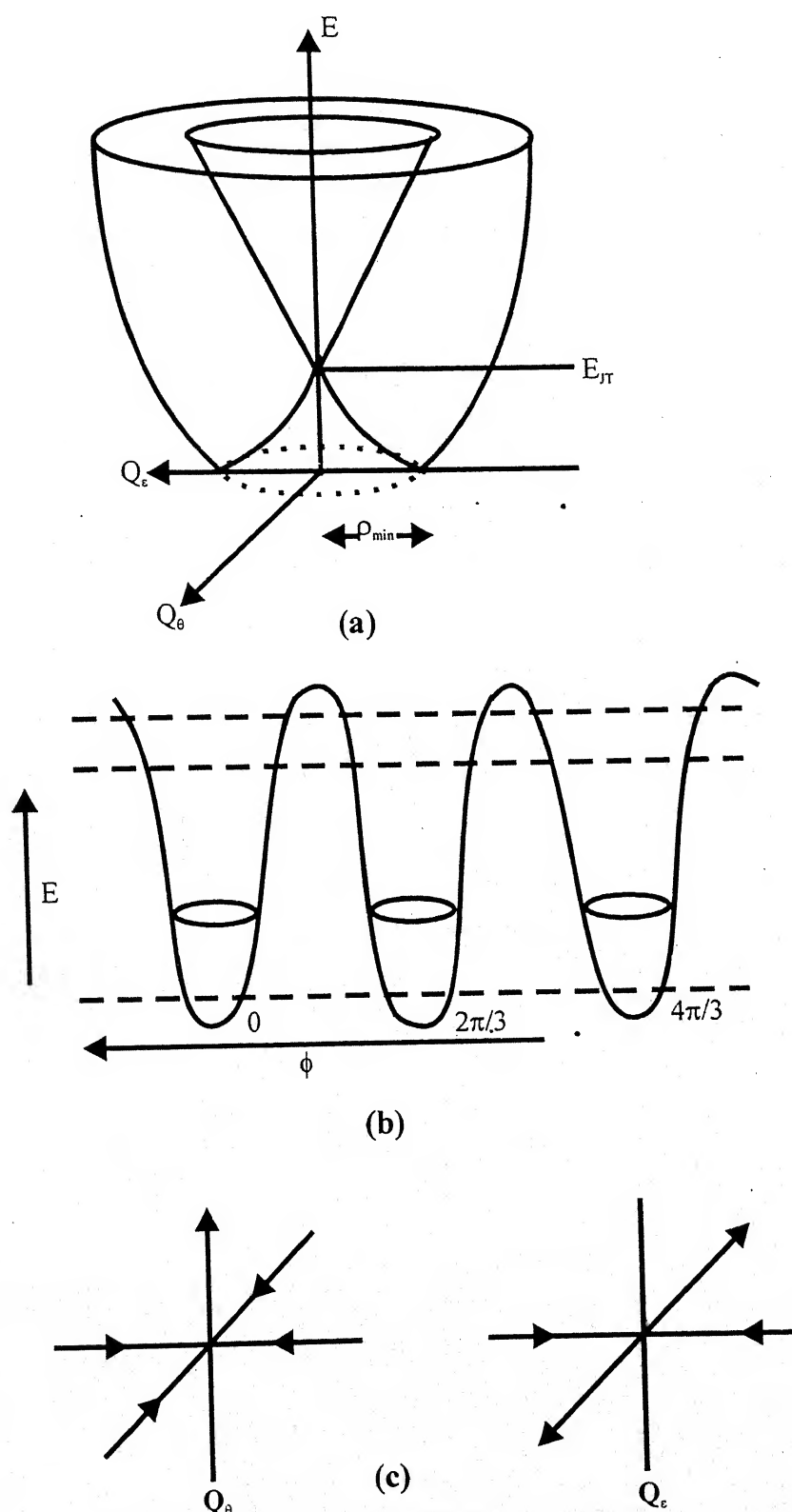


Fig. 4.7

- (a) Potential energy surface for a doubly degenerate state. E_{JT} corresponds to the JT stabilization energy (ρ_{min} has ϕ invariance).
- (b) Inclusion of warping terms removes the degeneracy in ϕ . The results is three minimal energy configurations with identical energy.

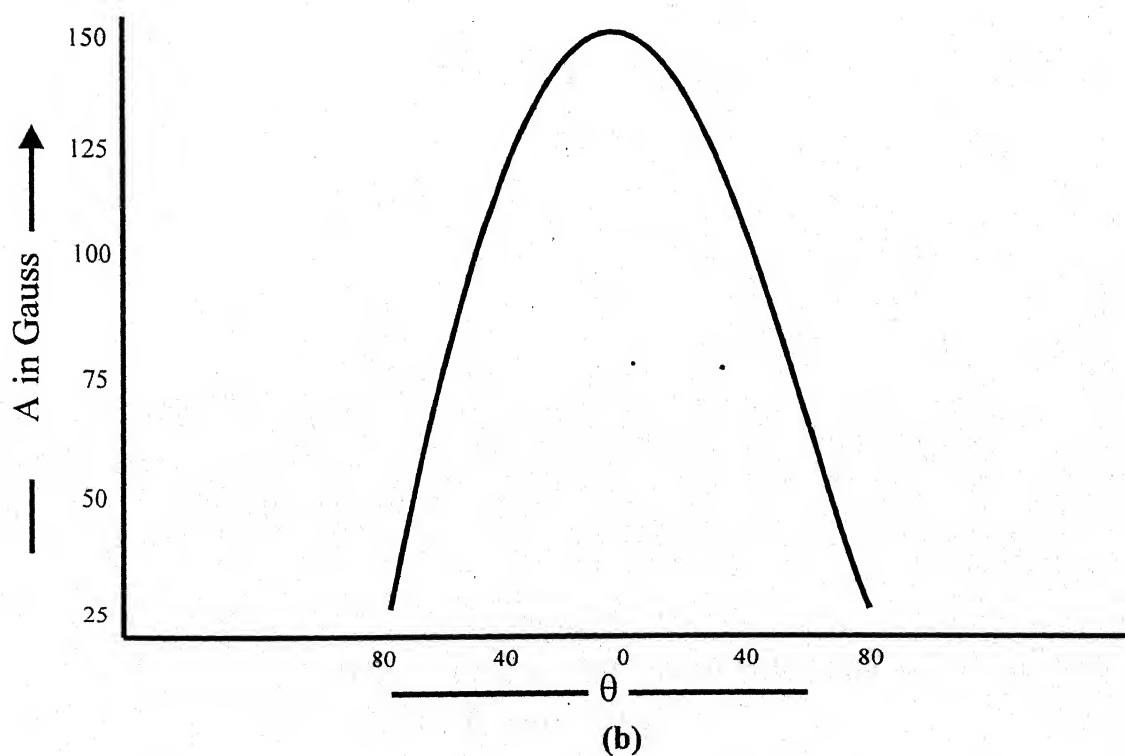
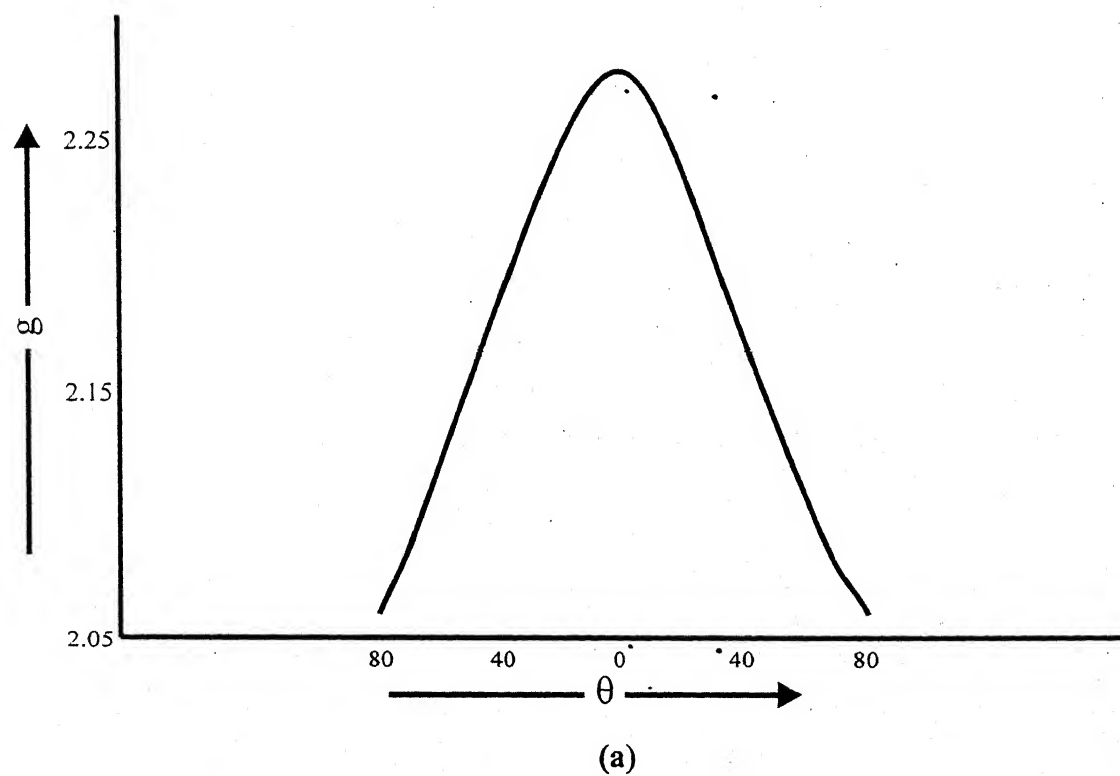


Fig. 4.8

- (a) $\text{Cu}^{2+} : \text{CdIm}_6(\text{NO}_3)_2$ Z-X plane g anisotropy
 (b) $\text{Cu}^{2+} : \text{CdIm}_6(\text{NO}_3)_2$ Z-X plane a anisotropy

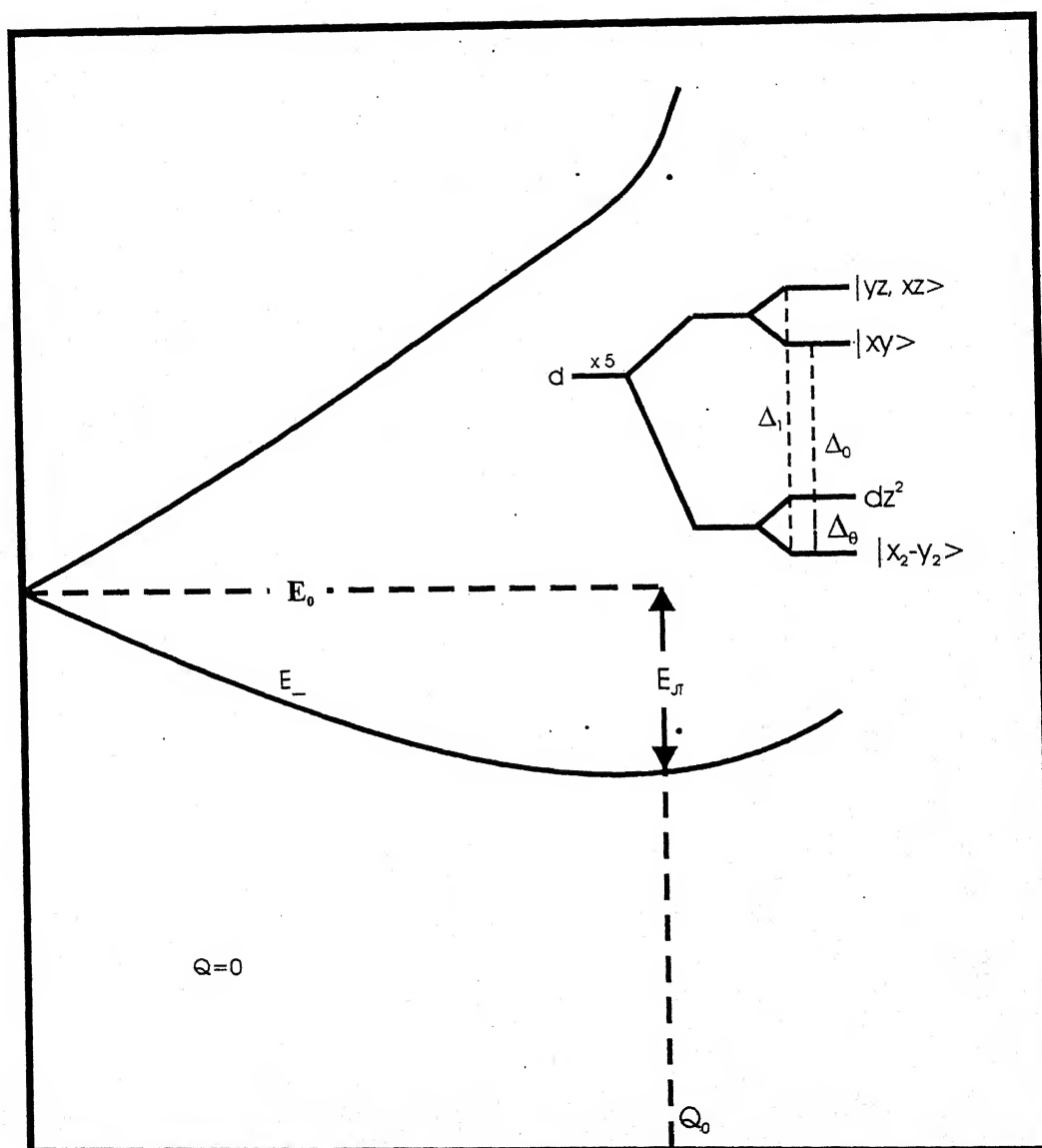


Fig. 4.9

E_0 is the energy of the doubly degenerate state.

E_{JT} is the JT energy and $\Delta_\theta = 4E_{JT}$

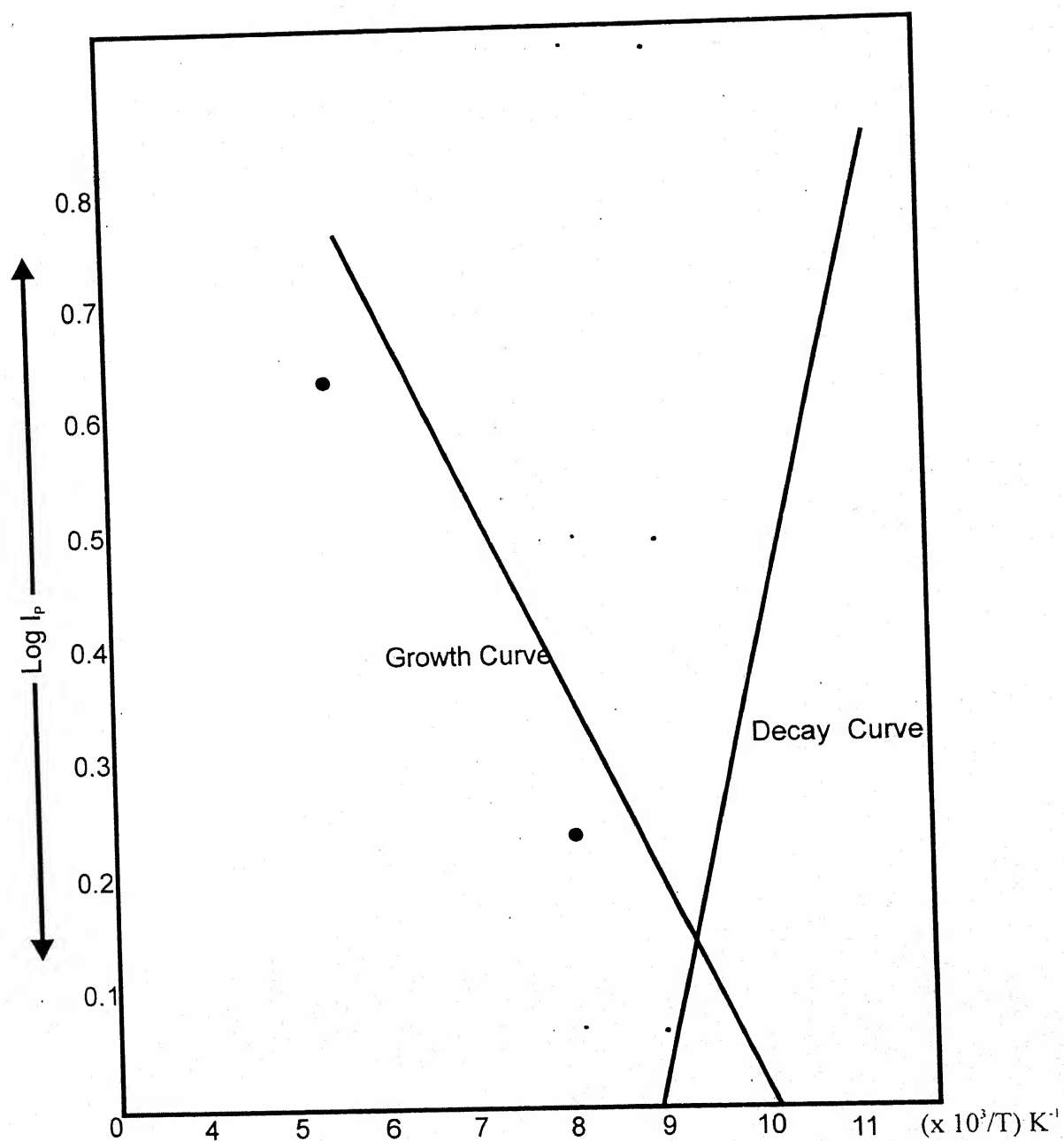
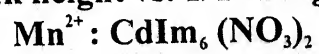


Fig. 4.10

Plot of peak height vs. $1/T$ along $H \parallel c$ axis.



REFERENCE

1. A.D. Mighell and A. Santoro, Acta Cryst. B27 2089 (1975).
2. R.K. Sharma, K.V. Lingam, B.N. Bhattacharya. Abstracted in Nucl. Phys. Solid State Phys. Symp. (India) (1979).
3. A. Abragam and B. Bleaney. Electron Paramagnetic Resonance of Transition Ions. Clarendon Press (1970) pp. 374.
4. S. Gresswind (Ed.), Electron Paramagnetic Resonance, Plenum Press, New York pp. 10 (1972).
5. Van Vleck, J. Chem. Phys., **7** 72 (1939).
6. M.D. Sturge, in solid state Phys., (F. Seitz, D. Tumbell and H. Ehrenreich, ed.), Vol. **20** pp92, Acad. Press, New York (1967).
7. K.K.S. Suvendran, Ph.D. Thesis, IIT, Bombay (1980).
8. V. Opik and M.H.L. Pryce, Proc. Royal Soc. (London), **A238**, 401 (1950).
9. W. Hayes and J. Wilkens, Proc. Royal Soc. (London), **A281**, 341 (1964).
10. A. Abragam and B. Bleaney, Electron Paramagnetic Resonance of Transition Ions, Clarendon Press, P. 175 (1970).
11. F. Hduj and S.M. Quick, Phys. Rev., **B6**, 3169 (1974).

12. R.R. Sharma, T.P. Das and R. Orbach, Phys. Rev. **171**, 378 (1968).
13. M.C.M. O'Brein, Proc. Roy. Soc. (London) **A281**, 323 (1964).
14. F. Hduj, R.G. Wilson, and N.E. Hedgecock, Phys. Rev. **B1** 3609 (1970).
15. R.H. Bercherts and H. Kanzaki, Phys. Rev. Vol.2, 23 (1970).
16. P.R. Levstein, C.A. Steren and A.M. Genaro, Chemical Phys. (Netherland) **120, 3**, 449(1980).
17. J. Goslar and W. Hilczner, Ferroelectrics (UK) **80** 651 (1988).
18. G.C. Rex and S. Sehlick, Polymer (UK) **28** 12, 2134 (1987).
19. K. Madhukar, B. Madhu and B.A. Sastry, J. Phys. Soc. Japan (Japan) **58**, 1, 336 (1989).
20. S.K. Mishra and C. Wang; J. Phys. Condens. Matter. (UK) **1**, 4, 777 (1989).
21. S.N. Rao and Y.P. Reddy, Solid State Communications (USA) **78**, 12, 1025 (1991).

CHAPTER – 5

ELECTRON PARAMAGNETIC RESONANCE OF Mn^{2+} ION IN NICKEL ACETATE TETRAHYDRATE

5.1 INTRODUCTION

The most commonly used dilutants, for reducing the interaction between paramagnetic ions, are diamagnetic ions in magnetically dilute mixed crystals(1). Besides, some paramagnetic ions are also found to act as proper dilutants under certain conditions. Paramagnetic ions whose spin-lattice relaxation time is short at room temperature can be used in place of the diamagnetic ions till high enough temperatures, so that the spin-lattice relaxation time of the diluting ions does not approach the Larmor precession period of the resonating paramagnetic ion (2,3). Besides, paramagnetic ions whose ground state splitting due to the surrounding crystalline field (ZFS) is much larger than the irradiating microwave frequency, can also be used in place of the diluting diamagnetic ions (3). The ions which belong to this class are those with even electrons and hence have no Kramers degeneracy, and Ni^{2+} is a good example in the iron group series. The present chapter deals with the EPR studies of Mn^{2+} doped nickel acetate tetrahydrate $[\text{Ni}(\text{CH}_3\text{COO})_2 \cdot 4\text{H}_2\text{O}]$ at room temperature.

5.2 CRYSTAL STRUCTURE

The crystal structure of $\text{Ni}(\text{CH}_3\text{COO})_2 \cdot 4\text{H}_2\text{O}$ has been determined by van Niekerk and Schoening (4). The unit cell is monoclinic with

$$a_0 = 4.75 \text{ \AA}, b_0 = 11.77 \text{ \AA}, c_0 = 8.44 \text{ \AA} \text{ and } \beta = 93^\circ 36'$$

and contains two molecules related by the operation of the space group $P2_1/C$. For the space group $P2_1/C$, the positions of the atoms are,

$$(0,0,0) \text{ and } (0, \frac{1}{2}, \frac{1}{2}) \text{ for nickel atom}$$

and

$$\pm (x, y, z; x, \frac{1}{2} - y, z + \frac{1}{2}) \text{ for other atoms and molecules.}$$

Each nickel atom is surrounded by a distorted octahedron of four water molecules at distances 2.06 \AA and 2.11 \AA , and two oxygen atoms of the two acetate groups at 2.12 \AA .

The crystals of $\text{Ni}(\text{CH}_3\text{COO})_2 \cdot 4\text{H}_2\text{O}$ grow as prismatic needles along the c axis(5). The projection of the unit cell of $\text{Ni}(\text{CH}_3\text{COO})_2 \cdot 4\text{H}_2\text{O}$ along its a_0 axis is given in Fig.5.1(6).

5.3 RESULTS AND DISCUSSION

(i). Analysis of the spectra:

The EPR of Mn^{2+} in $\text{Ni}(\text{CH}_3\text{COO})_2 \cdot 4\text{H}_2\text{O}$ has been studied at room temperature. The different magnetic complexes were found by studying the angular variation of the resonance spectrum. The z axes of these complexes were obtained by getting the maximum spread of the fine-structure separation. Two fine-structure maxima were obtained corresponding to the two magnetic complexes of Mn^{2+} substituting for Ni^{2+} in the bimolecular unit cell. The two z axes make an angle of $\sim 58^\circ$ with each other and $\sim 60^\circ$ with the crystallographic b axis.

From these observations, it has been concluded that $\text{Mn}-\text{H}_2\text{O}$ (1) forms the z -axis of the distorted octahedron of four water molecules and two oxygen atoms surrounding the Mn^{2+} ion substituting for Ni^{2+} .

The EPR spectrum for the Zeeman-field direction along the z axis of one of the magnetic complexes of Mn^{2+} is shown in Fig. 5.2. This has been analysed for the spin-Hamiltonian constants and these are,

$$g_z = 1.996 \pm 0.005, D = +462 \pm 5G, A = -90 \pm 5G$$

$$|E| = 90 \pm 10G, \text{ and } |B| = 90 \pm 10G.$$

(ii). Effect of Ni^{2+} on the EPR of Mn^{2+} :

As far as the general resonance properties – like the symmetry and the strength of the crystalline field at Mn^{2+} , the angle between the z axes – are concerned, the present system behaves like a system where Mn^{2+} is doped in an iso structural diamagnetic lattice, viz., magnesium acetate tetrahydrate $[\text{Mg}(\text{CH}_3\text{COO})_2 \cdot 4\text{H}_2\text{O}]$. In addition, however, a regular increase in the linewidth of Mn^{2+} resonance lines with the Zeeman- field intensity, and a shift in the g_z value towards the negative side, from the corresponding value of Mn^{2+} in isostructural $\text{Mg}(\text{CH}_3\text{COO})_2 \cdot 4\text{H}_2\text{O}$, have been observed.

Ni^{2+} has a $(3d)^8$ outershell configuration and a ground and a ground state 3F_4 . Under an octahedrally coordinated crystalline, field, the ground state of this even electron system is orbitally non-degenerate (7). Under the action of the crystalline field of orthorhombic or lower symmetry, the spin degeneracy is also removed (7). The separations between the ground state spin triplet are $|D| - |E|$ and $|2E|$, where D and E are the fine-structure constants for Ni^{2+} in that particular system. These for $\text{Ni}(\text{CH}_3\text{COO})_2 \cdot 4\text{H}_2\text{O}$ are, (8).

$$D = -5.61 \text{ cm}^{-1} \text{ and } E = -0.83 \text{ cm}^{-1}.$$

These splittings are much larger than the X-band microwave frequency ($\sim 0.3 \text{ cm}^{-1}$) and hence the non-observation of the EPR of Ni^{2+} .

Moriya and Obata (9) have given a detailed account of the effect of paramagnetic ions whose spin is quenched by the crystalline field (like Ni^{2+} , to be referred to as lattice spin), on the EPR of a resonating paramagnetic ion (like Mn^{2+}) introduced in the system. Similar effects relating to the g value have been discussed and observed by Hutchings and Wolf (10). For these systems when the Zeeman field is set on, magnetic moments are induced on the lattice spins due to polarization effect. This introduces an additional magnetic field at the resonating spin, proportional to the magnitude of the thermal equilibrium value of the lattice spin and the coupling constant between the two spins. The frequency dependence of the fluctuations of this lattice spin, about its thermal equilibrium value, which for the case of Zeeman interaction smaller than the ZFS of the lattice spin, gives rise to the dependence of the spin-lattice and spin-spin relaxation times of the resonating spin on the Zeeman-field intensity, and hence the line-width variation of the Mn^{2+} resonance lines with the Zeeman-field intensity.

The magnitude of the g tensor along the z axis, for the present system, is smaller than the free spin g value, while in

case of the EPR of Mn^{2+} in isostructural $\text{Mg}(\text{CH}_3\text{COO})_2 \cdot 4\text{H}_2\text{O}$, (11) at room temperature, this was observed to be 2.0069, larger than the free spin g value. The positive g shift, from the free spin g value, in the case of Mn^{2+} in $\text{Mg}(\text{CH}_3\text{COO})_2 \cdot 4\text{H}_2\text{O}$ has been explained on the basis of the effect of the covalent bonding between the Mn^{2+} ion and the surrounding ligands. $\text{Ni}(\text{CH}_3\text{COO})_2 \cdot 4\text{H}_2\text{O}$ is isostructural to $\text{Mg}(\text{CH}_3\text{COO})_2 \cdot 4\text{H}_2\text{O}$ (6), and one expects the same magnitude of ZFS of Mn^{2+} in this case also (which is really the case), and a corresponding positive g -shift, from the free spin g value. The negative shift in the g_z value in the case of Mn^{2+} in $\text{Ni}(\text{CH}_3\text{COO})_2 \cdot 4\text{H}_2\text{O}$, from that of the Mn^{2+} in $\text{Mg}(\text{CH}_3\text{COO})_2 \cdot 4\text{H}_2\text{O}$, has been attributed to the polarization effect of Ni^{2+} , which produces a local magnetic field at the Mn^{2+} ion in addition to the Zeeman field. From the shift in g_z value of Mn^{2+} in $\text{Mg}(\text{CH}_3\text{COO})_2 \cdot 4\text{H}_2\text{O}$, from the corresponding value for Mn^{2+} in $\text{Mg}(\text{CH}_3\text{COO})_2 \cdot 4\text{H}_2\text{O}$, the intensity of the local magnetic field at Mn^{2+} due to Ni^{2+} has been found to be $\sim 20\text{G}$, for the Zeeman-field direction along the z axis of one of the magnetic complexes.

A best fit calculation has been made of the linewidths of the Mn^{2+} resonance lines (peak-to-peak width of the derivative signal) for linear and quadratic variations with the Zeeman-field intensity, along the z axis of one of the magnetic complexes using the linear regression technique (12-15). Due to the

overlap of the lines of the second magnetic complex, and the weak intensity of the transition at larger Zeeman-field intensities, the number of resonance transitions considered for the best fit was limited. The linewidth of the Mn^{2+} resonance transition (ΔH) and the corresponding Zeeman-field intensity (H) considered (16-20) for the best fit are given in Table 5.I, wherein only well resolved lines have been taken.

The equation used have been, $\Delta H = a + bH$, (5.3.1)

For the case of linear variation of ΔH with H , and

$$\Delta H = c + dH^2, \quad (5.3.2)$$

For the case of quadratic variation. The values of these parameters are,

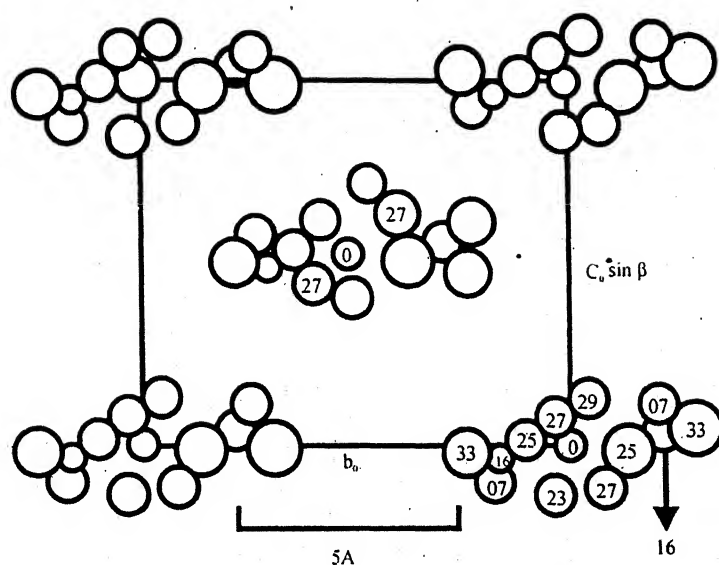
$a = 10.0\text{G}$, $b = 0.0091$ and the root-mean-square (RMS) deviation = 2.574G ,

and $c = 21.2\text{G}$, $d = 1.57 \times 10^{-6}\text{G}^{-1}$, and $\text{RMS} = 3.18\text{G}$.

A brief report of the theory concerning the effect of Ni^{2+} diluting ions on the EPR of Mn^{2+} is given in the Appendix.

Table 5.I
The Zeeman-Field Intensity (H) and the
Corresponding Linewidth (ΔH) of Mn^{2+} Resonance Lines
in $Ni(CH_3COO)_2 \cdot 4H_2O$

H (Gauss)	ΔH (Gauss)	$\Delta H/H$
1285	20.3	0.01579
1370	21.7	0.01584
1455	23.7	0.01629
2212	27.1	0.01225
2396	31.9	0.01331
2570	33.9	0.01323
2660	40.7	0.01530
4013	47.5	0.0118
4190	47.5	0.0113
4478	48.8	0.0109



- 0 Ni
- 27 H₂O (1)
- 23 H₂O (2)
- 25 O (1)
- 07 O (2)
- 16 C
- 33 CH₃

Fig. 5.1

The monoclinic crystal structure of $\text{Ni}(\text{CH}_3\text{COO})_2 \cdot 4\text{H}_2\text{O}$ projected along its a_0 axis. The numbers inside the circles represent the positions of the atoms or molecules along the a_0 axis in units of the unit cell dimension along the a_0 axis. ($100 = 4.75\text{\AA}$). For the other molecule of the unit cell, the positions of Ni and H_2O (1) are given

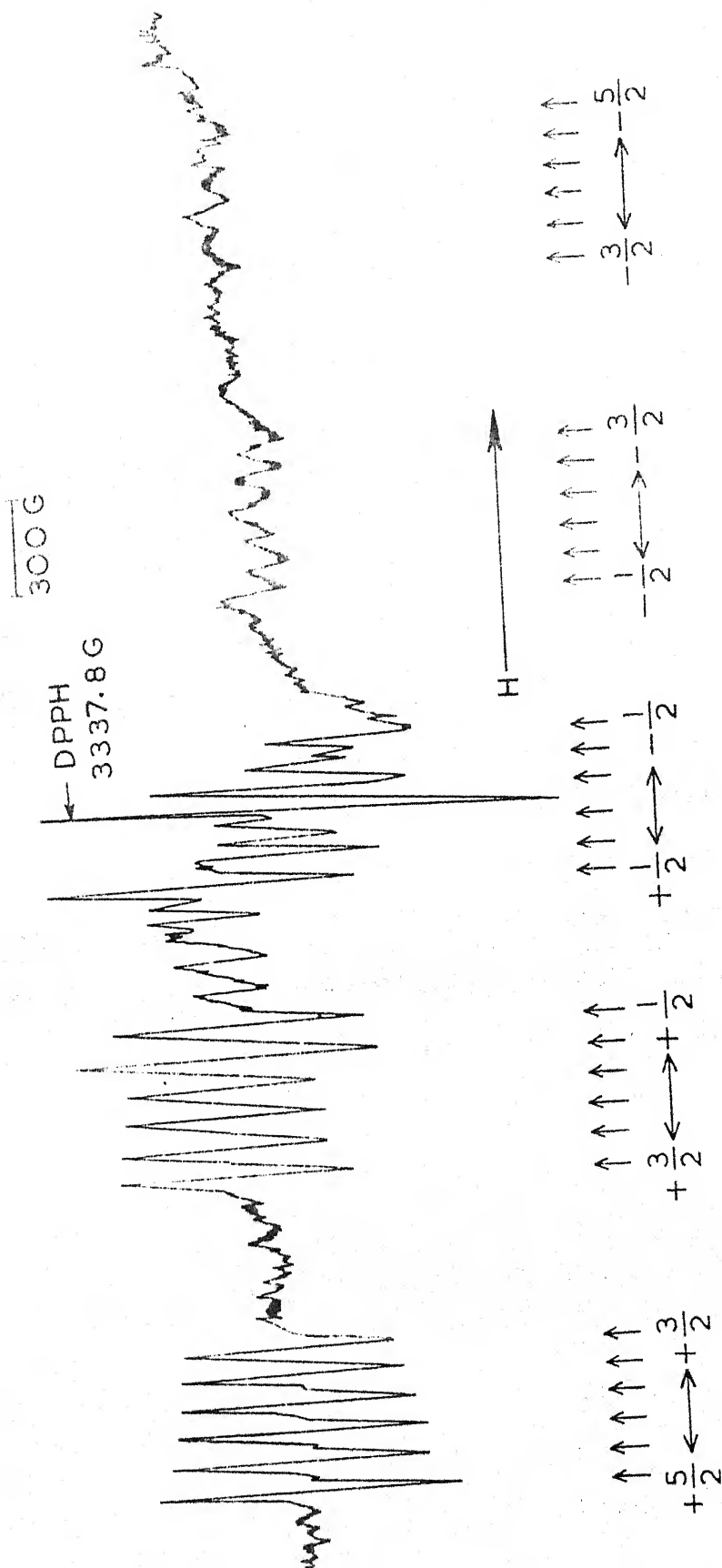


Fig. 5.2: EPR spectrum of Mn^{2+} in $\text{Ni}(\text{CH}_3\text{COO})_2 \cdot 4\text{H}_2\text{O}$ for the Zeeman-field direction along the z axis of one of the magnetic complexes of Mn^{2+} .

REFERENCES

1. B. Bleaney and D.J.E. Ingram, Proc. Phys. Soc. (London), **A63**, 408 (1950).
2. B. Bleaney, R.J. Elliott and H.E.D. Scovil, *ibid.* **A64**, 933 (1951).
3. K. Ono and I. Hayashi, J. Phys. Soc. Japan **8**, 561 (1953).
4. J.N. Van Niekerk and F.R.L. Schoening, Acta crystallogr. **6**, 609 (1953).
5. M.W. Porter and R.C. Spiller, 'The Barker Index of Crystals', Vol. 2, W. Heffer and Sons, Cambridge (1956).
6. R.W.G. Wyckoff. 'Crystal Structures, ' Vol.5, Interscience, New York (1966).
7. R. Schlapp and W.G. Penney, Phys. Rev. **42**, 666 (1932).
8. R.B. Flippen and S.A. Friedberg, *ibid.* **121**, 1591 (1961).
9. T. Moriya and Y. Obata, J. Phys. Soc. Japan **13**, 1333 (1958).
10. M.T. Hutchings and W.P. Wolf, Phys. Rev. Lett. **11**, 187 (1963).

11. T.J. Manakkil, Ph.D. Thesis, New Mexico State University, Las Cruces (1967).
12. B.J. Reddy, S Vedanand and G.Srinivaslu, Solid State Comm. (USA) **78**, 8, 751 (1991)
13. J.S. Phor, Radiat. Effects in Solids (UK) **116**, 1, 149 (1991)
14. V.K. Jain, G. Lehmann, Phys. Stat, Solidi B (East Germany) **159**, 2, 495 (1990).
15. A Bals, and S.I. Gorbachuk, Phys. Stat. Solidi. A (East Germany) **114**, 1, 305 (1989).
16. J.L. Rao, G.L. Narendra, B Sreedhar and S.V. Lakshman, Phys. Stat. Solidi B (East Germany) **153**, 1, 257 (1989).
17. S.K. Mishra Jainsheng Sun and S. Jerzak, Phys. Rev B. Cond. Matter (USA) **40**, 1, 54 (1989).
18. M. Umar, M.I. Haque and R.J. Singh. Phys. Stat. Solidi B (East Germany) **145**, 1 51 (1988).
19. R.S. Bansal, V.P. Seth and P. Chand, Phys. Scr. (Sweeden) **44**, 5 493 (1991).
20. Y. Nagarja Naidu, J. Lakshman Rao and S.V.J. Lakshman, Solid State Comm. (USA) **81**, 5, 437 (1992)

CHAPTER – 6

ELECTRON PARAMAGNETIC RESONANCE OF Mn^{2+} ION IN HEPTAHYDRATED SULFATES OF NICKEL AND MAGNESIUM

6.1 INTRODUCTION

In studying the EPR of paramagnetic ions, diamagnetic ions are most commonly used as the dilutants in magnetically dilute mixed crystals, so that there is no appreciable interaction between the paramagnetic ions themselves, or with the ions of the diluting medium (1). There exist certain paramagnetic ions, which can act as proper dilutants under certain condition. Paramagnetic ions whose spin-lattice relaxation time is short at room temperature can be used as dilutants till high enough temperatures, so that the spin-lattice relaxation time of the diluting ion does not approach the Larmor precession period of the resonating paramagnetic ion (2,3). Besides, paramagnetic ions whose ZFS is much larger than the irradiating microwave frequency, can also be used as dilutants (3). The ions which belong to the second class are those with even number of unpaired electrons, and hence have no Kramers degeneracy. In a crystalline field of lower-than-axial symmetry the orbital and spin degeneracies are completely removed, by the combined action of the crystalline-field and spin orbit interactions. Divalent nickel is a good example of this class of paramagnetic ions in the iron group series. In chapter-5 we have dealt with the EPR of Mn^{2+} in one of the nickel compounds, viz, $\text{Ni}(\text{CH}_3\text{COO})_2 \cdot 4\text{H}_2\text{O}$. The present chapter is an extension of the similar type of study in nickel sulfate heptahydrate ($\text{NiSO}_4 \cdot 7\text{H}_2\text{O}$), at room temperature. For

a comparative study, the EPR of Mn^{2+} in isostructural magnesium sulfate heptahydrate ($\text{MgSO}_4 \cdot 7\text{H}_2\text{O}$) has also been studied at room temperature.

6.2 CRYSTAL STRUCTURE

$\text{NiSO}_4 \cdot 7\text{H}_2\text{O}$ and $\text{MgSO}_4 \cdot 7\text{H}_2\text{O}$ are isostructural (4), with orthorhombic unit cell symmetry. The crystal structure of $\text{NiSO}_4 \cdot 7\text{H}_2\text{O}$ has been determined by Beevers and Schwartz (5). The unit cell is tetramolecular, the four molecules being related by the operation of the space group $\text{P}2_12_12_1$. The unit cell dimensions are (4),

For $\text{NiSO}_4 \cdot 7\text{H}_2\text{O}$:

$$a_0 = 11.86 \text{ \AA}, b_0 = 12.08 \text{ \AA}, \text{ and } c_0 = 6.81 \text{ \AA}.$$

and for $\text{MgSO}_4 \cdot 7\text{H}_2\text{O}$

$$a_0 = 11.91 \text{ \AA}, b_0 = 12.02 \text{ \AA}, \text{ and } c_0 = 6.87 \text{ \AA}.$$

For the space group operation $\text{P}2_12_12_1$, the atoms and molecules are in the position

$$(x, y, z; \bar{x}, \bar{y}, z + \frac{1}{2}; x + \frac{1}{2}, \frac{1}{2} - y, \bar{z}; \frac{1}{2} - x, y + \frac{1}{2}, \frac{1}{2} - z)$$

Each divalent cation is surrounded by six water molecules, $[\text{H}_2\text{O}(1)\text{-H}_2\text{O}(6)]$, at distances ranging from, in the case of

$\text{NiSO}_4 \cdot 7\text{H}_2\text{O}$, $1.93 \text{ \AA} - 2.40 \text{ \AA}$. The seventh water molecule, $\text{H}_2\text{O}(7)$, is not coordinated with a cation, but instead fills what would be a hole in the structure.

The single crystals of $\text{NiSO}_4 \cdot 7\text{H}_2\text{O}$ and $\text{MgSO}_4 \cdot 7\text{H}_2\text{O}$ grow as prismatic needles along the c axis⁶. the projection of the unit cell of $\text{NiSO}_4 \cdot 7\text{H}_2\text{O}$ along its c_0 axis is shown in fig. VII-1⁴.

6.3 RESULTS AND DISCUSSION

(i). Analysis of the spectra:

The EPR of Mn^{2+} in $\text{NiSO}_4 \cdot 7\text{H}_2\text{O}$ and $\text{MgSO}_4 \cdot 7\text{H}_2\text{O}$ has been studied at room temperature. Hayashi and Ono (7) have studied the EPR of Mn^{2+} in $\text{MgSO}_4 \cdot 7\text{H}_2\text{O}$, but the constants were not reported accurately. We have studied the system once again and determined the constants accurately, for comparison with the results on Mn^{2+} doped $\text{NiSO}_4 \cdot 7\text{H}_2\text{O}$. The different complexes of Mn^{2+} in $\text{NiSO}_4 \cdot 7\text{H}_2\text{O}$ and $\text{MgSO}_4 \cdot 7\text{H}_2\text{O}$ were found by studying the angular variation of the resonance spectrum. The z axes of these complexes were obtained by getting the maximum spread of the fine-structure separation. Four fine structure maxima were obtained corresponding to the four magnetic complexes of Mn^{2+} substituting for Ni^{2+} and Mg^{2+} . The z axis of each Mn^{2+} complex in $\text{NiSO}_4 \cdot 7\text{H}_2\text{O}$ makes angles of $\sim 32^\circ$, $\sim 55^\circ$ and $\sim 55^\circ$ with the z axes of the other

three complexes. This coincides fairly closely with the supposition that the z axis of the distorted octahedron of six water molecules is along the line joining manganese and the water molecule at shortest distance from nickel, viz., $\text{H}_2\text{O}(3)$.

The EPR spectra of Mn^{2+} in $\text{NiSO}_4 \cdot 7\text{H}_2\text{O}$ and $\text{MgSO}_4 \cdot 7\text{H}_2\text{O}$ for the Zeeman-field direction along the z axis of the one of the magnetic complexes, are shown in Fig. 6.2 and 3, respectively. These have been analysed for the spin Hamiltonian constants, which are:-

For Mn^{2+} in $\text{NiSO}_4 \cdot 7\text{H}_2\text{O}$:

$$g_z = 1.995 \pm 0.005, D = +448 \pm 5\text{G}, A = -91 \pm 5\text{G},$$

$$|E| = 74 \pm 10\text{G}, \text{ and } |B| = 87 \pm 10\text{G},$$

and for Mn^{2+} in $\text{MgSO}_4 \cdot 7\text{H}_2\text{O}$:

$$g_z = 2.003 \pm 0.005, D = +412 \pm 5\text{G}, A = -92 \pm 5\text{G},$$

$$|E| = 95 \pm 10\text{G}, \text{ and } |B| = 87 \pm 10\text{G},$$

The crystal-field parameters D and E in the two systems are very nearly the same, indicating that the configuration of water molecules at Ni^{2+} and Mg^{2+} is very nearly same. The observed differences may be due to small differences in the distances of the water molecules from the cations in the two cases.

(ii). Effect of Ni^{2+} on the EPR of Mn^{2+} :

As far as the general resonance properties like the symmetry and the strength of the crystalline field at Mn^{2+} , the angle between the axes – are concerned, both the systems, $\text{NiSO}_4 \cdot 7\text{H}_2\text{O}$ and $\text{MgSO}_4 \cdot 7\text{H}_2\text{O}$, behave in the same manner. In addition, in the case of Mn^{2+} in $\text{NiSO}_4 \cdot 7\text{H}_2\text{O}$, we have observed a regular increase in the linewidth of Mn^{2+} resonance lines with the Zeeman-field intensity, and a shift in the g_z value towards the negative side, from the corresponding value for Mn^{2+} in $\text{MgSO}_4 \cdot 7\text{H}_2\text{O}$.

The ground state spin triplet of Ni^{2+} in an octahedral crystalline field, under the combined action of crystalline field of lower than axial symmetry and spin orbit interaction, has its spin degeneracy completely removed (8). The separations between the components of the ground state triplet are $|D| - |E|$ and $|2E|$, where D and E are the fine structure constants of Ni^{2+} in that particular system. For Ni^{2+} in $\text{NiSO}_4 \cdot 7\text{H}_2\text{O}$ these are (9),

$$D = -3.56\text{cm}^{-1} \quad \text{and} \quad E = 1.5\text{cm}^{-1}.$$

These splitting are much larger than the x-band microwave frequency ($\sim 0.3\text{cm}^{-1}$) and hence the non observation of the EPR of Ni^{2+} .

The effect of lattice spin, for the case where the spin angular momentum is completely quenched, on the EPR of Mn^{2+} introduced in that system has been studied detailedly by Moriya and Obata (10) and the effects relating to the g value have been discussed

and observed by Hutchings and Wolf(11). For these systems, when the Zeeman field is set on, magnetic moments are induced on the lattice spins, due to polarization effect (12-17). This introduces an additional magnetic field at the resonating spin (Mn^{2+}), proportional to the magnitude of the thermal equilibrium value of the lattice spin and the coupling constant between the resonating and lattice spins. The frequency dependence of the fluctuations of this lattice spin, about its thermal equilibrium value, which for the Zeeman interaction smaller than the ZFS of the lattice spin, gives rise to the dependence of the spin-lattice and spin-spin relaxation times of the resonating spin on the Zeeman-field intensity. Hence the linewidth of Mn^{2+} resonance lines exhibit a direct dependence on the Zeeman-field intensity. From the observed g_z shift in the case of Mn^{2+} in $NiSO_4 \cdot 7H_2O$ from the corresponding value for Mn^{2+} in isostructural $MgSO_4 \cdot 7H_2O$, it has been possible to calculate the intensity of the additional magnetic field at Mn^{2+} due to Ni^{2+} in $NiSO_4 \cdot 7H_2O$. Assuming that the g_z shift is entirely due to the effect of Ni^{2+} , the additional magnetic field is $\sim 15G$ at Mn^{2+} , for the Zeeman field direction along the z axis of that complex.

A best fit calculation has been made of the linewidths of the Mn^{2+} resonance lines (18-21) (peak-to-peak width of the derivative signal) for linear and quadratic variations with the Zeeman-field intensity along the z axis of a magnetic complex. The method used has been the linear regression theory. Only those transitions whose

lines are clearly resolved have been considered for the best fit, and some representative values of these are given in Table 6.I.

Eqs. (5.1) and (5.2) were used for the best fit calculation and the parameters obtained are,

$$a = 6.51G, \quad b = 3.0 \times 10^{-3}, \quad \text{and} \quad RMS = 0.63G$$

$$\text{and } c = 16.89G, \quad d = 0.1 \times 10^{-6} G^{-1} \text{ and } RMS = 2.34G.$$

A brief report of the theory concerning the effect of Ni^{2+} diluting ions on the EPR of Mn^{2+} is given in the Appendix.

Table-6.I

The Zeeman-field Intensity (H) and the Corresponding linewidth (ΔH) of Mn^{2+} Resonance Lines in $NiSO_4 \cdot 7H_2O$

H (Gauss)	ΔH (Gauss)	$\Delta H/H$
2510	13.1	0.005219
3122	16.5	0.005285
3569	18.1	0.005071
4448	20.3	0.004563
5166	21.6	0.004181
5266	22.0	0.004177

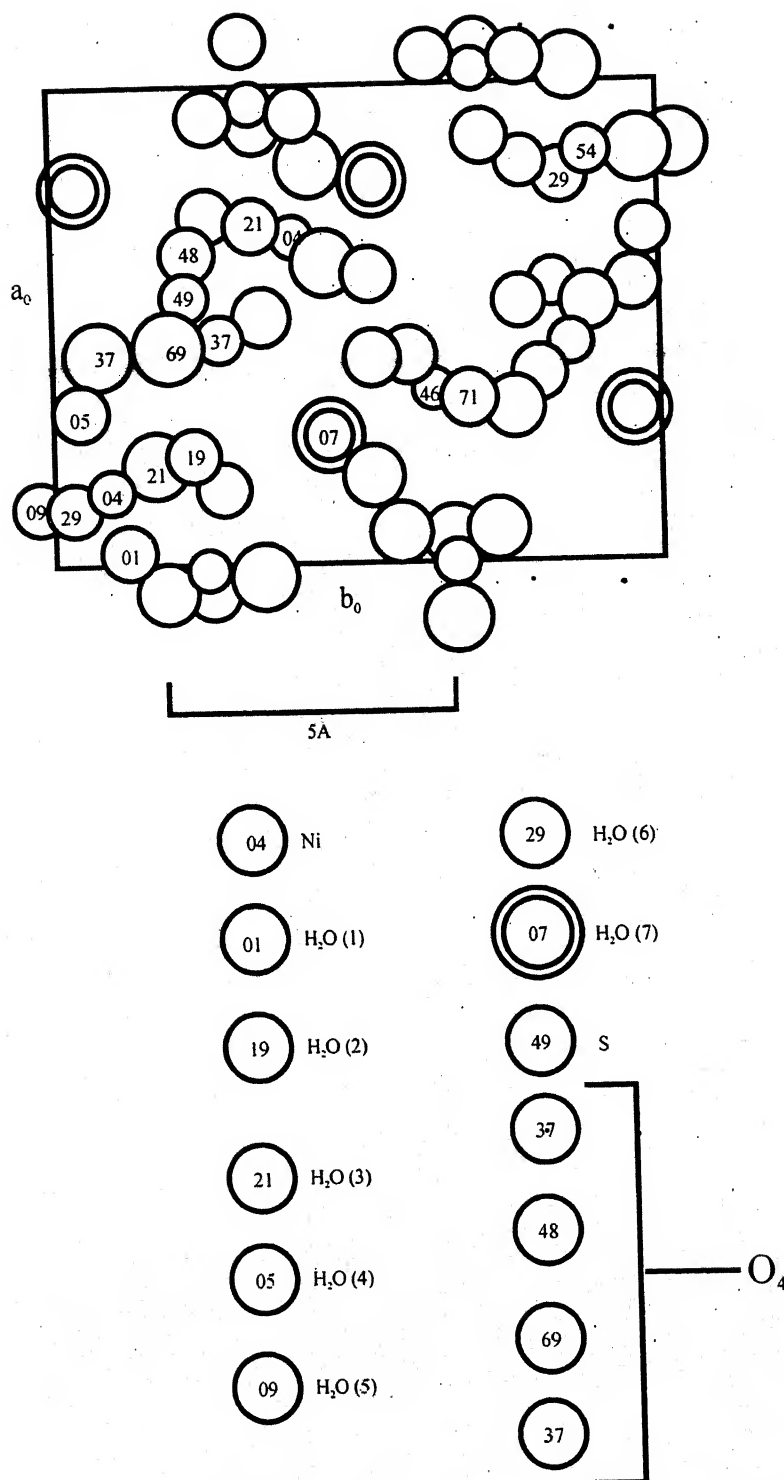


Fig 6.1

The orthorhombic crystal structure of $\text{NiSO}_4 \cdot 7\text{H}_2\text{O}$ projected along its C_0 axis. The numbers inside the circles represents the positions of the atoms or molecules along the C_0 axis in units of the unit cell dimension along the C_0 axis ($100 = 6.81\text{ Å}$). The seventh H_2O , which is not coordinated to the nickel atom, is doubly ringed. For the other molecules the positions of Ni and H_2O (3) are given.

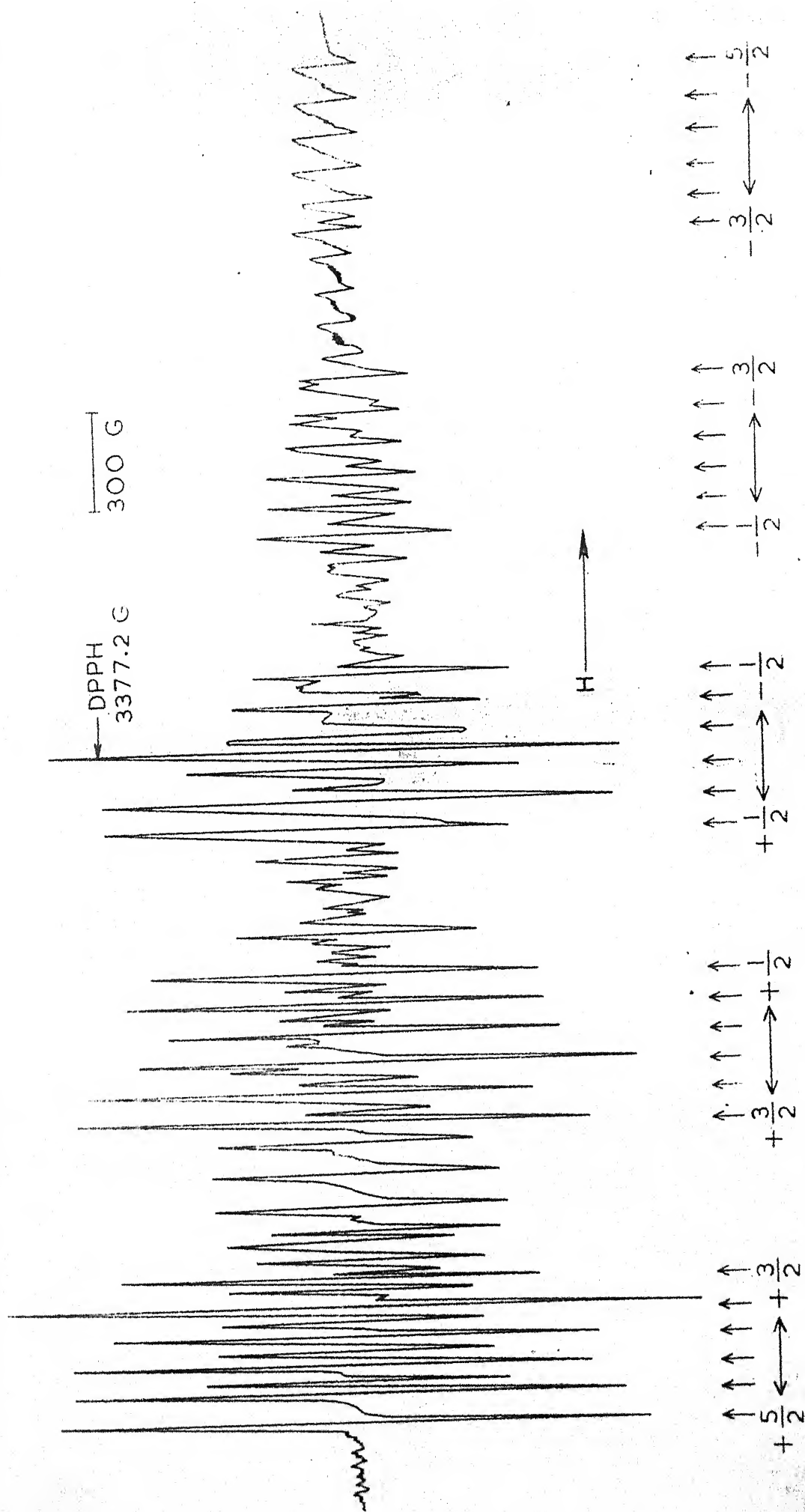


Fig. 6.2: EPR spectrum of Mn^{2+} in $NiSO_4 \cdot 7H_2O$ for the Zeeman-field direction along the z axis of one of the magnetic complexes of Mn^{2+} .

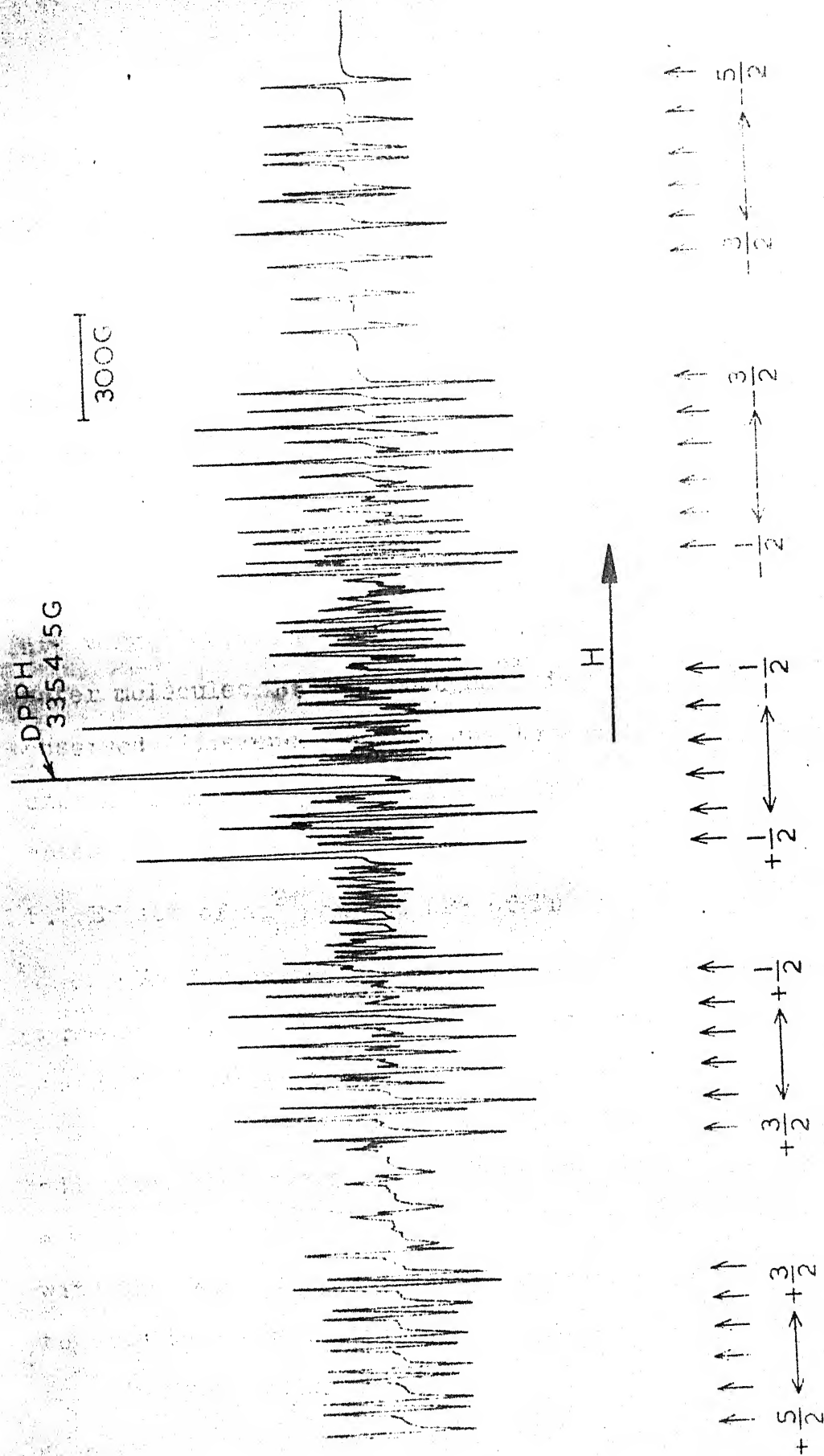


Fig. 6.3: EPR spectrum of Mn^{2+} in $\text{MgSO}_4 \cdot 7\text{H}_2\text{O}$ for the Zeeman-field direction along the z axis of one of the magnetic complexes of Mn^{2+} .

REFERENCES:

1. B. Bleaney and D.J.E. Ingram, Proc. Phys. Soc. (London) **Δ 63**, 408 (1950).
2. B. Bleaney, R.J. Elliott, and H.E.D. Scovil, Ibid. **Δ 64**, 933 (1951).
3. K. Ono and I. Hayashi, J. Phys. Soc. Japan **8**, 561 (1953).
4. R.W.G. Wyckoff, 'Crystal Structures', Vol 3, p. 839. Inter-science, New York (1965).
5. C.A. Beevers and C.M. Schwartz, Z. Kristallogr. **91A**, 157 (1935).
6. M.W. Porter and R.C. Spiller, 'The Barker Index of Crystals', Vol.1, W. Heffer and Sons, Combridge (1951).
7. I. Hayashi and K. Ono, J. Phys. Soc. Japan **8**, 270 (1953).
8. R. Schlapp and W.G. Penney, Phys. Rev. **42**, 666 (1932),
9. K. Ono, J. Phys. Soc. Japan **8**, 802 (1953).
10. T. Moriya and Y. Obata, ibid. **13**, 1333 (1958).

11. M.T. Hutchings and W.P. Wolf, Phys. Rev. Lett. **11**, 187 (1963).
12. Y. Nagraja, J. Lakshman Rao and S.V.J. Lakshman Solid Stat Communication (USA) **81**, 5 437 (1992).
13. R. Hrabanski, Solid State Comm. (USA) **64**, 1, 117 (1987)
14. O.S. Torosyan, L.S. Bezhanova, Sov. J. Contemp. Phys. (USA) **22**, 1, 29 (1987).
15. J. Robeiro, J. Phys. (France) **49**, 5, 813 (1988).
16. Y. Yang Zhou, Phys. Stat. Solidi B (East Germany) **147**, No. 1, 273 (1988).
17. K.L. Wan, S.L. Hutton and J.E. Drumheller, J. Chem. Phys. (USA) **86**, 7, 3801 (1987)
18. K.P. Such and Lehman, Mol. Phys. (GB) **60**, 3, 553 (1987).
19. E.Diamauero, J. Phys & Chem. Solids (GB) **48**, 1, 29 (1987).
20. P. Chand and G.C. Upreti, Solid Stat Comm. (USA) **56**, 2, 225 (1985).
21. S.K. Mishra. W. Changlu, Solid State Comm. (USA) **59**, 6, 409 (1986).

APPENDIX

Effect of Ni^{2+} Diluting ions on the EPR of Mn^{2+}

Chapters 5 and 6 describe the EPR of Mn^{2+} in single crystals of Ni^{2+} salts, and the results therein have been interpreted on the basis of the theoretical study by Moriya and Obata.¹ Here a brief summary of their work is presented.

The $(3d)^8$ configuration of Ni^{2+} in an octahedrally coordinated crystalline field has an orbital singlet as its ground state². The spin degeneracy is also removed completely in the presence of a crystalline field of lower than axial symmetry, by the combined action of the crystalline field and spin-orbit interactions.² Thus, in such an environment, both the orbital and spin angular momenta are completely quenched for the ground state of the Ni^{2+} ion. In such a case the diagonal component (low frequency component) of the ground state magnetic moment is zero, in the absence of the externally applied Zeeman field and the Ni^{2+} ion is non magnetic. When the Zeeman field (H) is set on, magnetic moments are induced on this non magnetic state, because of the matrix elements connecting the ground state, $|0\rangle$ and the high lying electronic states, $|n\rangle$, (high frequency component of the magnetic

1. T. Moriya and Y. Obata, J. Phys. Soc. Japan **13**, 1333 (1958).

2. R. Schlapp and W.G. Penney, Phys. Rev. **42**, 666 (1932).

moment), due to the polarization effect. The induced magnetic moment is proportional to H and $|\langle n|M|O \rangle|^2$, where M is the magnetic moment operator along the Zeeman-field direction³. Since the low-frequency component is zero we have

$$W_l = 0 \quad (\text{A.1})$$

the energy of this system can be written, upto second order in H , as

$$\begin{aligned} E &= W_0 + W_2 H^2 \\ &= W_0 + \sum_{\mu} W_{2\mu} H_{\mu}^2 \end{aligned} \quad (\text{A.2})$$

Moriya and Obata¹ have discussed the EPR of a resonating spin (Mn^{2+}) introduced in a salt where the Ni^{2+} are the diluting ions, and the effect of Ni^{2+} on the EPR of Mn^{2+} . At temperatures (T) such that $kT < \Delta$ ($=E_n - E_0$), the thermal equilibrium value of the Ni^{2+} spin is given as .

$$\langle S_{\mu} \rangle = \sum_m f_m (S_{\mu})_{mm} \quad (\text{A.3})$$

m is the summation over the various spin-states of the Ni spin and f_m is the statistical factor given by

$$f_m = \exp(-E_m / kT) / \sum_m \exp(-E_m / kT), \quad (\text{A.4})$$

3. C. Kittel 'Introduction to Solid State Physics', App. E. P-578, Asia Publishing House, Lucknow (1966)

and $(S_\mu)_{mm}$ are the diagonal elements of the μ -th component of the Ni^{2+} spin. Then the spin S of Ni^{2+} can be written as the contribution of two terms as

$$S = \langle S \rangle + \delta S, \quad (\text{A.5})$$

where δS is the fluctuation of the spin from its thermal equilibrium value.

Now we consider the Hamiltonian of the Mn^{2+} ion, with the effect of the Ni^{2+} ion on it. This is written as

$$\mathcal{H} = \mathcal{H}_{\text{Mn}} + \mathcal{H}_{\text{Mn-Ni}} \quad (\text{A.6})$$

Where \mathcal{H}_{Mn} is the Zeeman term in the spin Hamiltonian of Mn^{2+} , and

$$\mathcal{H}_{\text{Mn-Ni}} = \text{constant} \times \sum_{v=1}^3 \psi_v \sum_j \sum_\mu \phi_j^{v\mu} S_{j\mu} \quad (\text{A.7})$$

ψ is the v -th component of the Mn^{2+} spin, $\phi_j^{v\mu}$ is the coupling constant between Mn^{2+} and Ni^{2+} spins, like the dipolar or exchange coupling, and $S_{j\mu}$ is the μ -th component of the j -th Ni^{2+} spin, where more than one Ni^{2+} ion are contributing to $\mathcal{H}_{\text{Mn-Ni}}$. Eq. (A.6) is written as

$$\mathcal{H} = \mathcal{H}_0 + \mathcal{H}'. \quad (\text{A.8})$$

where

$$\mathcal{H}_0 = g\beta \left(\bar{H} + \text{constant} \times \sum_{\nu} \sum_{\mu} \phi_j^{\nu\mu} S_{j\mu} \right) \bar{\Psi} \quad (\text{A.9})$$

and

$$\mathcal{H}' = \text{constant} \times \left(\sum_{\nu} \sum_j \sum_{\mu} \phi_j^{\nu\mu} S_{j\mu} \right) \bar{\Psi}. \quad (\text{A.10})$$

The thermal equilibrium value of the Ni^{2+} spin produces an additional field at Mn^{2+} , proportional to $\phi_j^{\nu\mu}$ and $\langle S_{j\mu} \rangle$, Eq. (A.9), in addition to the Zeeman field. This additional field results in the g-shift, which has been calculated from the g value of the EPR of Mn^{2+} in an isostructural diamagnetic salt.

The effect of the fluctuations of the Ni^{2+} spin is obtained by considering the effect of \mathcal{H}' on \mathcal{H}_0 . This has been done by considering the motional effect, with the combination coming from the secular and non-secular effects.⁴ This leads to the dependence of $1/T_1$ and $1/T_2$ on $\langle \delta S_{\mu}(t) \delta S_{\nu} \rangle$, where T_1 and T_2 are the spin lattice and spin-spin relaxation times of Mn^{2+} , and

$$\delta S_{\mu}(t) = \exp(it \mathcal{H}_{\text{Ni}}/\hbar) \delta S_{\mu} \exp(-it \mathcal{H}_{\text{Ni}}/\hbar). \quad (\text{A.11})$$

$\langle \delta S_{\mu}(t) \delta S_{\nu} \rangle$ is further related to the difference between the isothermal and isolated susceptibilities (χ_T and χ_{is}) in the following way.

$$\langle \delta S_{\mu}(t) \delta S_{\nu} \rangle = \sum_n G_{\mu\nu}^{(n)}(t) \quad (\text{A.12})$$

4. R. Kubo and K. Tomita, J. Phys. Soc. Japan **9**, 888 (1954)

where $G_{\mu\nu}^{(n)}(t)$ is the 'auto-moment' of the Ni^{2+} spin

$$G_{\mu\nu}^{(n)}(t) = \langle (S_\mu)_{nn} (S_\nu)_{nn} \rangle - \langle S_\mu \rangle \langle S_\nu \rangle \quad (\text{A.13})$$

and hence

$$g_\mu^2 g_\nu^2 \beta^2 G_{\mu\nu}^{(n)}(t) = \langle \frac{\partial E}{\partial H_\mu} \frac{\partial E}{\partial H_\nu} \rangle - \langle \frac{\partial E}{\partial H_\mu} \rangle \langle \frac{\partial E}{\partial H_\nu} \rangle \quad kT \quad (\chi_T - \chi_{is})_{\mu\nu} \quad (\text{A.14})$$

where g_μ, g_ν are the μ -th and ν -th component of the g value of the Ni^{2+} ion in that particular compound. Since E is given by Eq. (A.2), we have

$$kT (\chi_T - \chi_{is})_{\mu\nu} = 2 (\langle W_{2\mu} W_{2\nu} \rangle - \langle W_{2\mu} \rangle \langle W_{2\nu} \rangle) H_\mu H_\nu. \quad (\text{A.15})$$

a function of the Zeeman-field intensity. Thus $1/T_1$ and $1/T_2$, and hence the widths of Mn^{2+} resonance lines, exhibit a direct dependence on the Zeeman-field intensity.

The results that have been obtained in the EPR of Mn^{2+} in the two Ni^{2+} salts are in conformity with these predictions of the theory of Moriya and Obata¹.

GENERAL REFERENCES

- (i) D.J.E. Ingram, "Spectroscopy at radio and microwave frequencies; Butter-worths, London (1955).
- (ii) W. Gordy, "Theory and Application of Electron Spin Resonance" (John Wiley & Sons, Inc, 1972).
- (iii) C.P. Poole Jr. and H.A. Farah, "The Theory of magnetic resonance" (John Wiley & Sons Inc. 1972).
- (iv) W.Low "Paramagnetic resonance in solids" (Academic press, New York and London 1960).
- (v) A. Abragam, B. Bleaney, "Electron Paramagnetic Resonance of Transition Ions (Clarendon press, Oxford 1970).
- (vi) C.J. Ballhausen, Introduction to legand field theory (McGraw Hill Book Co. Inc. New Delhi 1962).
- (vii) M.W. Porter and R.C. Spiller, Barker Index of crystals, Haffer Cambridge (1956).
- (viii) R.W.G. Wyckoff, Crystal Structure, (Vol. 3, Interscience Publ. 1965).
- (ix) K.A. Muller and H. Thomas, "Structural Phase Transitions I' (Springer Verlag Berlin, Heidelberg, New York 1981).
- (x) F.J. Owens, C.P. Poole Jr. and H.A. Farah, Magnetic Resonance of Phase Transitions, Academic Press (1979).
- (xi) A.Carrington and A.D. Mclachlen, Introduction to Magnetic Resonance (Chapman and Hall, 1979).
- (xii) J.E. Wertz and J.R. Bolton, Electron Spin Resonance; Elementary theory and Practical Applications, McGraw Hill (1972).
- (xiii) J.W. Orton, Electron Paramagnetic Resonance, Iliffe Books Ltd. London (1968).
- (xiv) B.D. Cullity, Elements of X-ray diffraction, Addison-Wisley Pub. Company, Inc. California (1978).
- (xv) Kaiser and L. Kavad, Electron Spin Resonance of first row transition Metal Complex ions, John Wiley (1968).
- (xvi) R.K. Watts : Points Defects in crystals. John-Wiley & Sons (1977).